ÉCOLE DE TECHNOLOGIE SUPÉRIEURE
UNIVERSITÉ DU QUÉBEC

THESIS PRESENTED TO
ÉCOLE DE TECHNOLOGIE SUPÉRIEURE

IN PARTIAL FULFILLMENT OF THE REQUIREMENTS FOR
A MASTER'S DEGREE IN MECHANICAL ENGINEERING
M. Eng.

BY
Joël BÉDARD

IMPROVEMENT OF SHORT-TERM NUMERICAL WIND PREDICTIONS

MONTRÉAL, SEPTEMBER 16 2010

BOARD OF EXAMINERS

THIS THESIS HAS BEEN EVALUATED

BY THE FOLLOWING BOARD OF EXAMINERS

Dr. Christian Masson, Thesis Supervisor
Département de génie mécanique à l'École de Technologie Supérieure

Dr. Yves Gagnon, Thesis Co-supervisor
Faculté des études supérieures et de la recherche à l'Université de Moncton

Dr. Wei Yu, Thesis Co-supervisor
Meteorological Research Division at Environment Canada

Dr. Robert Benoit, President of the Board of Examiners
Département de génie mécanique à l'École de Technologie Supérieure

Dr. Stéphane Bélair, External Examiner
Meteorological Research Division at Environment Canada

THIS THESIS HAS BEEN PRESENTED AND DEFENDED

BEFORE A BOARD OF EXAMINERS AND PUBLIC

SEPTEMBER 2ND 2010

AT ÉCOLE DE TECHNOLOGIE SUPÉRIEURE

ACKNOWLEDGEMENTS

This project, part of the Wind Energy Strategic Network (WESNet), is funded by the Natural Sciences and Engineering Research Council (NSERC) of Canada, and by the Canada Research Chair in the Aerodynamics of Wind Turbines in Nordic Environment (École de Technologie Supérieure), the K.-C.-Irving Chair in Sustainable Development (Université de Moncton) and the Environmental Numerical Prediction Research Section of the Meteorological Research Division (Environment Canada). The author also acknowledges the contributions of the Wind Energy Institute of Canada (WEICan) in this research program.

On a personal note, I wish to thank my directors Christian Masson, Yves Gagnon and Wei Yu for their advices and support in carrying out this work. More specifically, I am grateful to have had Christian Masson give me the opportunity to work in his lab and to Yves Gagnon for introducing me to different parties involved in the wind energy sector. Also, a very special thanks to Wei Yu for his scientific supervision and his devotion to the project: he integrated me into the Meteorological Research Division team at Environment Canada. Thanks to André Plante, Laurent Chardon, Djamel Bouhemhem and others colleagues from the Meteorological Research Division team for their technical support and advices. Also, thanks to Nicolas Gasset and Robert Benoit from the Canada Research Chair in the Aerodynamics of Wind Turbines in Nordic Environment (École de Technologie Supérieure) for many fruitful discussions.

Moreover, I wish to thank the WEICan staff and Mathieu Landry from the K.-C.-Irving Chair in Sustainable Development (Université de Moncton) for their technical support with atmospheric measurements and their warm welcoming during my stay in the Maritimes. I am also grateful to Linda Mallette (École de Technologie Supérieure) for her precious help with the official recognition of the competencies acquired at Université de Moncton. Also, thanks to the members of the present jury for their precious comments and their judicious evaluation. On a final note, very special thanks are reserved to my family and my friends for being with me, for your constant support and your infinite patience. Thank you very much!

IMPROVEMENT OF SHORT-TERM NUMERICAL WIND PREDICTIONS

Joël BÉDARD

RÉSUMÉ

Avec la croissance soutenue de l'énergie éolienne sur les marchés énergétiques, les opérateurs des réseaux électriques ont de plus en plus de défis à relever en matière d'équilibrage de réseau, le tout afin de minimiser les coûts associés à la gestion des autres sources énergétiques. Le vent étant une source énergétique variable, la prévision de la puissance éolienne est donc l'une des solutions qui permettra à ce type d'énergie de devenir viable du point de vue économique, tant sur les marchés régulés que dans les marchés ouverts. Dorénavant, il semble qu'il y ait un besoin urgent pour des modèles permettant de prédire de manière fiable la puissance éolienne à court-terme (0 – 48 h); ceci, afin de maintenir l'intégration de l'énergie éolienne dans le portefeuille énergétique des différentes juridictions.

En fonction des besoins de l'industrie éolienne, « Environnement Canada » effectue, depuis trois ans, des prévisions météorologiques expérimentales dans l'est canadien à l'aide d'un modèle de prévisions numériques à aire limitée (GEM-LAM 2.5 km). La région couverte englobe la péninsule gaspésienne ainsi qu'une partie des provinces maritimes. Cette région couvre plusieurs sites éoliens tels que North Cape. Ce site est situé à l'Ile du Prince Édouard où le Wind Energy Institute of Canada opère un centre d'essais éolien. Une analyse préliminaire des prévisions et une inspection minutieuse de ce site ont permis de démontrer que, bien que la résolution du modèle soit déjà relativement haute, elle manque tout de même de raffinement afin de bien représenter les phénomènes météorologiques pour ce site côtier à topographie complexe. Pour cette raison, un module géophysique de traitement statistique des sorties (Geophysic Model Output Statistic (GMOS)) a été développé et appliqué afin de permettre une optimisation de l'utilisation du modèle de prévision météorologique à des fins de prévision de la puissance éolienne à court-terme. GMOS diffère des MOS couramment utilisés dans les centres météorologiques par les aspects suivants : 1) il prend en compte les paramètres géophysiques régionaux (hauteur topographique, rugosité de surface, etc.) ainsi

que la direction du vent; 2) il peut être directement appliqué pour corriger les sorties de différents modèles numériques sans entraînement, bien qu'un entraînement soit bénéfique.

Ce module statistique a été entrainé et testé pour le site de North Cape, où il a réduit l'erreur quadratique des prévisions de 25 à 30 %. Cette amélioration significative est observable pour tous les horizons temporels ainsi que pour la majorité des conditions météorologiques. De plus, la signature topographique de l'erreur de prévision a été éliminée suite à l'application du GMOS. D'ailleurs, le modèle de prévision numérique combiné au GMOS offre une prévision supérieure à celle de la persistance dès un horizon de 2 h. Ce gain n'était observable qu'à partir d'un horizon de 4 h sans l'utilisation du GMOS. Enfin, une validation effectuée pour un site établi à Bouctouche (Nouveau Brunswick), présentant des améliorations similaires des prévisions de vent de surface, a permis de démontrer l'applicabilité générale de la méthode.

Cette étude, présentant un module statistique permettant l'optimisation de l'utilisation des prévisions météorologiques à haute résolution, a aussi contribué au développement d'une méthodologie afin de mieux comprendre les erreurs de prévisions reliées aux différentes conditions météorologiques. Cet outil d'analyse a permis d'évaluer la contribution d'erreur de phase et d'amplitude pour des conditions atmosphériques normales ainsi que pour divers évènements météorologiques à caractère dynamique tels que les variations subites de vitesse du vent, le passage de dépressions etc. Une compréhension accrue des erreurs de prévisions ainsi que l'acquisition de prévisions éoliennes plus précises permettront d'augmenter la valeur économique de l'énergie éolienne sur le marché.

Mots- Clés : énergie éolienne, prévision de puissance, prévisions numériques, couche limite atmosphérique, vent de surface, sites complexes, statistiques de sortie, analyse d'erreur

IMPROVEMENT OF SHORT-TERM NUMERICAL WIND PREDICTIONS

Joël BÉDARD

ABSTRACT

With the sustained growth of wind energy installed capacity for electricity generation, electricity system operators have increasing challenges balancing the electricity grid, notably in regards to minimizing the cost of other energy sources dispatch. Due to the variability of wind, wind power generation forecasting is an important issue for the economic viability of wind energy, whether in regulated or open markets. Therefore, there is a pressing need for robust short-term (up to 48 hours) surface wind forecast models, and eventually wind power forecast models, in order to sustain the integration of wind energy in electricity portfolios of jurisdictions.

Computed for the needs of the wind energy industry, three years of experimental meteorological forecasts in Eastern Canada are available from Environment Canada Numerical Weather Prediction (NWP) model configured on a limited-area (GEM-LAM 2.5 km) for wind power predictions. These data include forecasts for the region of North Cape (Prince Edward Island) where the Wind Energy Institute of Canada runs a test site for wind turbines. Although the model spatial resolution is already relatively high (2.5 km), preliminary statistical analysis and site inspection revealed that the model does not have sufficient grid spacing refinement to properly represent the meteorological phenomena on this complex coastal site. For this reason, a Geophysic Model Output Statistic (GMOS) module has been developed and applied to optimize the use of the short-term NWP. GMOS differs from other MOS that are widely used by meteorological centers in the following aspects: 1) it takes into accounts the surrounding geophysical parameters such as surface roughness, terrain height, etc. along with the wind direction; 2) GMOS can be directly applied for model output correction without any training although a training of the GMOS will further improve the results.

This statistical module was trained and tested over the North Cape site and it basically improves the predictions RMSE by 25 – 30 % for all time horizons and almost all meteorological conditions. Also, the topographic signature of the forecast error due to insufficient grid refinement is eliminated and the NWP combined with the GMOS now outperforms the persistence model after a 2 h horizon, instead of 4 h without the GMOS. Ultimately, in order to generalize the results, this methodology has been validated by an independent test case performed on a site located in Bouctouche (New Brunswick). Similar improvements on the GEM-LAM 2.5km forecasts were observed thus, showing the general applicability of the GMOS.

Although the current study presents an optimization of the use of short-term NWP for wind power forecasts using a statistical module, it also contributes to the development of a methodology and an analysis tool to assess and understand the NWP uncertainties on the amplitude and the phase of the surface wind forecast errors for different meteorological situations. A better knowledge of the wind speed and wind power forecast uncertainties, along with more accurate short-term wind forecast models, will increase the economic value of wind energy on the market.

Keywords: wind energy, wind power forecast, numerical weather prediction, atmospheric boundary layer, surface wind, complex sites, model output statistics, uncertainty analysis

TABLE OF CONTENT

Page

LIST OF TABLES

Page

LIST OF FIGURES

Page

ABBREVIATIONS AND ACRONYMS

AGL	Above ground level
ANN	Artificial neural networks
AST	Atlantic standard time
AVG	Average
AWS	Associated Weather Services
CFD	Computational fluid dynamics
DISP	Dispersion
E	East
MP	Multi-point
D-MP	Directional multi-point
ENE	East North East
ESE	East South East
GEM	Global environment multiscale model
GMOS	Geophysic model output statistic
GMT	Greenwich mean time
IEC	International Electrotechnical Commission
IREQ	Hydro-Quebec's Research Institute
LAM	Limited area model
LMS	Least mean square
MAE	Mean absolute error
MAX	Maximum
MIN	Minimum
MLP	Multilayer perceptron
MOS	Model output statistics
N	North

NB	New Brunswick
NE	North East
NN	Nearest neighbour
NNE	North North East
NNW	North North West
NSERC	Natural Sciences and Engineering Research Council of Canada
NW	North West
NWP	Numerical weather prediction
PEI	Prince Edward Island
RMSE	Root mean squared error
S	South
SDBias	Difference between standard deviations
SE	South East
SSE	South South East
SSW	South South West
STD	Standard deviation
SW	South West
USA	United States of America
W	West
WEICan	Wind Energy Institute of Canada
WESNet	Wind Energy Strategic Network
WNW	West North West
WSW	West South West

INTRODUCTION

Due to the global warming and to the many consequences of energy generation, industries and governments are promoting and developing power generation from renewable sources such as wind power. This type of energy has reduced impacts on the environment compared to more conventional power plants like nuclear, oil, natural gas and coal. As a matter of fact, in some European countries, up to 21 % of the energy generation comes from wind power (e.g. Portugal 9 %, Spain 12 % and Denmark 21 % (Global Wind Energy Council, 2008)) and this type of clean energy is also increasingly being adapted and used in North America.

One of the major concerns of integrating wind energy into electricity grids is the variability of the wind, and therefore, the power. With the sustained growth of wind energy installed capacity for electricity generation, electrical system operators need large amounts of spinning reserves from other energy sources to compensate for the fluctuations from the wind power, thus greatly affecting the cost of energy production. They also have increasing challenges optimizing the energy sources dispatch and minimizing the electrical network balancing costs. Therefore, wind power generation forecasting is an important issue for the economic efficiency of wind energy. More robust short-term (up to 48 hours) wind power forecasts will contribute to optimize the scheduling of conventional power plants and optimize the value of wind energy within the market in order to sustain the integration of wind energy in electricity portfolios of jurisdictions.

Three years of experimental meteorological forecasts in eastern Canada are available from Environment Canada Global Environment Multiscale Numerical Weather Prediction (NWP) model configured on a limited-area uniform 2.5 km horizontal grid spacing (GEM-LAM 2.5 km) for wind power predictions. These data also include forecasts for the region of North Cape on Prince Edward Island (PEI, Canada) where the Wind Energy Institute of Canada (WEICan) runs a test site for wind turbines and the PEI Energy Corporation operates a 10 MW wind farm. WEICan records wind speed at six different heights as well as wind direction, temperature and barometric pressure at single heights from a 60m mast, while the

PEI Energy Corporation records the total power production, the wind speed and the wind direction of each turbine at the same site. The forecasts, the power production and the atmospheric measurements use the same data format and the same time intervals (hourly averages), which facilitates model evaluation. With these two partners, it is thus possible to correlate model uncertainties to site characteristics or meteorological events and finally, to improve the forecast method itself.

The first chapter of this thesis gives a brief introduction of the state of the art on short-term wind forecasting and uncertainties, while an analysis of the database quality is performed in Chapter 2. Since data from different sources are available, a simple methodology is used to identify outliers. Data from both forecast and measured series associated to outlying data are removed in order to prevent errors due to outliers. Also, since vertical heat fluxes and temperature stratification have an impact on the vertical wind profile (see Chapter 1), low level thermal stability values derived from forecast outputs are integrated in the vertical interpolation of the wind speed to the anemometer height in order to improve the accuracy of this interpolation (Chapter 3).

In order to improve the Numerical Weather Predictions (NWP), a preliminary analysis over the North Cape site is conducted to define the parameters that shall be used to implement a Geophysic Model Output Statistics (GMOS) module (Chapter 4). The main objective of this research work is to improve short-term wind forecasting model by developing and applying different types of statistical modules (linear regressions, Artificial Neural Networks (ANN), etc.) to predict more precisely the wind speed as a function of the site characteristics and meteorological parameters (Chapter 5). Statistical techniques have been preferred over physical micro-scale models as they are computationally inexpensive (see Chapter 1). Calibration of the GMOS is done using one year of data and then, the evaluation phase takes place over the remaining period. Note that, in order to generalize the results, a validation of the complete methodology is also performed using a similar meteorological tower owned by Université de Moncton which is located in Bouctouche (New Brunswick (NB), Canada).

Throughout this work, in order to express the forecast error characteristics, many statistical criteria and error indicators are computed while figures and graphs are produced to illustrate the different results. Mainly, the mean absolute error (MAE) evaluates the error directly in terms of wind speed prediction; the root mean squared error (RMSE) evaluates the error in terms of wind speed prediction and verifies the error distribution; the bias evaluates the systematic error. Note that the standard deviation (STD), being a component of the RMSE, can also be used to verify the error distribution, but as the RMSE will be decomposed in Chapter 6 to represent different characteristics of the forecast errors, this criteria is preferred over the STD. In all cases, these criteria are normalized with the site annual mean wind speed to maintain the results independent from the site itself. Furthermore, to compare different models, an improvement indicator is also used. The final section of this thesis (Chapter 6) presents the analysis of the short-term wind forecasts uncertainties. This expanded work is done using amplitude and phase error description as well as exploratory analyses to detail the uncertainty characteristics and different error tendencies or evolution in time. This analysis is used as a dynamic approach to evaluate the contribution of meteorological events to forecast errors; meteorological situations related to high uncertainty of short-term wind predictions can then be identified.

The objective of the current study is to optimize the use of short-term NWP for complex sites by applying statistical methods. The conclusions of this assessment contribute to the development of the forecast model with Environment Canada by applying the GMOS developed and notably by identifying meteorological events with high uncertainties by means of the evaluation protocol being developed. Ultimately, a better knowledge of these uncertainties and better wind forecasts will increase the economic value of wind energy in the market.

CHAPTER 1

LITERATURE REVIEW

1.1 Numerical wind power prediction models

Landberg et al. (2003) and Giebel et al. (2003) provide complete reviews of wind power prediction models. They show that most short-term wind power forecast models use the available regional NWP as input parameters, usually geostrophic wind speed and direction. Generally, those NWP models have a coarse spatial resolution ranging from 5 to 25 km. Therefore, the first step in wind power predictions is to estimate the wind resources at the exact wind farm location (wind speed and direction). This downscaling operation is generally done using a physical Limited Area Model (LAM) with higher resolution (meso-scale or micro-scale) and employing the global NWP as initial lateral boundary conditions. Also, high resolution topography and surface roughness measurements are used to characterize the site.

Then the wind speed at the site is generally scaled down to the turbine rotor height by applying a logarithmic vertical profile for neutral atmospheric stability. Landberg (1998) shows that it is also possible to correlate the geostrophic wind with the surface wind by using a simple relation, assuming the geostrophic drag law as a linear function. Considering different surface roughness, along with the geostrophic wind speed and direction, he points out that it is possible to predict surface wind speed directly from the geostrophic wind under neutral atmosphere. He also demonstrates that the variation in the wind direction with height (Ekman spiral) is one of the most difficult parameter to predict and cannot be simplified into a simple relation. Nonetheless, wind speed can be predicted using simple methods with a relatively good accuracy (in comparison with micro-scale models). Finally, correlations are generally developed using the turbine power curves to convert the surface wind to electrical power. The wind power forecast models can also take into account the wind farm layout to integrate the wake effect of a turbine on the aerodynamics of the whole wind farm into the final wind power forecast.

1.2 Model output statistics

Most wind power prediction models use Model Output Statistics (MOS) to correct biases and the general amplitude errors (auto-regressive statistical models, ANN, etc.). When used off-line, MOS are calibrated using historical wind farm data in order to search for the optimal statistical parameters. If the power production data are available online, MOS can be calibrated in real time. Therefore, online data offer many advantages. Tuning off-line MOS needs considerable efforts compared to self calibrating MOS; online MOS adapts themselves to annual and seasonal variations, farm layout and data quality. Also, Kariniotakis et al (2004) show that Kalman filtering techniques clearly improve NWP systematic errors for linear (e.g. temperature) and non-linear parameters (e.g. wind speed). Since statistical techniques are computationally inexpensive, they conclude that it is worthwhile using them. With a proper MOS, systematic errors remain low. Thus, there remain two types of random errors still occurring in wind power forecast: amplitude and phase errors. The amplitude error misjudges the intensity of a meteorological event and the phase error misplaces the event in time. Therefore, since the wind power forecast is affected by both the intensity and occurrence of the wind, work is needed to assess the uncertainties of models on the amplitude and the phase errors of wind speed forecasts.

1.3 Reference models

When comparing different NWP models to obtain their performance evaluation, it is interesting to first define a reference model using only simple physical considerations (Madsen et al., 2004). Ten years ago, persistence models, where the future wind is assumed to be the same as the last measured wind speed, along with climatology predictions, using the annual mean wind speed, were used as reference models. These basic models were used for their simplicity and because persistence is excellent for short-term forecasts up to 3 - 6 hours (Landberg and Watson, 1994; Liu, 2009). This is explained by the fact that the atmospheric motion is driven by pressures systems which changes much more slowly than wind turbulence, since the time scale of pressures systems is in the order of days.

More recently, Nielsen et al. (1998, p. 29) defined a new reference model because they found that "it is not reasonable to use the persistence model when the forecast length is more than a few hours." Thus, they merged both the persistence and the climatology prediction models. To get the new reference model, they linearly combine the old reference models for each forecast horizon. This new model performs better than both individual models for all time horizons. Since then, this new reference model is used to compare the different NWP models being analyzed for different time horizons. Note that the new reference model has to be calibrated with measured time series to determine the statistical parameters using the autocorrelation of the wind speed from measured time series (Madsen et al., 2004). Therefore, it is important to split the database and clearly define the calibration data (as for any learning model) and the test data for the error analysis. Then the performance evaluation of the model has to be done with the test data.

1.4 Performance evaluation of models

Before carrying out the performance evaluation with different criteria, it is important to verify the quality of the data. One can perform a visual check of the data to ensure that there are no outliers within the data (e.g., zero wind speed due to icing of an anemometer) or, if data are available from different measurements, they can be compared directly to identify the outliers. Kariniotakis et al. (2004) also points out that it is necessary to use common data (NWP, power production and atmospheric measurements) and common data format for proper model comparison. Then, in the standardized protocol for performance evaluation of prediction models (Madsen et al., 2004), a guideline is presented to properly use statistical criteria to determine the power prediction uncertainties. It is recommended using many statistical criteria, to express different error characteristics.

In order to evaluate the errors directly in terms of amplitude, it is recommended to use the MAE, while the STD is used to evaluate the error distribution to get the confidence interval based on the Gaussian distribution. Note that larger absolute errors have larger effects on the RMSE than on the MAE. Therefore, when used along with the MAE, the RMSE can be used

to obtain details on the error distribution. The bias can still be computed to verify the systematic error, since there is no perfect MOS. In all cases, it is important to normalize these criteria with the installed power capacity of the wind farm or the mean wind speed. This operation makes the results independent from the wind farm or the site itself. When the objective is to compare prediction models, it is recommended to use the improvement criterion, also referred to as "skill" score. This criterion is defined as the difference between the error of the reference model ($\in_{\mathrm{ref}}$) and the analyzed model error ($\in_{\mathrm{model}}$), normalized with the reference model error ($\in_{\mathrm{ref}}$).

$$I_{model} = \left(\in_{ref} - \in_{model}\right) \Big/ \in_{ref} \Rightarrow I_{model} \in]-\infty, 1] \tag{1.1}$$

The improvement can be computed for each of the criteria presented above. An improvement score of zero means that the model performs as well as the reference model. Conversely, a perfect model would get a score of one; while a negative score means that the reference model performs better than the analyzed model.

Madsen et al. (2004) also recommend the use of exploratory analyses to detail the uncertainty analysis. A histogram plot or a cumulative squared error graph can help to illustrate different error tendencies or evolution in time. These analyses can point out a time period that needs further investigations (due to changes in the NWP). Kariniotakis et al. (2004) use the forecast with errors lower than 10% to visually compare the analyzed models in a graph. They also use the minimum and maximum values of the errors as exploratory analyses to characterize the model uncertainties. The general results of the performance evaluations need to be expressed for a precise time horizon (generally 6 or 12 h), for some time periods (seasonal) or for meteorological events.

1.5 Benefit of ensemble forecasts

It is well known that the accuracy of the NWP models is a major concern in wind power predictions. Doubling the spatial and temporal resolution of the NWP models would increase the computational time by a factor of at least eight. But the exact same computational time could be used to run an ensemble of eight members (combining different NWP models) in order to obtain a better forecast. A solution to this problem is to use NWP ensembles to significantly reduce the RMSE. It is shown that a combination of an ensemble of predictions outperforms the individual NWP members (Lange et al., 2006) and ensemble forecasts can also give the confidence level of the predictions. Such combination is done by statistically weighting the NWP for different weather classes. Ensemble forecast can be achieved either by using different NWP models, by using different parameterization of the same model or by varying the input data (Nielsen et al. 2004 and Nielsen et al. 2007a).

Nielsen et al. (2007a) point out that the operational robustness (reliability or accuracy) of a model is highly increased by using data from different sources. Nielsen et al. (2004) also achieve ensemble forecasts using different parameterization of the same model or by using perturbed initial conditions. Statistical methods combining the NWP and the new reference model is another way to get sophisticated bias correction (e.g. Wind Power Prediction Tool model). Based on a combination of the different forecast properties (variance, kurtosis, skewness, etc.) and the weather conditions, with low linear correlation between the different members, ensemble forecast almost guarantee improvements of the model (Nielsen et al., 2007b). In this work, it is also recommended to realize ensemble forecast using only few good uncorrelated forecasts, rather than a multitude of correlated forecasts. The statistical weighting and bias correction of the ensemble forecast can be computed using error, variance or meteorological characteristics criteria. Like MOS, ensemble forecast models tend to give better results (lower MAE and higher correlation) with regular recalibration or online auto-calibration (Nielsen et al., 2007b).

1.6 Challenges to overcome

In most wind farm applications, the end users (wind farm managers, transmission system operators, energy service suppliers and traders) are not the ones who run the NWP models; rather, they only use the predictions. The end users experience directly the consequences of the forecast errors, such as the variation in the price of energy on the market, supply contracts, operating costs and security concerns. Therefore, it is important to provide an appropriate estimate of the forecast error.

Many studies show that it is difficult to forecast sudden and pronounced changes in the weather produced by meteorological events such as the passage of a meso-scale front. For instances, Lange and Heinemann (2003) show that forecast errors are highly related to the local meteorological events. Days with typical meteorological conditions can be classified using synoptic meteorology (historical data including pressure as well as wind speed and direction). They use one average error value per day to compare the different groups and they find a profound difference within different weather situations. Dynamic events, like low pressure systems, produce much higher forecast uncertainties than quasi static ones, such as high pressure systems. Cutler et al. (2007) have similar conclusions about wind power ramps (high phase and amplitude errors).

Kariniotakis et al. (2004) point out an important diurnal variations of the MAE for some European NWP models, indicating that there is still a lot of work to do to integrate surface heat fluxes (Landberg and Watson, 1994) and temperature stratification (Lange and Heinemann, 2003) in these models. These phenomena related to atmospheric stability are still quite difficult to predict. Similarly, Kariniotakis et al. (2004) observe that model uncertainties are directly related to the terrain complexity. In another study, Nielsen et al. (2007a) show that using planetary boundary layer stability measures derived from meteorological forecasts improves the forecast for complex sites. These results suggest including some physical parameters (atmospheric stability or terrain characteristics) in MOS to get more accurate predictions, especially for sudden meteorological events.

Subsequently, according to the needs of electrical systems operators, the objective of the present study is to develop a GMOS which integrates terrain and wind characteristics to improve the wind forecast of a NWP model, particularly in complex terrain. Also, it is intended to integrate stability as derived from meteorological forecast in the vertical interpolation of the wind speed forecast. The purpose of these assessments is to contribute to the development of the forecast model used at Environment Canada by applying such techniques and notably by identifying meteorological events with high uncertainties by means of an evaluation protocol. Finally, phase, amplitude and systematic errors decomposition intend to help defining NWP research priorities in improving wind energy forecasting.

CHAPTER 2

MEASUREMENT DATA

At the North Cape site, the WEICan records wind speed at six different heights as well as wind direction, temperature and barometric pressure using a mast located at 47.054082 N, 63.99865 W (see Figure 2.1). Except for the atmospheric pressure, the exact same data is gathered at the Bouctouche tower located at 46.472217 N, 64.73915 W (see Figure 2.2). These 60 m towers have respectively a 0.3 m (triangular lattice tower) and 0.152 m (tubular tower) width. Figures 2.1 - 2.2 present the location of both sites: the cross represents the anemometer tower while the grid represents a subset of the Environment Canada GEM-LAM horizontal grid for wind predictions. Tables 2.1 - 2.2 present the different sensor types and their configuration on both towers.

Figure 2.1 North Cape site location (PEI, Canada).

Figure 2.2 Bouctouche site location (NB, Canada).

Table 2.1 Sensor descriptions and positioning on the North Cape anemometer tower

#	**Sensor model**	**Height (m)**	**Boom length (m)**	**Orientation (°)**
N1	NRG Type 40 Maximum Anemometer	9.83	0.89	295
N2	NRG Type 40 Maximum Anemometer	16.95	0.97	295
N3	NRG Type 40 Maximum Anemometer	26.96	1.02	295
N4	NRG Type 40 Maximum Anemometer	39.79	1.06	295
N5	Barometric Pressure Sensor 61205V	41.50	-	-
N6	NRG 200 Series Wind Vane	48.82	0.83	55
N7	Campbell Scientific Temperature Probe-107/108	49.22	-	-
N8	NRG Type 40 Maximum Anemometer	49.70	1.32	295
N9	NRG Type 40 Maximum Anemometer	58.37	1.44	295

Note that the atmospheric measurements (10 minute averages and STD from 1Hz data), along with the forecasts, use the same data format and the same time intervals which allows proper model evaluation. It is important to note that the first year of the measurement data is

used to train the different statistical modules that are implemented for both sites (Chapter 5). Then, for the evaluation phase (Chapter 6), it is suggested to use at least eight month of data (one complete year is recommended) in order to produce results that are representative of the model behaviour in an actual wind power plant, which operates all year around. This recommendation is based on the fact that model evaluation over shorter period than eight months shows non representative results: insufficient evaluation data put emphasis on a certain season, which is not desirable when assessing the evaluation of the general performance of a model. Yet, two complete years of data (May 2007 to April 2009) are available for the North Cape site, but only 22 month of data (July 2008 to April 2010) are available for the Bouctouche site. Therefore, the first year of both time series is used for the training phase and the remaining period is set as the validation database.

Table 2.2 Sensor descriptions and positioning on the Bouctouche anemometer tower

#	**Sensor model**	**Height (m)**	**Boom length (m)**	**Orientation (°)**
B1	NRG Type 40 Maximum Anemometer	10.0	1.5	315
B2	Campbell Scientific Temperature Probe 107/108	3.0	-	-
B3	NRG Type 40 Maximum Anemometer	30.0	1.5	315
B4	NRG Type 40 Maximum Anemometer	40.0	1.5	315
B5	NRG Type 40 Maximum Anemometer	50.0	1.5	315
B6	NRG 200 Series Wind Vane	58.0	1.5	345
B7	NRG Type 40 Maximum Anemometer	60.0	1.5	315
B8	NRG Type 40 Maximum Anemometer	60.2	1.5	135

With the training and validation databases set for both sites, it is now possible to perform the data quality analysis. Since measurements from different sensors are available, a simple methodology is used in section 2.1 to identify outliers. Then, in section 2.2, an analysis is performed to select the appropriate anemometers that have to be used to test and validate the NWP model. In Tables 2.1 - 2.2, it is possible to note that every sensor is mounted no closer

than 1.5 times the tower width to avoid high flow distortion due to the mast (Kaimal, 1994) which is analyzed in detail in section 2.3. Thus, a complete analysis of the measurements uncertainty is conducted to verify that the database is suited for the NWP model evaluation. Finally, section 2.4 presents the wind characteristics on the sites.

2.1 Data quality analysis

Before processing the data and assessing any model validation, it is essential to analyse the quality of the data sets. Following the data validation methodology proposed by the Associate Weather Services (AWS) Scientific (1997), a computer based routine is coded to automatically identify suspect values. Then a case-by-case verification is done to ensure that only erroneous values are removed from the database, permitting a high data recovery rate. The validation procedure, illustrated in Figure 2.3, is grouped in three different categories: data sequence checks, measured parameter checks and data treatment. The data sequence check is done to ensure that the records are complete. Verifying the number of records for each parameter compared to the time series allows to find missing sequential values. In fact, for the North Cape site, some icing events and some electrical failure are already indicated in the files by WEICan and hourly data are removed. This first check indicates the total number of record available for the analysis among the raw data.

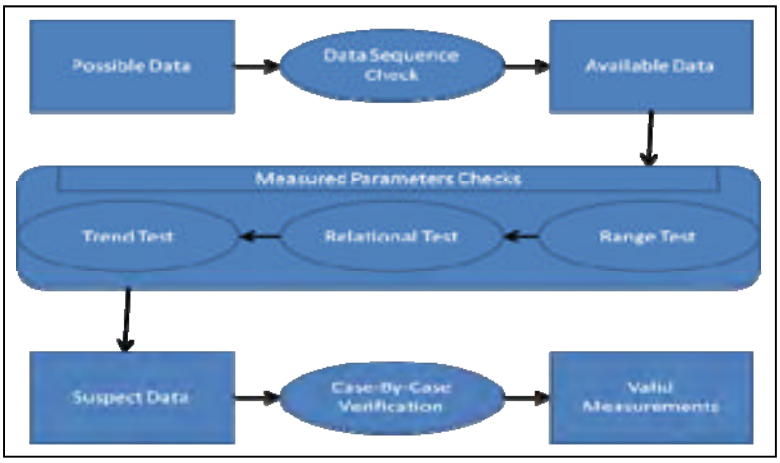

Figure 2.3 Quality control flow diagram.

Subsequently, it is possible to verify the records of each measured parameters. Since a single criterion is unlikely to detect every problematic situation, three different types of test are used to identify outliers. A range test is used to ensure that all collected data are logged into physical value ranges: there should not be any negative values (except for the temperature); usual sensor calibration gives an offset value of 0 or 0.035 m/s for zero wind speed; measured values should not exceed a reasonable range of values, such as 30 m/s average speed and 40 m/s maximum gust speed for example.

On the other hand, since data are available from different sensors, a relational test is also performed to compare the output of the anemometers located on the same tower. This relational test allows verifying that the sensors represent an appropriate vertical profile of the wind. Note that the North Cape site is surrounded on the East, North and West sides by a coastal cliff which has an average height of 13 m (see Chapter 3). Gasset et al. (2005) have shown that such a cliff affect the wind speed near the ground up to a distance of ten times the cliff's height. Even though the tower is further than 130 m away from the cliffs, sensors #1N and #2N have not been used in this study because the turbulent kinetic energy of the flow still appears to be influenced by the cliff in this area up to twice the cliff's height above ground level (AGL) (Gasset et al., 2005). Similarly, the Bouctouche site is surrounded by a forest canopy; therefore, for the same reasons, the 10 m anemometer on Bouctouche mast (#1B) is not used.

The last check, the trend check, verifies if the temporal variation of a measured parameter exceeds the usual physical behaviour due to the inertia of the atmospheric system. The validation criteria proposed by AWS Scientific (1997) for sites located in the United States of America (USA) are not used in this study due to differences in climate regime between USA and Canada. Instead, "normal fluctuation" ranges are determined according to the eastern Canadian climate, which is consistent with the measurements. The validation criteria that are used for the Canadian sites are listed in Tables 2.3 - 2.5. Note that a violation of one of these criteria flags the data as suspect. Afterward, all identified events are verified case-by-case to ensure that only erroneous values are removed from the database.

Table 2.3 Sensor range test criteria for the eastern Canadian climate

Parameter type	**Sample parameter (10 min)**	**Validation criteria**
Wind speed	Average	0.035 < AVG < 30 m/s
	Standard deviation	0 < STD < 4 m/s STD = 0 only if AVG = 0.035 m/s
	Maximum & minimum gust	0.035 < MIN or MAX < 40 m/s
Barometric pressure	Average	96 < AVG < 104 kPa
Wind direction	Average	0 ≤ AVG < 360 °
	Standard deviation	0 < STD < 90 ° STD = 0 only if AVG < 5 m/s
Temperature	Average	-25 < AVG < 35 °C

Table 2.4 Sensor relational test criteria for the eastern Canadian climate

Parameter type	**Sample parameter (10 min)**	**Validation criteria**
Average wind speed	30 m / 40 m difference	≤ 2 m/s
	30 m / 50 m difference	≤ 2.5 m/s
	30 m / 60 m difference	≤ 3 m/s
	40 m / 50 m difference	≤ 2 m/s
	40 m / 60 m difference	≤ 2.5 m/s
	50 m / 60 m difference	≤ 2 m/s
Maximum wind gust speed	30 m / 40 m difference	≤ 5 m/s
	30 m / 50 m difference	≤ 5 m/s
	30 m / 60 m difference	≤ 5 m/s
	40 m / 50 m difference	≤ 5 m/s
	40 m / 60 m difference	≤ 5 m/s
	50 m / 60 m difference	≤ 5 m/s

Table 2.5 Sensor trend test criteria for the eastern Canadian climate

Parameter type	**Sample parameter (10 min)**	**Validation criteria**
Average wind speed	Mean variation	≤ 10 m/s within 1 h
Average temperature	Mean variation	≤ 7 °C within 1 h
	Sign change	≤ 2 within 3 h Only if daily AVG < 3°C
Average barometric pressure	Mean variation	≤ 1.5 kPa within 3 h

Once the validation methodology is applied, the case by case verification show that the measured parameter checks point to suspicious data (Figures 2.4 – 2.7). Figure 2.4 shows an event (North Cape, February 27th, 2008) where wind data is removed from the database due to the icing of the anemometers. Looking at the temperature profile which is slightly under the freezing point and looking at the wind vane that has a constant direction with no variation (STD equal to zero); it is very likely that there was effectively an icing event. All parameters show regular fluctuations within the day but the wind speed and direction are not valid from 10:00 AM; the wind speed has been removed from the database and the wind vane was iced in the North-East direction. Since the wind speed was over 10 m/s before the icing event, the icing of the anemometer causes an artificial decreasing trend in the wind speed which is detected by the validation methodology. Also, the method identifies high variations of the wind speed caused by malfunctioning sensors or created artificially by missing data. In almost all cases, the verification of the data associated with suspicious wind ramps (identified by the method) showed an abnormal behaviour of the sensors. Overall, only one normal wind increase is pointed out as suspect data: this event is therefore reincorporated in the database and all erroneous data (e.g. the event showed in Figure 2.4) are removed.

Furthermore, applying the same data validation methodology, another type of suspect data where some maximum wind speeds are recorded to a peaking value over 1 000 m/s is being pointed out repeatedly. Because of these abnormal wind gusts, the STD of the wind speed also reaches an extremely large value. The mean wind speed is also found to be abnormally

large. The mean wind speed and STD, as well as the average wind direction and STD, for one irregular event can be observed in Figure 2.5. Monitoring the graphs of Figure 2.5, one can see that the identified time series (North Cape, June 25th, 2007) contain three aberrant data which do not represent properly the physical behaviour of the wind speed between 13:00 and 18:00. It can also be observed that there is a high wind direction STD as the wind direction changes suddenly and repeatedly during this event. This might show a dynamic meteorological event occurring that day, but there is no low pressure system that could explain such large change in wind speed. The temperature is above zero which confirms that there is no icing event. The 60 m anemometer records extremely high wind gust which are abnormal. This implies that there is an electrical issue with the sensor: the electrical output does not always match the input wind speed. Again, these observations show that the methodology used to remove data from malfunctioning anemometers is proper and those outlying data are removed from the database.

This verification also shows that the computer based methodology is able to point out irregular behaviour of the atmospheric boundary layer wind profile. Figure 2.6 shows an event (North Cape, June 4th, 2007) where the measured wind speeds are not following a regular vertical profile: greater wind speed at higher measurement locations should be observed. It is important to note that, because of the turbulent nature of the wind, it is possible to observe short moments (up to few hours) where the wind does not follow this profile, but this phenomenon should not be observed for long time period. For a period longer than 6 h during that day (from 15:00 to 22:00), the averaged wind speeds are following a non physical profile (i.e. lower wind speeds measured by the 60 m anemometer) due to a malfunctioning anemometer. Consequently, all situations of irregular vertical profile of the wind speed found by the methodology are removed to assure data quality.

Finally, some other erroneous data are found to be suspect. Figure 2.7 shows an event (North Cape, June 6th, 2007) where the pressure and temperature sensors are malfunctioning between 14:00 and 15:00. Normally, temperature and pressure are parameters that have a

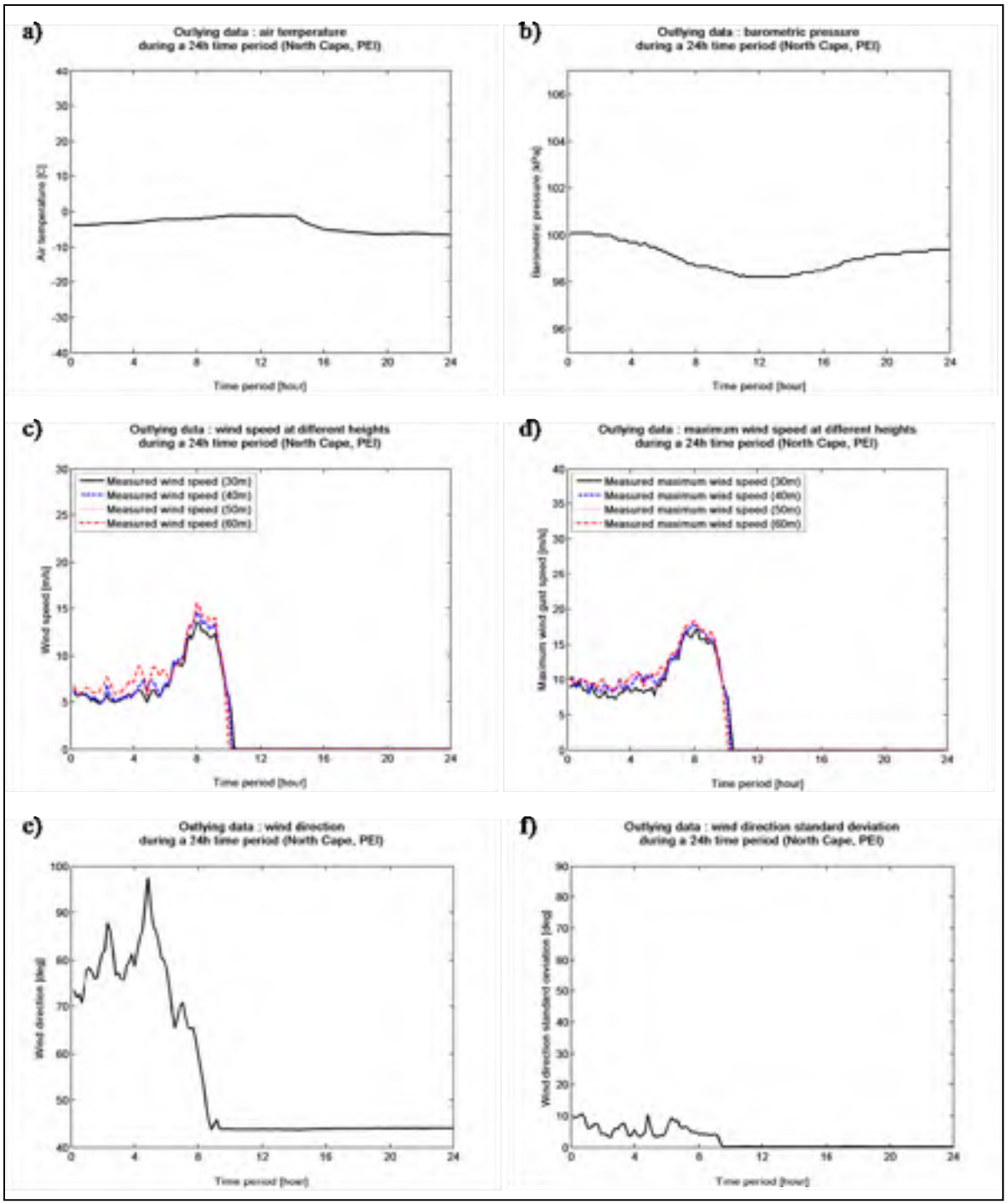

Figure 2.4 Time series of a suspect icing event: a) air temperature, b) barometric pressure, c) average wind speed, d) maximum wind speed, e) average wind direction and f) STD of the wind direction.

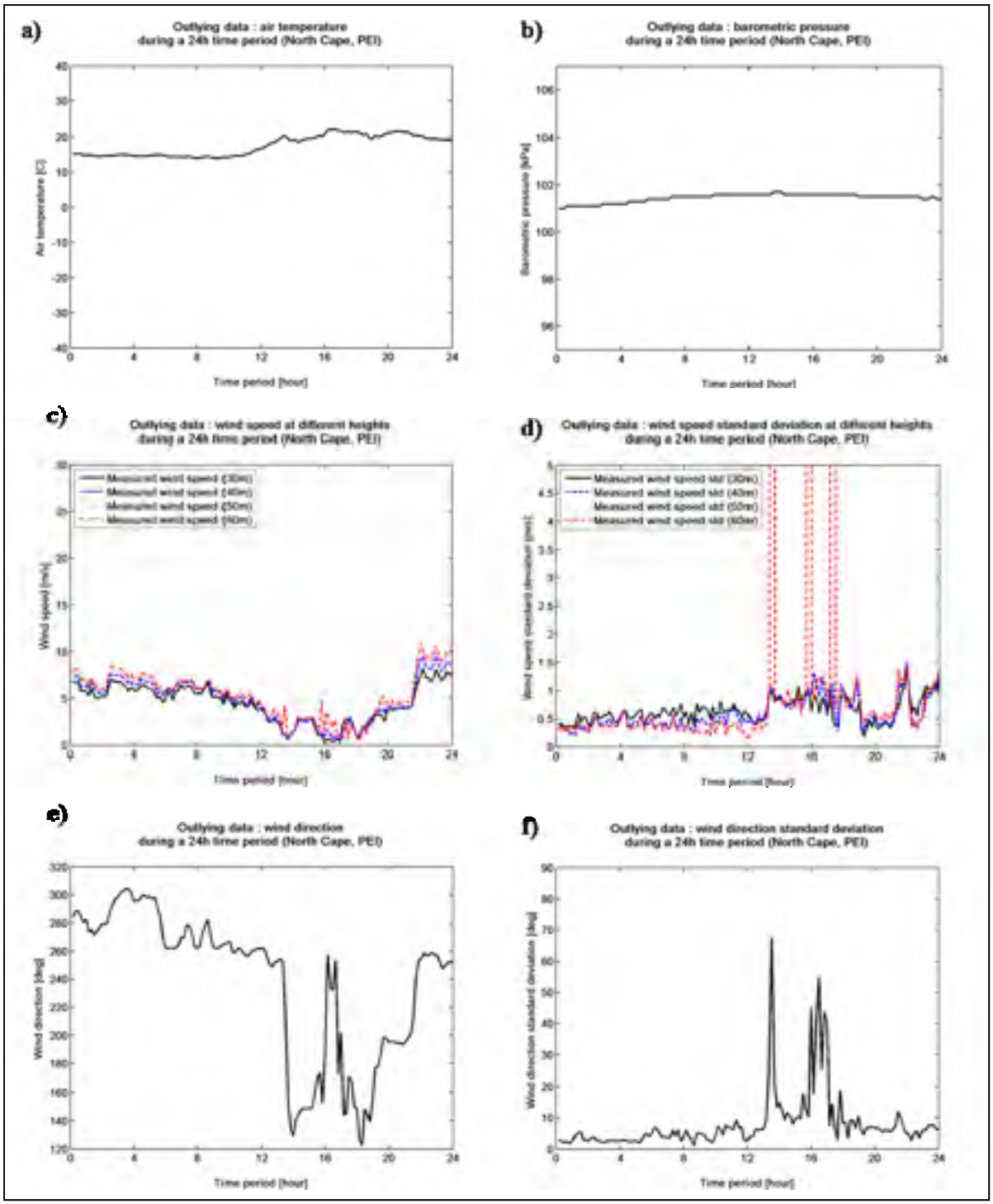

Figure 2.5 Time series of suspect wind gusts: a) air temperature, b) barometric pressure, c) average wind speed, d) maximum wind speed, e) average wind direction and f) STD of the wind direction.

high inertia and change slowly in time: these variables shall not fluctuate suddenly nor shall they venture out of certain physical limits. During this event, the pressure sensor suddenly drops down to 10 kPa as the temperature sensor measures -90°C while all other sensors seem to function properly. Such fluctuations are not physically possible and many events (~ 12/year) similar to this particular one are identified within the database. This method allows removing those erroneous data.

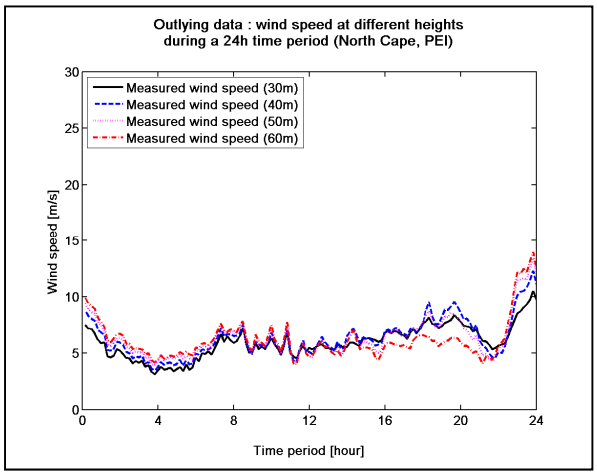

Figure 2.6 Time series of a suspect vertical wind profile: average wind speed.

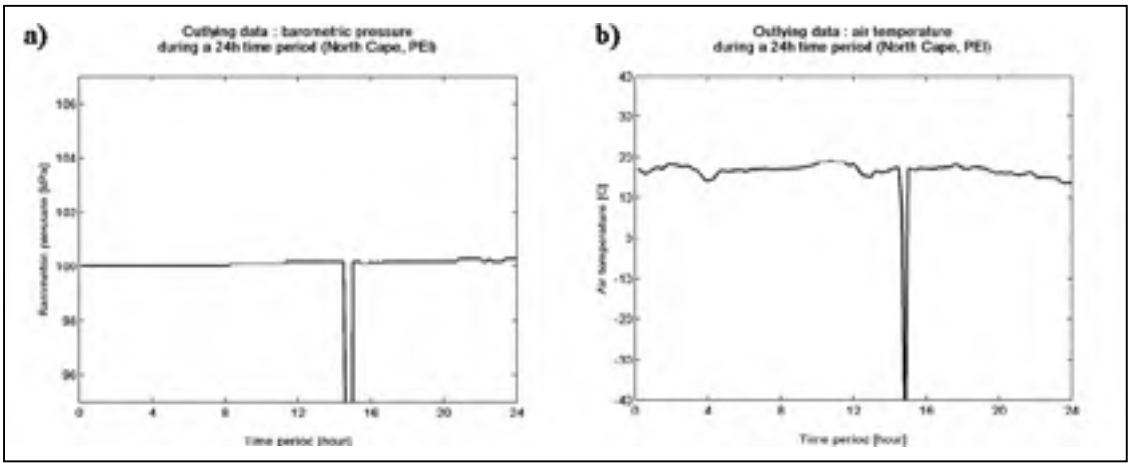

Figure 2.7 Time series of a suspect event: a) barometric pressure and b) temperature.

Ultimately, the main parameters (temperature, pressure, wind speed and direction) are plotted over the complete time series. This final visual check done on the entire time series of each parameter allows to quickly validate that all evident erroneous data are found by the methodology. The complete verification shows that the method has been able to identify many types of erroneous values. Only few normal events are recognized as suspect data, but with the case-by-case verification, they have been kept in the database. These verifications induce a high data recovery rate while minimizing the risk of keeping erroneous values. Two complete hours of data is removed for every event (one before and one after) to ensure that the sensors are fully functional due to the inertia of some events, like icing.

Moreover, as mentioned earlier, locating the anemometer on a boom at least 1.5 times longer than the tower width generally protects the instruments from the disturbed flow due to the tower, but it does not keep the sensors away from tower shadowing. In fact, the tower shades the sensor and reduces the downwind wind speed significantly (Hunter et al., 1999). This effect mainly covers a downwind angle of 30° on both sides of the tower for a total angle of 60° where the data should be excluded (Kaimal, 1994). For the same positioning, a wind vane suffers a maximum deflection of 5° due to tower shadowing (Kaimal, 1994), but since the wind directions are binned into 16 sectors of 22.5° each, such deflection does not affect much the binned value of the wind direction. Subsequently, records when the anemometers are located downwind to the tower are removed from the database (i.e. E, ESE and SE directions for the North Cape site and ESE, SE and SSE directions for the Bouctouche site).

Furthermore, as the NWP model is set for output at hourly time steps representing the instantaneous average wind speed, the last 10 min measurements of each hour is used to describe the average wind speed at the same time stamp (see section 2.3 for a description of temporal averages). Subsequently, for a single outlying datum within the measurement database, data from both the forecast and the measured series associated to the same time period are removed in order to compare identical databases. Note that before using any onsite measurements, it is essential to offset the forecast time series since the predictions are done using the Greenwich Mean Time (GMT) zone while the measurements are acquired on

the Atlantic Standard Time format (AST = GMT-4). Finally, according to the following equations, the data recovery rate is calculated using the total possible records, with the number of available records and available forecast records included in the database as well as the number of invalid records and the number of shadowed records that are removed:

$$Available\ Records\ Ratio = \frac{Available\ Records}{Possible\ Records} \times 100 \quad (2.1)$$

$$Valid\ Records\ Ratio = \frac{Valid\ Records}{Available\ Records} \times 100 \quad (2.2)$$

$$Valid\ Records = Data\ Available - Invalid\ Records \quad (2.3)$$

$$Shadow\ Free\ Records\ Ratio = \left(1 - \frac{Shadowed\ Records}{Valid\ Records}\right) \times 100 \quad (2.4)$$

$$Available\ Forecast\ Ratio = \frac{Available\ Forecast\ Records}{Valid\ Records - Downwind\ Records} \times 100 \quad (2.5)$$

$$Data\ Recovery\ Rate = \frac{Available\ Forecast\ Records}{Data\ Records\ Possible} \times 100 \quad (2.6)$$

Table 2.6 presents monthly and annual results for each of the parameters that are previously computed using two years of data from North Cape. The results for Bouctouche site are quite similar and they are shown in the annexes (see Annex I: Table A.I.1). These tables show that many measurement data are not available during the cold season (January to March), mainly due to icing of the instruments. Also, it is possible to observe that the data validation methodology removed many data from the database from December to March also due to the high occurrence icing events. In addition, this methodology removed a significant number of data during the months of May, June and July because the North Cape 60 m anemometer did experience electrical problems as mentioned earlier (i.e. high measured gust speeds). Data have also been removed downwind of the tower to avoid measurements

suffering from shadowing and the number of data removed depends on the wind frequency for the given wind direction of each month. As the instruments are purposely installed on the most frequent upwind direction, the number of downwind data removed is relatively low. On the other hand, the available forecast ratio does not rely on any environmental variables; it depends on the computational capability to run the model. Since it is an experimental forecast for the wind energy sector, Environment Canada operational forecast always prevails. Therefore, these forecasts have been executed on a dedicated cluster located at Hydro-Quebec's Research Institute (IREQ) and this is the reason why the available forecast ratio is 100% (not in real time). Finally, the total data recovery rate related to the present study is 78.84%. This amount of data is sufficient for the purpose of validating a forecast model.

Table 2.6 Data recovery rates for every month of the sample year (North Cape)

Month	**Available Records Ratio (%)**	**Valid Records Ratio (%)**	**Shadow Free Records Ratio (%)**	**Available Forecast Ratio (%)**	**Data Recovery Rate (%)**
January	95.36	88.23	95.37	100.0	80.24
February	95.61	80.20	89.61	100.0	68.71
March	89.52	84.98	92.23	100.0	70.16
April	97.50	87.39	88.92	100.0	75.76
May	99.80	87.47	86.14	100.0	75.20
June	99.86	91.31	78.83	100.0	71.88
July	99.80	91.72	92.07	100.0	84.28
August	100.0	95.90	83.18	100.0	79.77
September	100.0	94.44	92.13	100.0	87.01
October	98.92	94.02	93.35	100.0	86.82
November	100.0	94.51	86.99	100.0	82.21
December	100.0	92.20	91.11	100.0	84.00
Annual	**98.03**	**90.20**	**89.16**	**100.0**	**78.84**

2.2 Anemometer selection

As a measurement mast presents many anemometers, one of them is selected to be compared with the NWP model outputs for model validation. This is the reason why four different logarithmic vertical wind profiles are plotted and the surface roughness is computed for the entire time series of the mean wind speed. The wind profiles are shown in Figure 2.8 and Tables 2.7 - 2.8 details the computed surface roughness. Similar wind profiles are found for the Bouctouche site in the annexes (see Annex II: Figure A.II.1). All parameters are computed from a neutral logarithmic equation comparing the wind speed at two different heights to interpolate the average wind speed to another location using equations 2.7 - 2.10. Note that the surface roughness describes the height where the wind speed is zero. This length is generally used in meteorology to define the ground surface and the obstacles on site. It is possible to compute the surface roughness (z_0) and the surface friction velocity (u_*) using wind speeds at two different heights:

$$U(z) = \frac{u_*}{k}\, ln(z/z_0) \tag{2.7}$$

$$u_* = \frac{k(U_2 - U_1)}{ln(z_2/z_1)} \tag{2.8}$$

$$z_0 = z_1 \left(\frac{z_2}{z_1}\right)^{U_1/(U_1 - U_2)} \tag{2.9}$$

$$U(z) = \frac{U_2\ ln(z/z_1) - U_1\ ln(z/z_2)}{ln(z_2/z_1)} \tag{2.10}$$

Where: $U(z)$ is the interpolated wind speed [m/s] at height z [m];

- U_1 and U_2 are the measured wind speed [m/s] at heights z_1 and z_2, respectively [m];
- k is the Von Karman similarity constant (0.4 [-]);
- u_* is a friction velocity scale from kinematic surface stress based on wind shear [m/s].

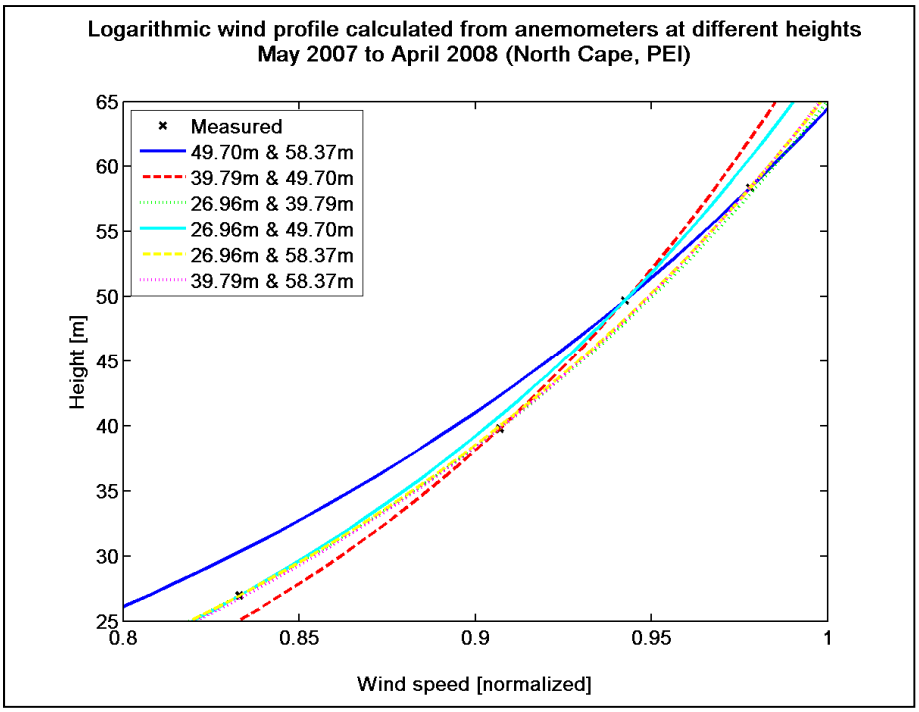

Figure 2.8 Logarithmic vertical wind speed profiles plotted from the mean wind speed at two different heights.

Table 2.7 Surface roughness computed from the mean wind speed at different heights (North Cape)

Anemometer height	Surface roughness on site (z_0)
49.70 m & 58.37 m	0.7033 m
39.79 m & 49.70 m	0.1362 m
26.96 m & 39.79 m	0.3335 m
26.96 m & 49.70 m	0.2552 m
26.96 m & 58.37 m	0.3180 m
39.79 m & 58.37 m	0.3002 m

Table 2.8 Surface roughness computed from the mean wind speed at different heights (Bouctouche)

Anemometer height	**Surface roughness on site (z_0)**
50 m & 60 m	1.9453 m
40 m & 50 m	4.2256 m
30 m & 40 m	3.4345 m
30 m & 50 m	3.7352 m
30 m & 60 m	3.3252 m
40 m & 60 m	3.2239 m

Subsequently, the comparison between the different logarithmic profiles derived from the annual average wind speed of each anemometer on the same tower (Figure 2.8) shows that the 50 m anemometer operates very close to all calculated profiles for the measurement period at both sites. Also, looking at Table 2.7, one can notice that the only set of anemometers giving a representative surface roughness for North Cape site is using the 30 m and the 50 m (i.e. surface roughness for a fallow field with many small wind turbines and few small buildings shall be slightly higher than 0.25 m (Manwell et al., 2002)). However, when assessing a wind power monitoring program, it is important to use the highest sensor as possible to be relatively close to current standard turbine hub heights. The quality control of the data shows that the 60 m anemometer often reads maximum wind gust speeds that are not physically possible. Therefore, the second option would be to choose the 50m anemometer which is working as predicted by the different logarithmic profiles and which gives a surface roughness value representative of the site characteristics. In addition, the two first NWP output levels are given for different pressure levels and are located relatively close to 45 m and 120 m above ground. These are sufficient reasons to choose the 50m sensor which is very close to the first level of the forecast model, while being very close to the wind vane, the temperature probe and the barometric pressure sensor that are also located between 40 and 50 m high. For these reasons, the sensor #8N (NRG Type 40 Maximum Anemometer, 49.7 m) is chosen to details the wind characteristics for the North Cape site.

The same methodology applied to the anemometers mounted on the Bouctouche mast lead to choose the sensor #5B (NRG Type 40 Maximum Anemometer, 50 m high) for the validation of the Environment Canada NWP model. It is also interesting to note that, looking at Table 2.8, the roughness length computed for the Bouctouche site is approximately 3.5 m. Such roughness length is generally associated to urban areas with very large buildings, which is not the case here. This site is actually surrounded by a forest canopy which has a roughness length of about 1.5 m (Manwell et al., 2002) as used in the inputs of the NWP model. Stull (1988) explains that a dense forest canopy could act like a displaced surface of height "d" (see Figure 2.9), which is not considered in the NWP model. Therefore, one shall expect that the wind speed forecast error is higher for the Bouctouche site than the North Cape site.

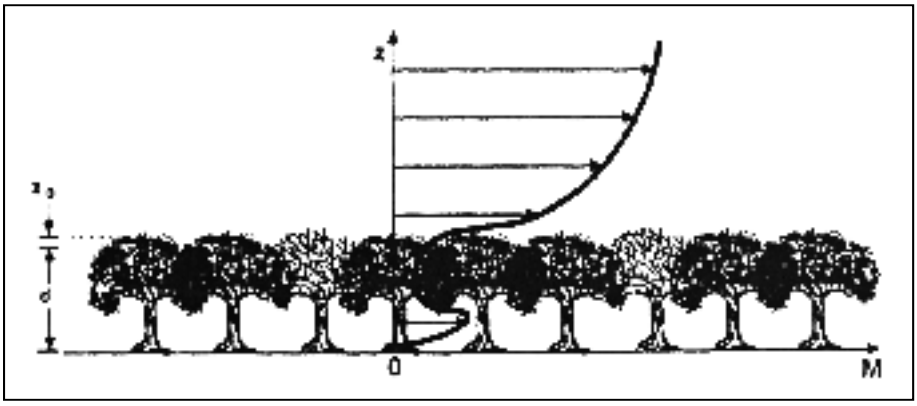

Figure 2.9 Vertical wind speed profiles over forest canopy.
(adapted from Stull, 1988, p. 381)

2.3 Atmospheric measurement uncertainty

Now that the anemometers have been chosen and that all erroneous values have been removed from the database, the measurement uncertainties can be computed in order to verify that the measurement dataset is well suited to evaluate the model. It is known that cup anemometer precision is of the order of 3 % (AWS Scientific, 1997), but it is also important to compute the wind speed deficit due to the flow distortion around the anemometer tower (excluding shading area) and the precision of the averaging technique.

First, the flow distortion in the surrounding area of the tower can be computed using the geometrical and conception parameters of the triangular lattice tower (IEC, 1998):

$$U_d = 100\% \times \left[1 - (0{,}062\ C_T^2 + 0{,}076\ C_T)\ (\frac{L}{R} - \ 0{,}082)\right] \tag{2.11}$$

$$C_T = 2{,}1\ t\ (1 - t) \tag{2.12}$$

Where: U_d is the wind speed deficit [%];

- C_T is the drag coefficient [-];
- t is the solidity of the tower ($0.1 < t < 0.3$);
- R is the distance to the mast centre [m];
- L is the mast leg distance (0.6025 [m]).

The distance to the mast center (R) can then be expressed as a function of the mast leg distance (L) and the boom length ($B_{\text{North Cape}} = 1.32$ m) for a triangular lattice mast:

$$R = \sqrt{\left(B + \frac{L}{2}\right)^2 + \left(\frac{L}{2}\tan 30°\right)^2} \tag{2.13}$$

As the anemometer tower solidity is not known, the highest recommended value is used in order to be conservative. Then, for the Bouctouche tubular mast, the wind speed deficit is computed as a function of distance ($d = 1.5$ m) from the centre of a tubular mast and mast diameter ($d = 0.152$ m). The relation is given in the IEC standard (1998) from a two dimensional Navier-Stokes analysis. Subsequently, the average centreline wind speed distortion is approximately 1.3 % for the North Cape tower and 0.1 % for the Bouctouche tower.

Afterwards, when characterizing experimentally a turbulent flow, the averaging technique precision shall be computed since measurements are usually averaged over many realizations

under similar conditions (i.e. ensemble averaging). In the atmospheric boundary layer, due to the stochastic behaviour of the turbulent flow, it is almost impossible to observe identical events and to perform ensemble averaging. Then, when describing the properties of the atmospheric air flow, data are averaged over time. Time averages are performed considering that they are equivalent to ensemble averages. This assumption is called the ergodic hypothesis (Lumley and Panofsky, 1964).

The atmosphere is also assumed to be statistically stationary during the averaging period (Tennekes and Lumley, 1972). Van Der Hoven (1957) shows that there is a gap between convection driven boundary layer scales (shorter than 0.001 Hz ~ 16.67 min) and synoptic scales (greater than 0.0001 Hz ~ 2.78 h) where the spectral intensity is negligible. Consequently, the atmosphere fluctuations can be assumed to be stationary for averaging period shorter than the convection driven scales (i.e. 10 min averages). Thus, considering that high frequency component of the wind, as turbulent wind gusts, have no significant contribution (zero average) in the mean meteorological phenomena. Conversely, when computing time averages, it is important to average over a sufficiently long sampling time (Panofsky and Dutton, 1983): this allows to properly describe the mean wind speed and limiting the statistical influence of the autocorrelation of the turbulence. Since the surface wind speed measurements are used for the NWP model validation, it is therefore important to estimate the error due to finite integration time.

When performing time averages, a common approach used in meteorology to express any parameter is to decompose each and every variable into a mean part and a perturbation part (Taylor's hypothesis). In equation 2.14, the perturbation or turbulent part (U') superimposed on the average part ($\overline{U}$) represents the instantaneous value (U) (Stull, 1988). These fluctuations are computed in the NWP model but are not commonly used as model outputs. For this reason, no distinction is made between mean or instantaneous parts after the present section since this study is only based on mean variable outputs. Therefore, in the rest of the document, for notational simplicity, this bar representing the average part of a variable will not be specified anymore.

$$U' = U - \overline{U} \tag{2.14}$$

Assuming a statistical stationary flow, the wind speed variance ($\sigma_U{}^2$) becomes stable (Kaimal, 1994) for long averaging time periods (i.e. larger than the interval over which the turbulence remains correlated and dependent of itself). The turbulence autocorrelation interval is also called the integral time scale (τ_U) and is defined as the integral of the autocorrelation function of the wind speed (R_U) over time (ε):

$$\tau_U = \frac{1}{\sigma_U{}^2} \int_0^\infty R_U(\varepsilon)\, d\varepsilon \tag{2.15}$$

$$R_U(\varepsilon) = \overline{U'(t)\, U'(t+\varepsilon)} \tag{2.16}$$

Figure 2.10 presents the relation between the autocorrelation function and the time lag for the anemometer previously selected for the North Cape site (49.7 m). The curve shows the average relation for approximately a four month period (mid August to late November 2009) at North Cape. In this figure, one can see that the wind speed gusts autocorrelation becomes negligible as the time lag increases. Computing the integral of the wind speed autocorrelation function at the wind test site with the 50 m anemometer (equation 2.15 – 2.16), the average integral time scale is 15.9 sec for the four month period at North Cape. Note that, since it is impossible to integrate the autocorrelation function to infinity using real data, the integral is computed over time up to the point where the autocorrelation functions reaches zero.

Considering that the wind energy industry and most meteorological assessments use 10 min averaging time period (T), the variance of the wind speed becomes stable since $T \gg \tau_U$. Subsequently, Tennekes and Lumley (1972) derive an equation to express the quadratic error due to finite integration time (E) as a function of the integral time scale (τ_U), the averaging period (T) and the variance of the wind speed in the averaging ensemble ($\sigma_U{}^2$) as follow:

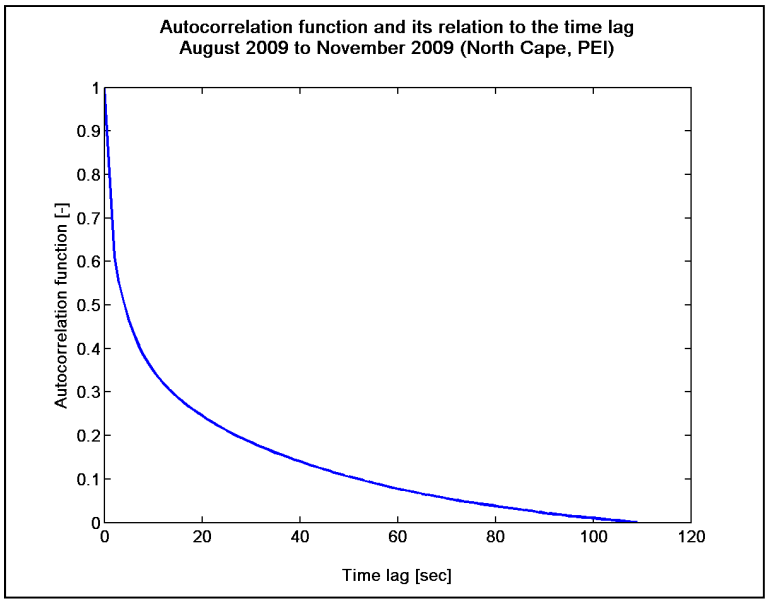

Figure 2.10 Instantaneous wind speed (1 Hz) autocorrelation function in relation with the time lag.

$$E \approx \frac{2\,\sigma_U{}^2\,\tau_U}{\bar{U}^2\,T} \tag{2.17}$$

Finally, assuming ergodicity of the atmospheric flow to perform time averages, the computed error level for the mean wind speed is approximately 2.6 %. Therefore, when performing the quadratic sum of the measurement uncertainties (measurement error ~ 3 %, flow distortion ~ 0.1 to 1.3 % and averaging technique precision ~ 2.6 %), the total measurement error level is approximately 4 % for both the triangular lattice tower at North Cape and the tubular mast at Bouctouche. Note that this value is in relation with the average measurement uncertainty performed using the North Cape specific anemometer for four month of measurements at 1 Hz sampling rate; it still gives a good evaluation of the order of magnitude of the measurement errors. From the preliminary analysis done in Chapter 4, the annual MAE and RMSE of the NWP model are 28.01 % and 36.77 % respectively. When compared to the error of the NWP model, the measurement error is an order of magnitude lower. Then, it is concluded that the data from the anemometer towers are well suited for the evaluation of the NWP model.

2.4 Wind characteristics

Once the measurement uncertainty has been evaluated, it is then important to evaluate the wind characteristics on the test sites that are considered in the present study. To do this evaluation, it is possible to plot different essential parameters for annual and seasonal time series. The wind frequency, the average wind speed and the wind energy ratio are calculated for each direction and the Weibull distributions are computed. Because of confidentiality agreements, all wind speeds are normalized using the annual average wind speed and the Weibull parameters are not given. The wind frequency roses, average wind speed roses, wind energy roses and Weibull distributions for annual and seasonal time series at the North Cape site can be observed in Figures 2.11 - 2.14, respectively. Figure 2.15 shows the annual and seasonal average diurnal cycle of the wind speed at North Cape. The wind characteristics at Bouctouche site appears to be quite similar to those observed at the North Cape site; these results are shown in the annexes (see Annex III: Figures A.III.1 – A.III.5).

Looking at Figure 2.11, one can see that the prevailing wind direction is from the western direction all year except during the spring season. Effectively, during that season, winds come from the western side as well as from the northern side. During the fall season, the wind is still often from the West, but its distribution is a little more spread out than the annual distribution. Then, Figures 2.12 - 2.13 show that the strongest winds are from the western side (i.e. from SW to NNW). These sites also get strong northern winds during winter and summer, while it gets strong winds from the SSE during the summer. Figure 2.14 shows that the wind is stronger in the winter and in the fall seasons. The summer season is characterized by very low wind speeds. Figure 2.15 confirms that the average wind speed is lower in summer and that it is higher in fall and winter. This figure also shows that there is generally a diurnal cycle of the wind speed reaching its minimum in late afternoon.

Once the data quality and the wind characteristics are assessed, it is possible to work on the development of a standard protocol to evaluate short-term wind prediction models, to correlate its uncertainties to meteorological events and finally, to improve the model itself.

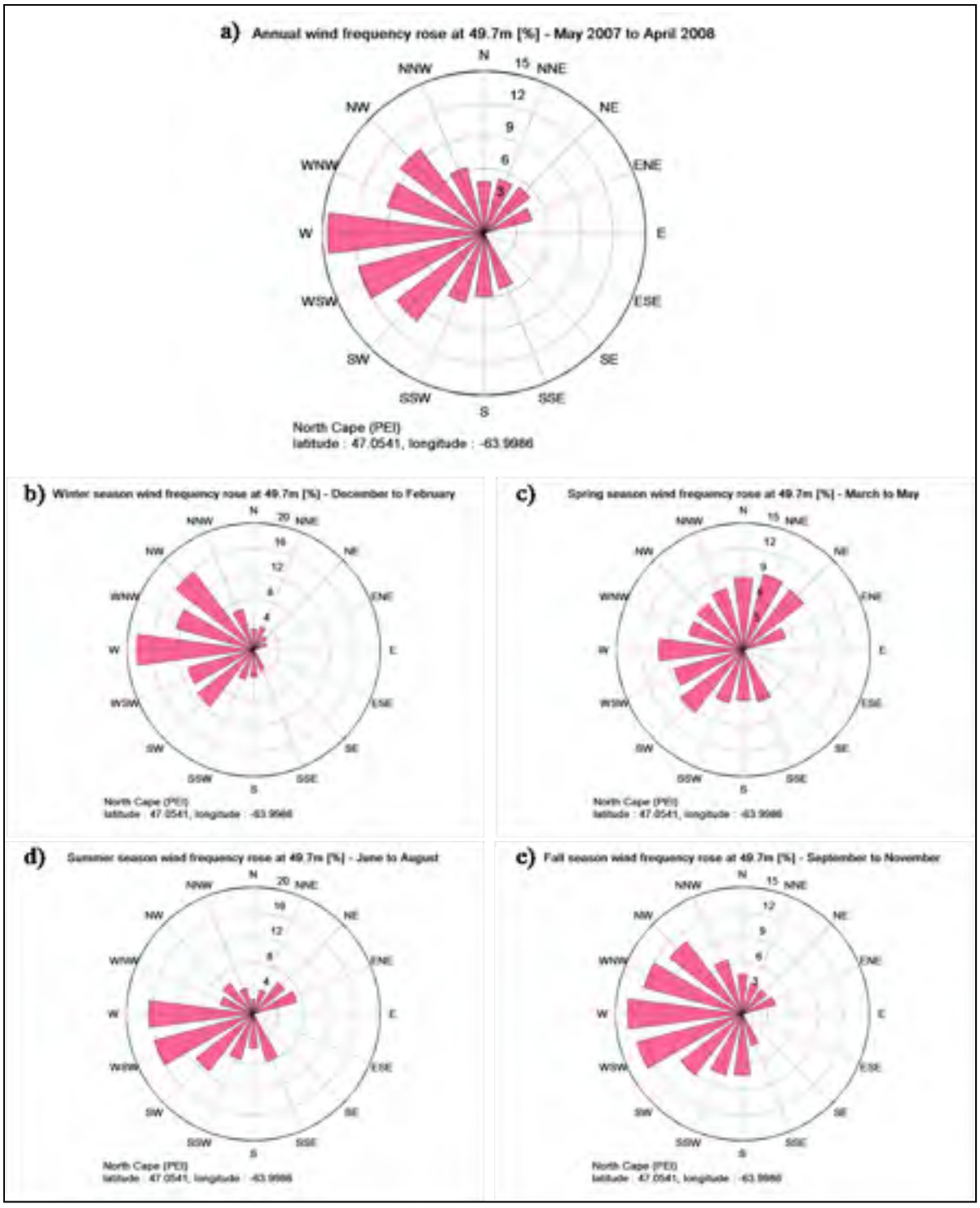

Figure 2.11 Annual and seasonal wind frequency roses at the North Cape site: a) annual, b) winter, c) spring, d) summer and e) fall.

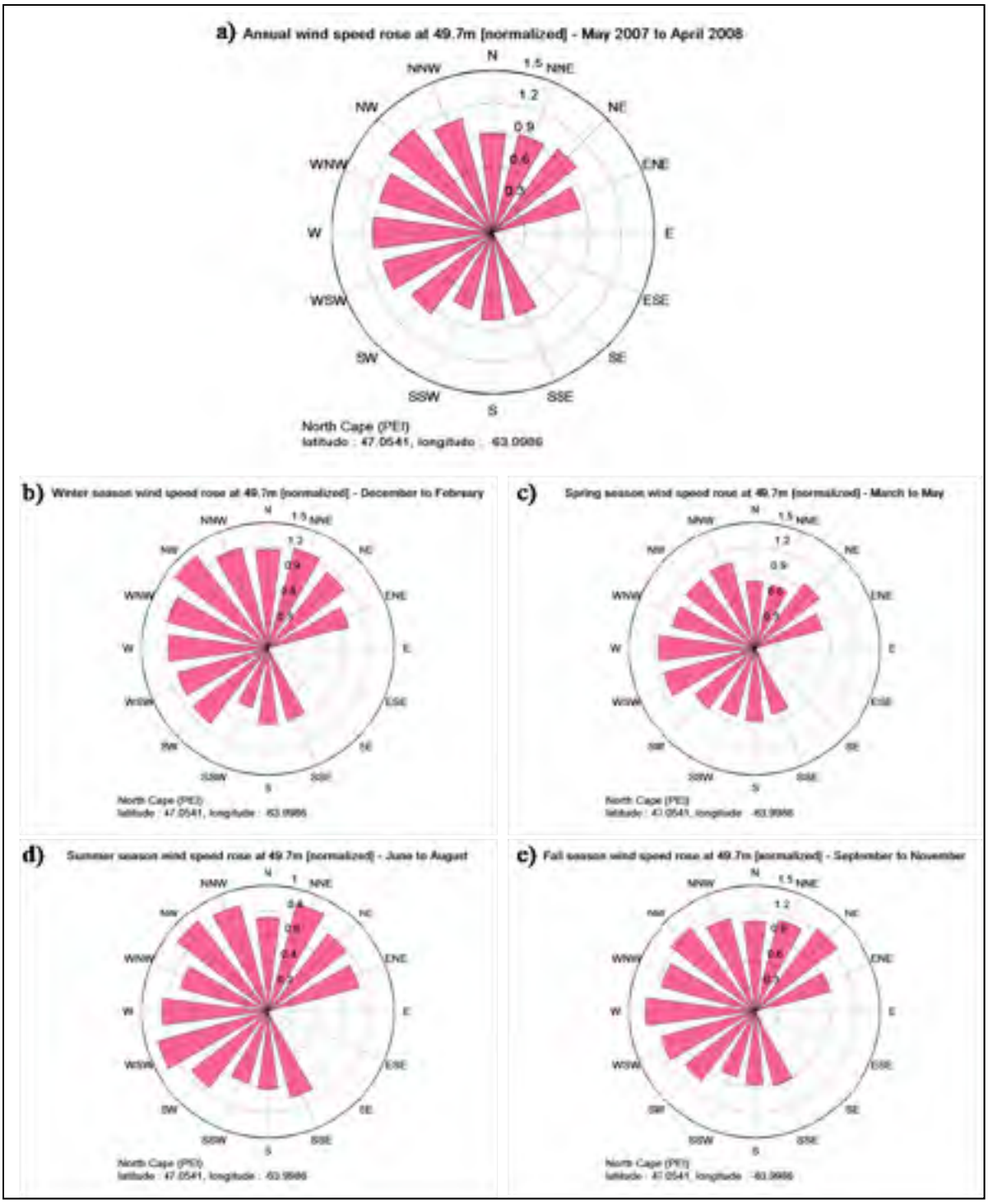

Figure 2.12 Annual and seasonal average wind speed roses at the North Cape site: a) annual, b) winter, c) spring, d) summer and e) fall.

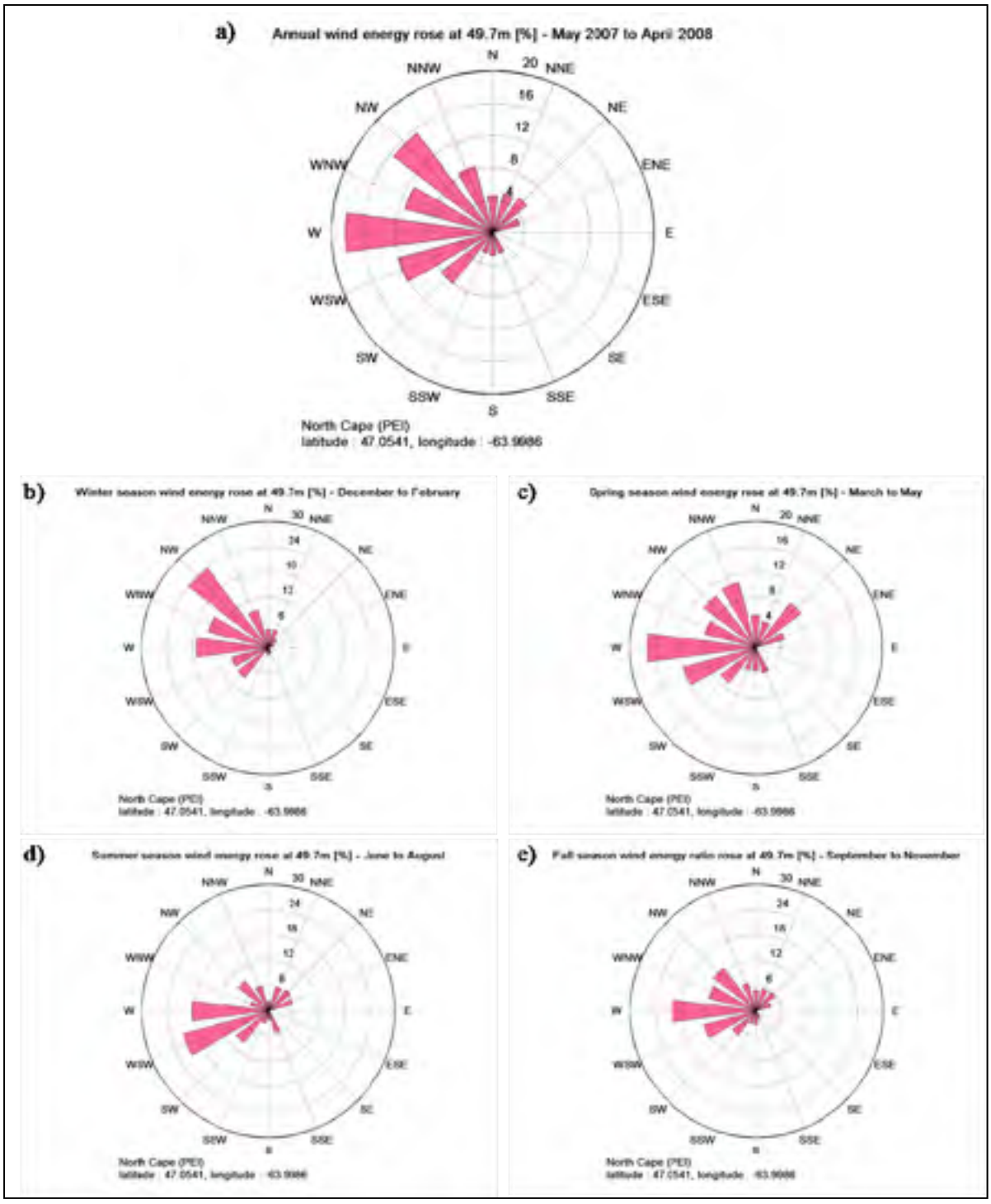

Figure 2.13 Annual and seasonal wind energy roses at the North Cape site: a) annual, b) winter, c) spring, d) summer and e) fall.

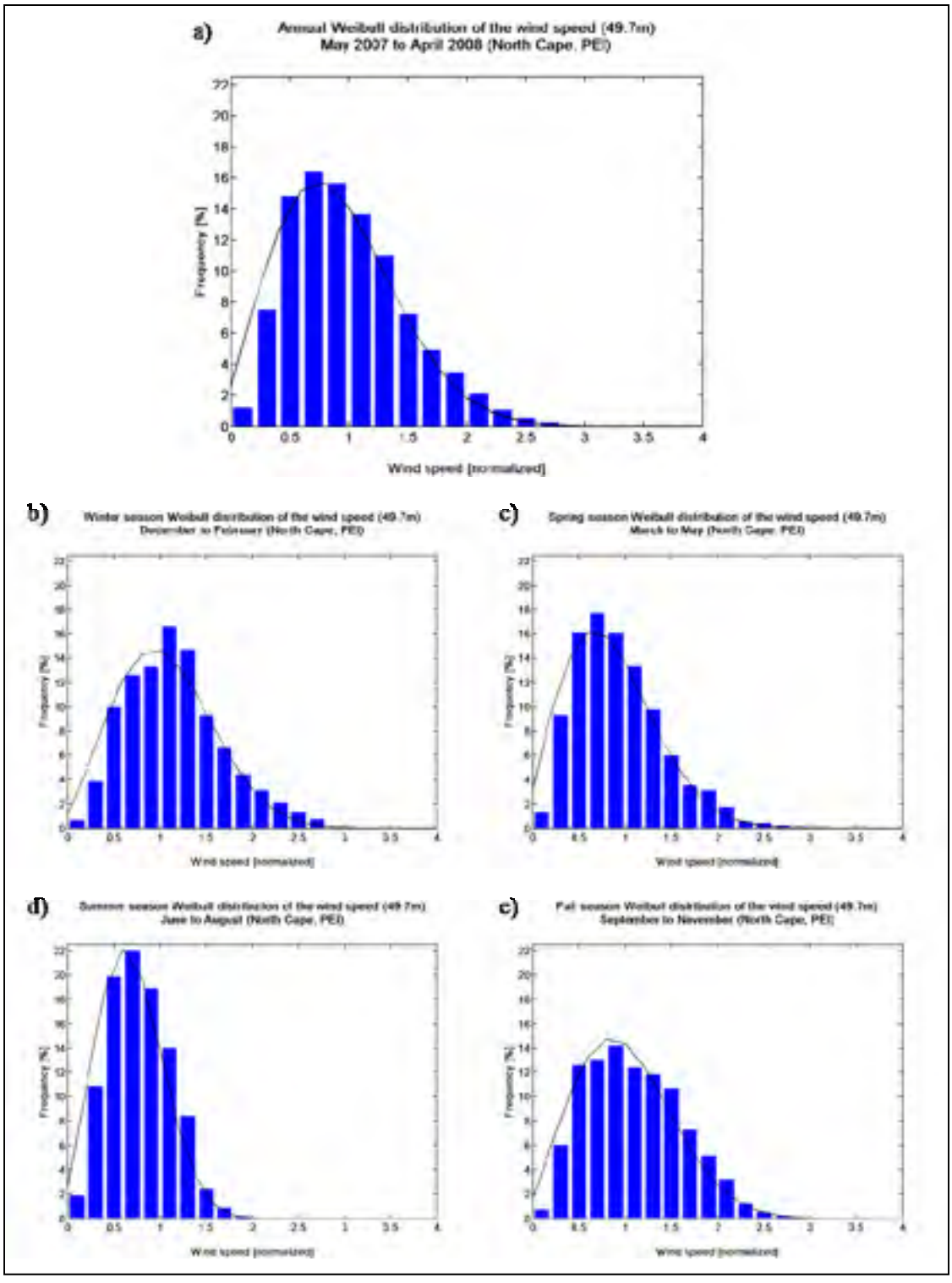

Figure 2.14 Annual and seasonal Weibull distributions of the wind speed at the North Cape site: a) annual, b) winter, c) spring, d) summer and e) fall.

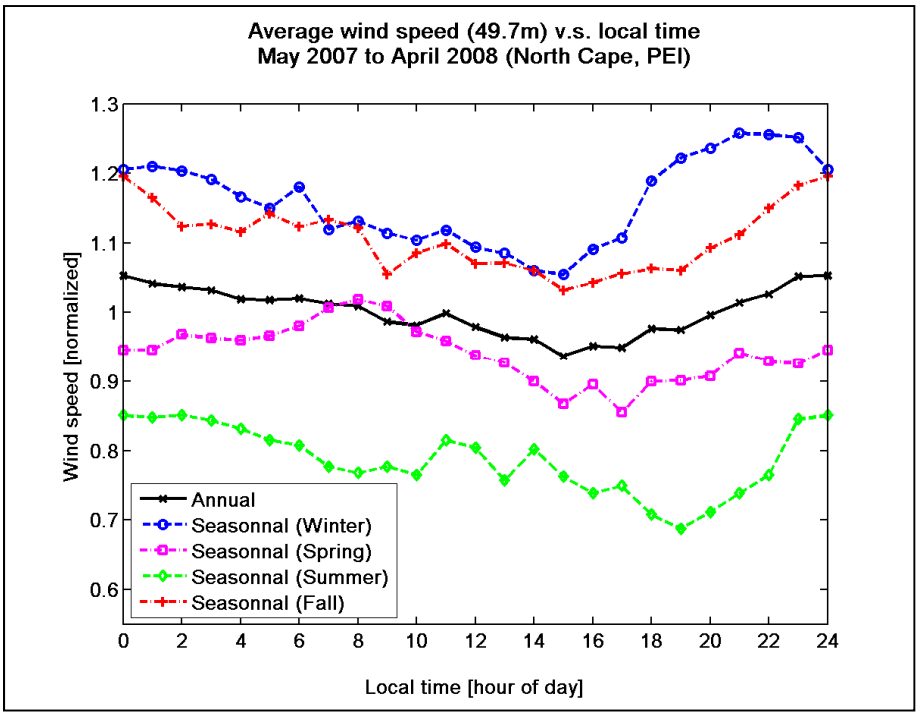

Figure 2.15 Annual and seasonal average wind speed diurnal cycles at the North Cape site.

CHAPTER 3

VERTICAL INTERPOLATION OF THE FORECASTS

As mentioned earlier in section 2.2, the first forecast output levels follow pressure levels (hybrids levels). They are approximately located at 45 m and 135 m AGL and the anemometers that are used to validate the forecasting model are located at 50 m AGL. As the forecast output heights vary in time (± 10 %), a vertical interpolation module has to be implemented in order to evaluate the wind speed at the appropriate height. Interpolation modules using different techniques are employed and compared to verify which algorithm is the most suitable for wind forecast applications. Power law profiles, logarithmic profiles for neutral and non-neutral atmospheres are tested in this section.

3.1 Power Law profiles

The Power Law is a simple profile representing the wind speed at a certain height (z). The wind speed is calculated using the wind speed (U_r) at a reference height (z_r):

$$U(z) = U_r \left(\frac{z}{z_r}\right)^{\alpha} \tag{3.1}$$

The exponent α can be computed using the wind speed at the reference height (Justus, 1978):

$$\alpha = \frac{0{,}37 - 0{,}088\ ln(U_r)}{1 - 0{,}088\ ln\left(\frac{z_r}{10}\right)} \tag{3.2}$$

It can also be computed as a function of the surface roughness (Counihan, 1975):

$$\alpha = 0{,}096\ log(z_0) + 0{,}016\ (log(z_0))^2 + 0{,}24 \tag{3.3}$$

3.2 Linear profiles

Vertical wind speed profiles can also be computed with a linear regression where the wind speed is interpolated using wind speed observations ($U(z)$) at two different heights (z_i):

$$U(z) = U_2 + (z - z_2)\frac{(U_1 - U_2)}{(z_1 - z_2)} \quad (3.4)$$

3.3 Logarithmic profiles

Logarithmic profile schemes use surface momentum, sensible heat and latent heat fluxes to describes the kinematic surface stress based on wind shear (friction velocity: u_*) and to compute the atmospheric stability in the surface layer (Stull, 1988). As a matter of fact, the momentum and heat fluxes are computed in the NWP model for each type of surfaces: water, frozen water, ground and snow covered ground. They are then aggregated into single fluxes (used as lower boundary conditions for the vertical diffusion) which are available as model outputs. In the present project, only fluxes related to the ground are relevant, but are not available in this database. Therefore, attempts using the aggregated fluxes to compute the logarithmic wind profiles have been done, but the wind profiles totally diverged from expected values. Subsequently, logarithmic wind profiles are computed using measured or forecasted wind speed at a reference height. Logarithmic wind speed profile for neutral flow is the scheme that is usually used in wind energy assessments, it is then tested for the vertical interpolation:

$$U(z) = \frac{u_*}{k}\, ln(z/z_0) \quad (3.5)$$

Where: $U(z)$ is the interpolated wind speed [m/s] at height z [m];

- u_* is a friction velocity scale from kinematic surface stress based on wind shear [m/s];
- k is the Von Karman similarity constant (0.4 [-]);
- z_0 is the forecast model surface roughness input [m].

Then, the friction velocity is computed using the wind speed (U_r) at a reference height (z_r):

$$u_* = \frac{U_r\, k}{ln(z_r/z_0)} \tag{3.6}$$

Where:u_* is a friction velocity scale from kinematic surface stress based on wind shear [m/s];

- U_r is the forecasted wind speed [m/s] at the output level height AGL z_r [m].
- k is the Von Karman similarity constant (0.4 [-]);
- z_0 is the forecast model surface roughness input [m].

Non neutral logarithmic profiles considering the atmospheric stability use a similar formulation adding a dimensionless wind shear parameter. The dimensionless wind shear ($\varphi(z/L)$) is generally a function of the height (z) and the Monin Obukhov length (L) (Businger et al., 1971; Delage, 1988; Delage and Girard, 1992; Mailhot, 1992; Delage, 1997). In our case, the Monin Obukhov length representing the atmospheric stability is computed in GEM-LAM, but is not stored in the database and it is not possible to properly compute it from the aggregated surface fluxes. Consequently, the dimensionless wind shear is considered constant in height and is approximated using a second wind speed observation at a reference height (wind speed forecast at the second level). Flow stability measures (φ) derived from forecast outputs are therefore integrated in the vertical interpolation (equations 3.7 – 3.9) to improve the NWP for complex sites such as North Cape since local since winds are affected on a local scale by thermal properties (Liu, 2009; Nielsen et al. 2007a).

$$U(z) = \frac{u_*}{k}\,\left(ln\left(\frac{z}{z_0}\right) - \varphi\right) \tag{3.7}$$

$$u_* = \frac{k(U_2 - U_1)}{ln(z_2/z_1)} \tag{3.8}$$

$$\varphi = \frac{\left(U_2\, ln\left(\frac{z_1}{z_0}\right) - U_1\, ln\left(\frac{z_2}{z_0}\right)\right)}{(U_2 - U_1)} \tag{3.9}$$

Where: φ is the stability function [-];

- z_0 is the forecast model surface roughness input [m];
- u_* is a friction velocity scale from kinematic surface stress based on wind shear [m/s];
- k is the Von Karman similarity constant (0.4 [-]);
- U is the forecasted wind speed [m/s] at the output level height AGL z [m].

3.4 Comparison of the different vertical interpolations

In order to verify which vertical interpolation scheme respects the most the physics of the flow, the interpolated wind speeds have been compared to measurements and the model output for two different computation points: the closest NWP point to the measurement mast (distance = 445 m; surface roughness = 0.001 m; ground ratio = 0 %), and the closest computation point that has geophysical characteristics (surface roughness and ground ratio) similar to the site (distance = 7 868 m; surface roughness = 0.3162 m; ground ratio = 100 %). Results for unstable / neutral and for stable atmospheric conditions are shown in Figures 3.1 - 3.4. Analysing Figures 3.1.a - 3.4.a, one can see that the Power Law from Justus (1978) do perform generally well, but the curvature is too pronounced for stable atmosphere as it is not enough pronounced for unstable/neutral atmospheric conditions. The exact same observation can be made for Counihan's Power Law profile (1975) in Figures 3.1.b - 3.4.b and for the neutral logarithmic profile in Figures 3.1.d - 3.4.d. These two last vertical profiles have very similar behaviours since they are both computed using the measured wind speed at the same reference height and the same surface roughness. As a result, these three methods do not properly represent the vertical wind profile for all meteorological conditions. Neither of them matches properly the behaviour of the flow since the profiles are forced to zero at the surface roughness height, independently of the atmospheric stability. As these three methods don't respect the physics of the flow and as they are not properly interpolating the wind speed for all atmospheric stability conditions, they are not used to interpolate the NWP outputs.

Furthermore, analysing Figures 3.1.c - 3.4.c, one can see that linear profiles are really not suited for vertical interpolation of the wind speed in the surface layer since the measured wind speed show a non-linear behaviour. Therefore, as the linear profile does not properly represent the surface wind speed profile, it is not used to interpolate the NWP outputs.

Conversely, the non-neutral logarithmic wind profile considers the atmospheric stability by computing the wind speed using the forecasts at the two first output levels. Therefore, when looking at Figures 3.1.e - 3.4.e, one can observe that the interpolated wind speed fits almost perfectly the measurements for unstable / neutral and stable atmospheric conditions. As this profile is computed from two forecasted wind speeds, it respects the dynamic behaviour of the meteorological system under different stability conditions. The results being similar for the Bouctouche site (see Annex IV: Figures A.IV.1 – A.IV.2), it is possible to state that the non-neutral logarithmic vertical wind profile performs better than the other profiles.

As a matter of fact, in the case where the NWP model would systematically over or under-predict the wind speed, non proper interpolation scheme like a linear profile could eventually give better results than other models when compared at a single height; this could explain the use of such profiles in the wind industry. However, when computing the integral of the wind speed over the area swept by a wind turbine to calculate the wind power, the results would not be coherent with the reality (see Table 3.1) since the wind turbines sweep a large area ranging from approximately 20 m to 150 m high (depending on the type of turbine). Therefore, it is important to choose judiciously the interpolation scheme to be used and to evaluate the order of magnitude of the interpolation error. As noted in the previous paragraphs, the non-neutral logarithmic vertical wind profile appears to be properly suited for vertical interpolation of the wind speed for wind power assessments. It is therefore used to interpolate the wind speed forecasts in the present study. Then, the difference between the best and the worst interpolation methods (non-neutral logarithmic vs linear profiles) is evaluated to approximate the order of magnitude of the forecast error that can be attributed to the vertical interpolation. Figure 3.5 shows the annual average vertical wind profiles and Table 3.1 shows the annual wind speed and power difference between those two profiles.

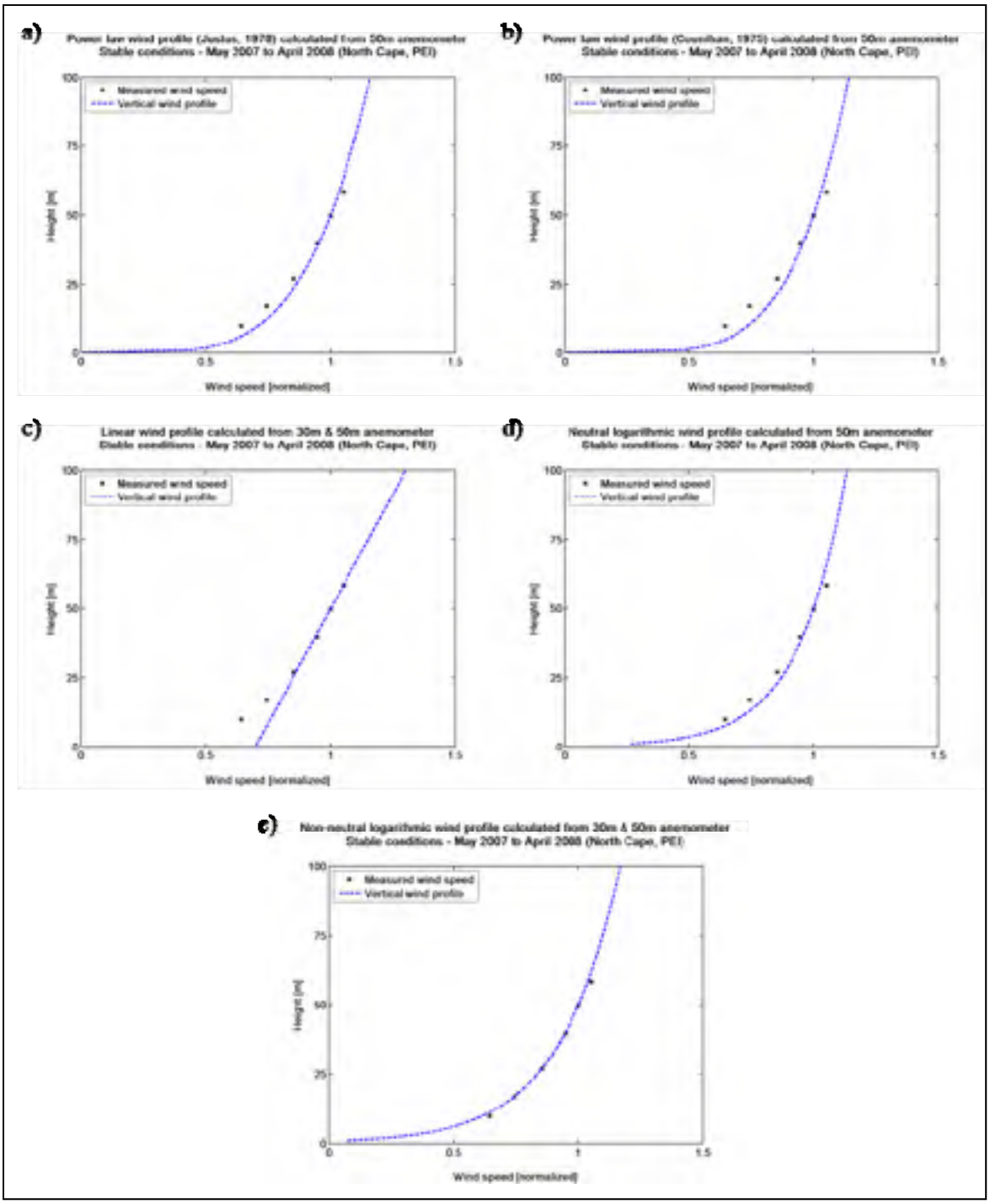

Figure 3.1 Vertical wind profiles under stable atmospheric conditions at the closest NWP point to the measurement mast (North Cape): a) Power Law profiles from Justus (1978), b) from Counihan (1975), c) linear profile, d) neutral and e) non-neutral logarithmic profiles.

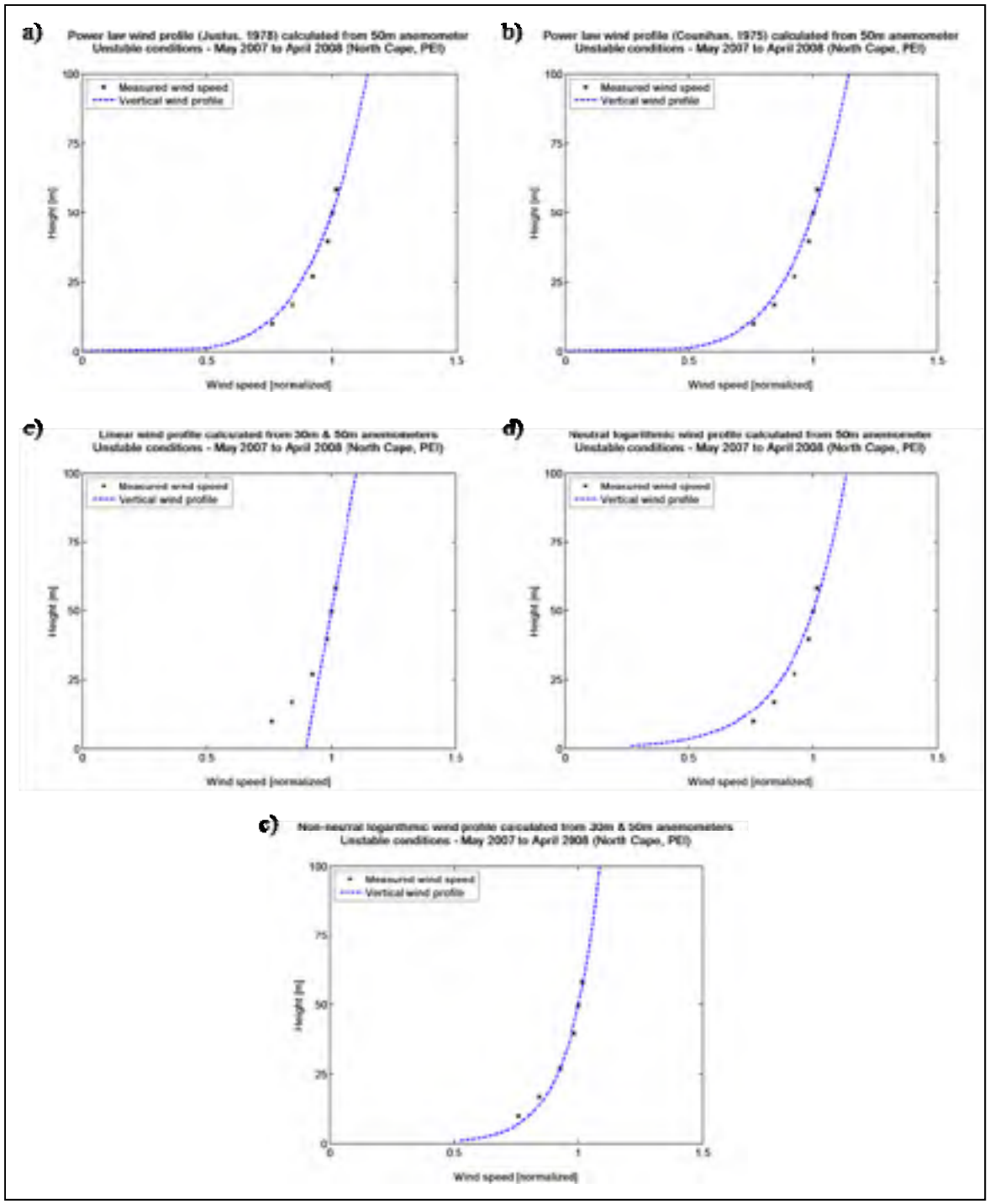

Figure 3.2 Vertical wind profiles under unstable/neutral atmospheric conditions at the closest NWP point to the measurement mast (North Cape): a) Power Law profiles from Justus (1978), b) from Counihan (1975), c) linear profile, d) neutral and e) non-neutral logarithmic profiles.

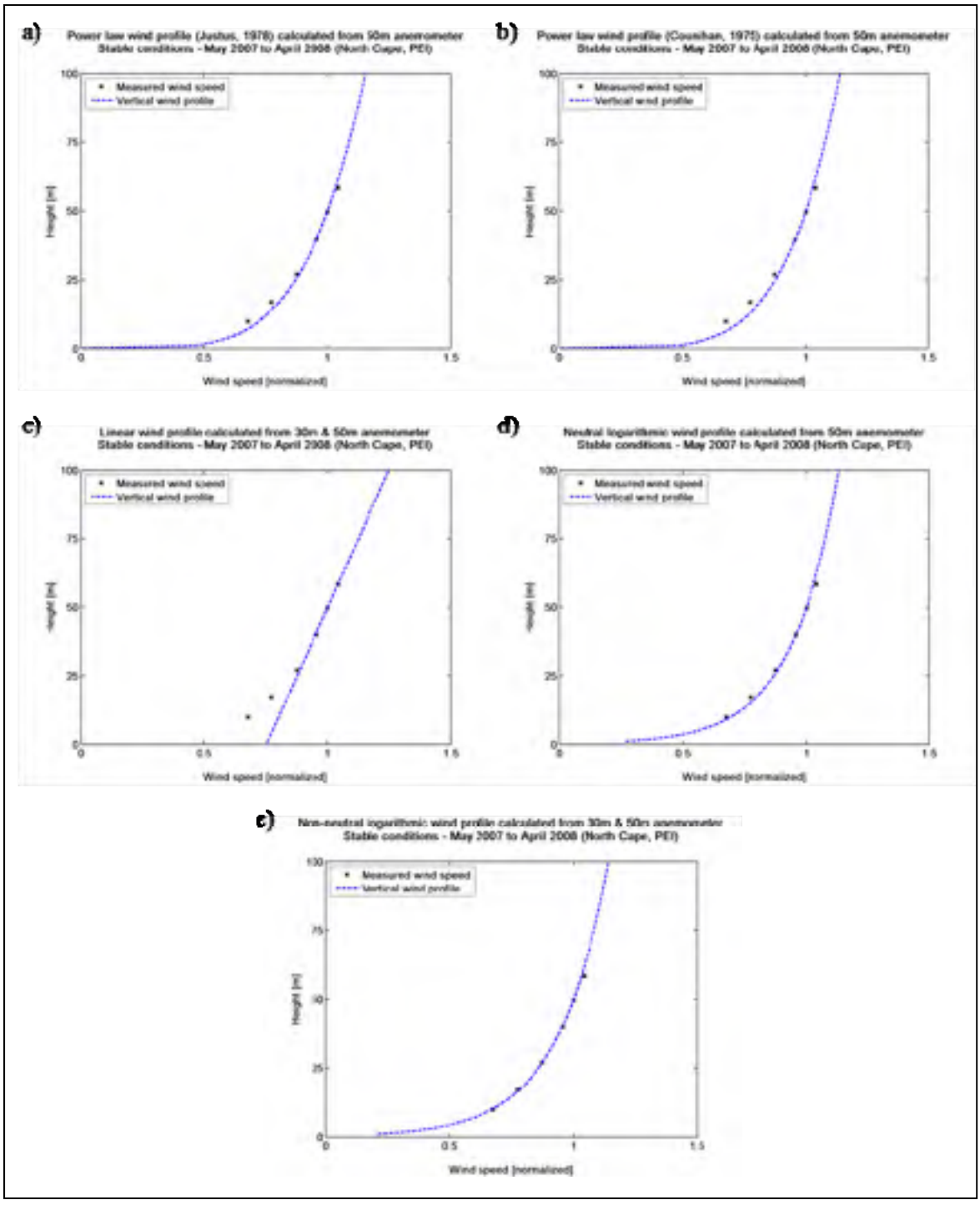

Figure 3.3 Vertical wind profiles under stable atmospheric conditions at the closest computation point with geographical characteristics similar to the site (North Cape): a) Power Law profiles from Justus (1978), b) from Counihan (1975), c) linear profile, d) neutral and e) non-neutral logarithmic profiles.

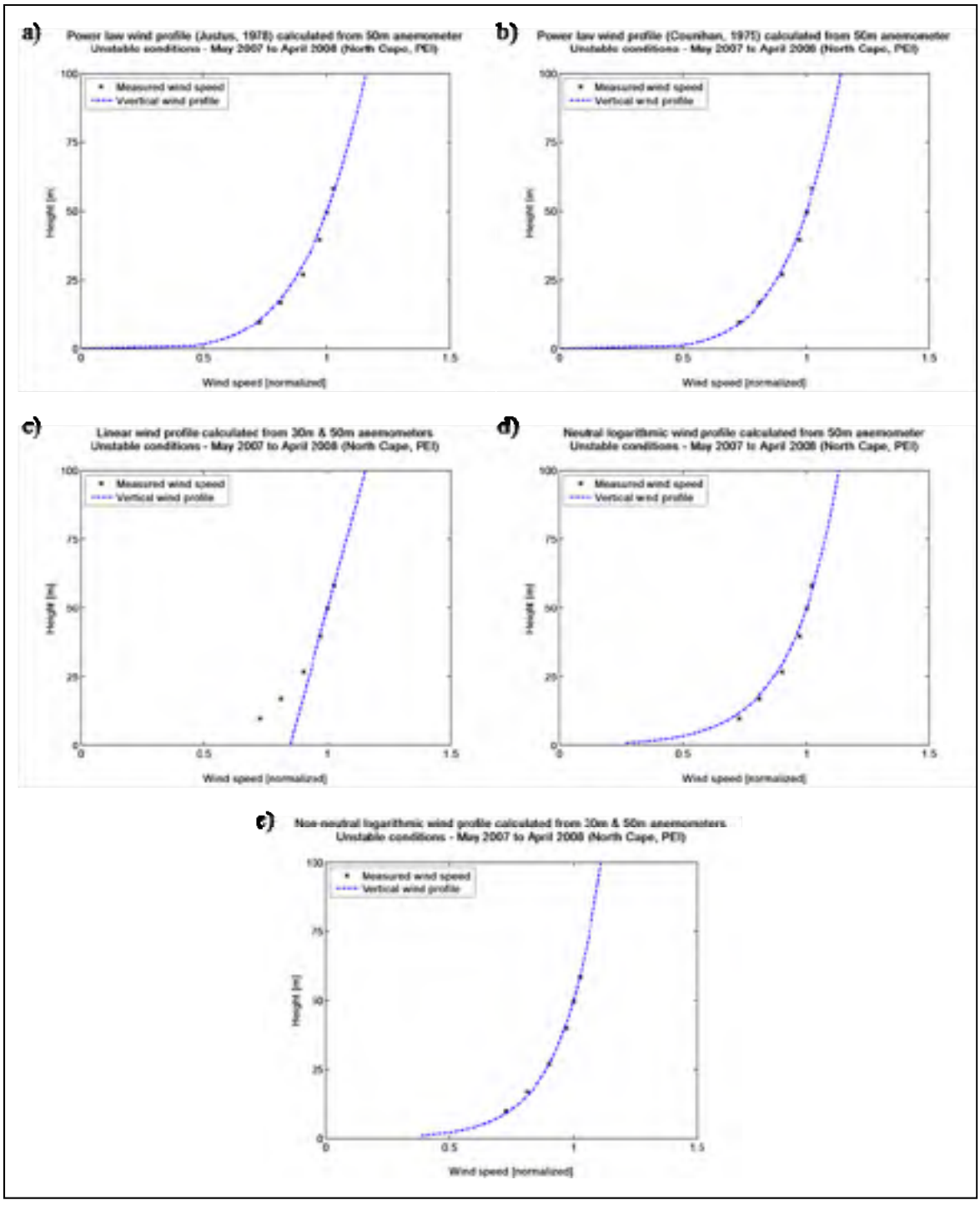

Figure 3.4 Vertical wind profiles under unstable/neutral atmospheric conditions at the closest computation NWP point with geographical characteristics similar to the site (North Cape): a) Power Law profiles from Justus (1978), b) from Counihan (1975), c) linear profile, d) neutral and e) non-neutral logarithmic profiles.

Looking at the measured wind speeds at different heights in Figure 3.5, one can observe that there is effectively a significant difference between the interpolated wind speeds from both methods. Then, the results presented in Table 3.1 show the interpolation differences in terms of wind speed and power for the two types of turbines already installed at North Cape: Vestas V47 and V90. Thus, it gives the order of magnitude of the error caused by the vertical interpolation of the wind speed. This table shows that the vertical interpolation difference is 0.35 % at the hub height of a V47 turbine (50 m AGL) and it becomes larger when getting away from the NWP forecast output heights (~ 45 and 135 m AGL). This difference is approximately 1.38 % at the hub height of a V90 turbine (90 m AGL). This table also shows that the difference is significantly higher (~ 3.16 %) when computing the power forecast of the Vestas V90 turbine. Thus, these results indicate that the vertical interpolation uncertainty has a significant impact on the forecasted power of a wind turbine (integrating the wind power density over the swept area). For these several reasons, the best vertical wind profile (non-neutral logarithmic) is ultimately implemented to interpolate the NWP outputs at the anemometer heights for the statistical analysis in this work.

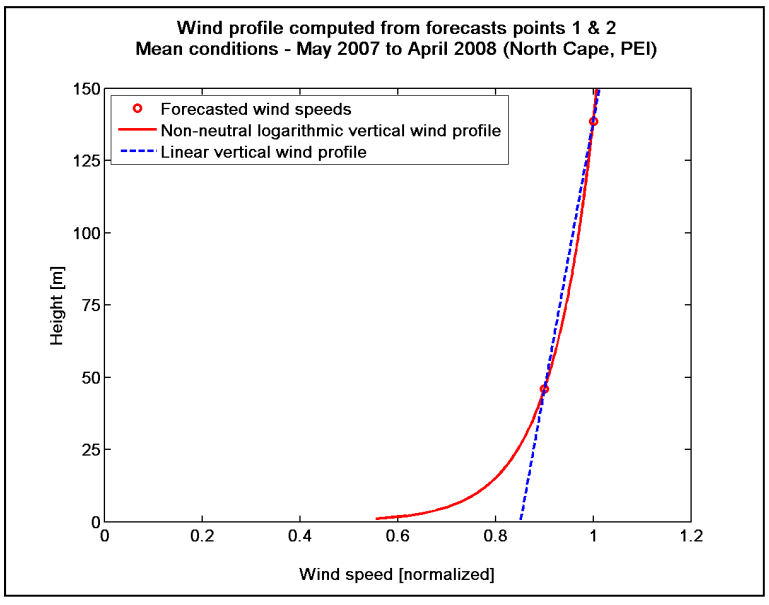

Figure 3.5 Comparison of non-neutral logarithmic and linear profiles at the North Cape site.

Table 3.1 Mean annual wind speed and power forecast difference between linear and non-neutral logarithmic vertical wind profiles

Turbine type	**Difference between linear and non-neutral logarithmic vertical wind profiles for mean annual atmospheric conditions**	
Vestas V47	Wind speed at hub height (50 m)	0.35 %
	Wind power for a Vestas V47 swept area (26 to 74 m)	0.29 %
Vestas V90	Wind speed at hub height (90 m)	1.38 %
	Wind power for a Vestas V90 swept area (45 to 135 m)	3.16 %

CHAPTER 4

NUMERICAL WEATHER PREDICTION MODEL

Short-term wind power forecast models are usually based on NWP models like GEM-LAM (Landberg et al., 2003 and Giebel et al., 2003). This NWP model applies fluid mechanics governing equations to describe the various dynamical processes taking place in the atmosphere using finite-difference method (Côté et al., 1998), i.e. the conservation equations (mass, energy, momentum and moisture) as well as the equation of state for perfect gases. As these dynamic equations are not solvable analytically, numerical algorithms are developed and physical parameterizations are used to close these equations. The idea of physical parameterization is to use the model variables to represent the mean effect of the sub-grid scale phenomena in the Earth's surface, the atmospheric boundary layer as well as the processes related to condensation, radiation, etc. For example, the turbulent kinetic energy (TKE) is calculated with a simplified approach where the TKE evolution is a function of the source-sink term, the viscous dissipation and redistribution term. Applying this simplified method significantly reduce the computation time and costs. A complete description of the physics library used in GEM-LAM is available from Environment Canada (Mailhot et al., 1998). One of the goals of this work is to describe and assess the forecast uncertainty related to the physics of the NWP models (see Chapters 5 - 6). Other error sources, such as measurements and interpolation, are detailed in the previous chapter.

4.1 Model outputs

Before getting any further, it is important to take a look at the variables available from Environment Canada NWP model. As mentioned earlier many physical and dynamical output variables are computed; but as the calculation domain and output files are large, only the most important parameters are stored for this experimental forecast assessment. Table 4.1 provides details of the main variables used in the present study and Table 4.2 describes the GEM-LAM output vertical levels. For accuracy and working simplicity, all variables are converted into the international units system (see Table 4.1). Also, since level heights are

expressed in meters above sea level, a conversion is done to make sure that all level heights are measured in meters AGL (see Table 4.2).

Table 4.1 Description of the GEM-LAM output parameters

Variables	**Units**	**Working units**	**Unit conversion**	**Level**
Hydrostatic pressure	mb	Pa	1mb = 100Pa = 0.1kPa	Level 1 & 2
Wind speed	Knot	m/s	1Knot = 0.514791m/s	Level 1 & 2
Wind direction	Deg.	Deg.	-	Level 1 & 2
Height	dam	m	1 dam = 10m	Level 1 & 2
Temperature	°C	K	°C + 273.1 = K	Level 1 & 2
Specific humidity	-	-	-	Level 1 & 2
Latitude	Deg.	Deg.	-	-
Longitude	Deg.	Deg.	-	-
Topographic height	m	m	-	-
Topographic mask	-	-	-	-
Surface roughness	m	m	-	-

Table 4.2 Description of the GEM-LAM output vertical levels

Levels	**Height definition**	**Conversion**	**Working height**
1	Height above sea level	H'1 = H1 - Topographic height	H'1 [m AGL]
2	Height above sea level	H'2 = H2 - Topographic height	H'2 [m AGL]

4.2 Stability parameter computation

An important parameter that is not included in the model outputs is the atmospheric stability parameter called the Richardson Number (Mailhot et al., 1998). This dimensionless number expresses the ratio between the buoyant forces and other mechanical forces producing turbulence. The turbulence can be generated by both buoyancy and wind shear. Then, the

Richardson Number can be either positive or negative depending on the vertical temperature gradient: negative if the buoyancy forces tend to generate turbulence through heat convection (unstable flow); positive if the buoyancy forces tend to suppress the turbulent motion generated by the wind shear (stable flow). Subsequently, a situation where there are no buoyancy forces (i.e. no vertical temperature gradient) is called a neutral flow. Generally, one can observe unstable flows during the day since the sun is warming up the ground which generates buoyant convection and, on the opposite, during night time, the ground loses heat through radiation and the air cools down close to the surface, thus generating statically stable buoyant forces.

As local temperature and wind speed gradients are quite difficult to measure with rawinsonde, meteorologists tend to replace local gradients by a series of discrete measures in the atmosphere. Using measurements from discrete heights tend to approximate the local gradients ($\Delta x \cong dx$). Using relatively close measuring points, it is then possible to compute the Richardson Number with discrete data. This approximated non dimensional ratio is then called the Bulk Richardson Number (Rb) and this approximation is applied to compute the forecasted atmospheric stability (Rb):

$$Rb = \frac{g\,\Delta\theta_V\,\Delta z}{\overline{\theta_V}\,(\Delta U)^2} \tag{4.1}$$

Where:g is the gravitational acceleration (9.81 [m/s^2]);

- U is the wind speed [m/s] at a specific height z [m];
- θ_V is the virtual potential temperature [K];
- $\overline{\theta_V}$ is the mean virtual potential temperature between two discrete points [K].

The virtual potential temperature θ_V refers to the temperature that would have a parcel of moist air that brought adiabatically up to the reference pressure level (see equations 4.2 – 4.3) (Stull, 1988). Meteorologists tend to use the potential virtual temperature (θ_V) instead of

the temperature, since θ_V allows to compare parcels of moist air at different heights as it conserves the mass and thermodynamic properties of the fluid.

$$\theta = T\ (P_0/P)^{0,286} \tag{4.2}$$

$$\theta_V = \theta\ (1 + 0{,}61\ r) \tag{4.3}$$

Where: P_0 is the reference pressure level (100 000 [Pa]);

- P is the measured pressure [Pa];
- θ_V is the virtual potential temperature [K];
- θ is the potential temperature [K];
- T is the average temperature measured [K];
- r is the specific humidity contained in the atmosphere (mixing ratio) [$kg_{vapor}/kg_{dry\ air}$].

Since the atmospheric stability measure is a characteristic of the surface boundary layer (wind speed, temperature and humidity gradients are larger near the surface), the parameters from the first two levels are used for this calculation (equations 4.1 – 4.3). The Bulk Richardson Number is finally computed for each grid point at each time step. Then, it is used in the subsequent statistical analysis where prediction uncertainties are compared to different parameters to detail the forecast errors under certain meteorological conditions.

4.3 Preliminary analysis

Canadian global and regional models cover a large physical area and, due to computational constraints, their grid spacing remains relatively large (30 and 15 km) compared to the size of a wind turbine. However, the local topography highly influences the wind characteristics on a site and the predictions errors (Kariniotakis et al., 2004). This is why limited area models (LAM), such as GEM-LAM (Environment Canada), are developed for meso-scale and local scale applications. In our study, this model is applied to specific domains, the Gaspésie region, where several wind farms are currently in operation. This model has a horizontal

resolution of 2.5 km and each computational point represents the average meteorological situation within an area of 2.5 km x 2.5 km. While GEM-LAM has a relatively fine spatial resolution, it is not yet capable to represent sharp topographic details such as a cliff or a coastal interface. Indeed, the model considers topographic changes between the computation points as steady topographic slopes. Therefore, cliffs are not modeled and coastal interfaces are only represented as surface ratios of ground within the 2.5 km x 2.5 km area.

Figures 4.1 - 4.2 show the complexity of the topography in North Cape (PEI). In Figure 4.2, the cross represents the anemometer tower while the grid represents a subset of the Environment Canada GEM-LAM horizontal grid for wind predictions. Looking at Figures 4.1 - 4.2, one can see that the WEICan wind test site is located on a complex terrain, considering that North Cape is surrounded (East, North and West) by a coastal cliff of approximately 13 m in height. Even though there is a computational grid point very near to the measurement mast (445 m), the model can't perceive that there is a sharp coastal cliff right in the middle of its domain. It only models the site as a slope over 2.5 km with a 1.1882 m average height and a 0 % ground covering proportion within that grid cell. These parameters are not representative of the site. Moreover, the surface roughness associated with the sea surface, as considered by the model, is approximately 0.001 m while the site is located on a fallow field with many small wind turbines and few small buildings and shall have a surface roughness around 0.25 m as defined previously.

Figure 4.1 Photos of North Cape and the cliffs surrounding the wind test site.

Figure 4.2 Plan of North Cape wind test site with part of the GEM-LAM horizontal grid.

Figure 4.3 presents the result of a statistical analysis showing a clear topographic signature in the prediction uncertainty for different wind directions at the North Cape site. Note that wind data from E, ESE and SE directions are removed from the database due to shadowing effect (see Chapter 2). Also, all results are normalized using the highest value of each graph due to confidentiality agreements.

When looking at Figure 4.3, it is clear that the wind forecast error is higher for the southern winds coming from the island since the air flow is exposed to sudden changes in surface properties (topography, surface roughness, thermal properties due to presence of land as well as wake effects) which is difficult to solve (Liu, 2009). Indeed, this topographic signature, also noted by Liu (2009), is due to the fact that the model computation point used (closest point) does not have the proper physical description (surface roughness and topography) to describe the analysed site. The model considers the position of that point to be in the Gulf of Saint-Lawrence, rather than on land, and thus, over-estimates the wind that is actually over a complex terrain and on land.

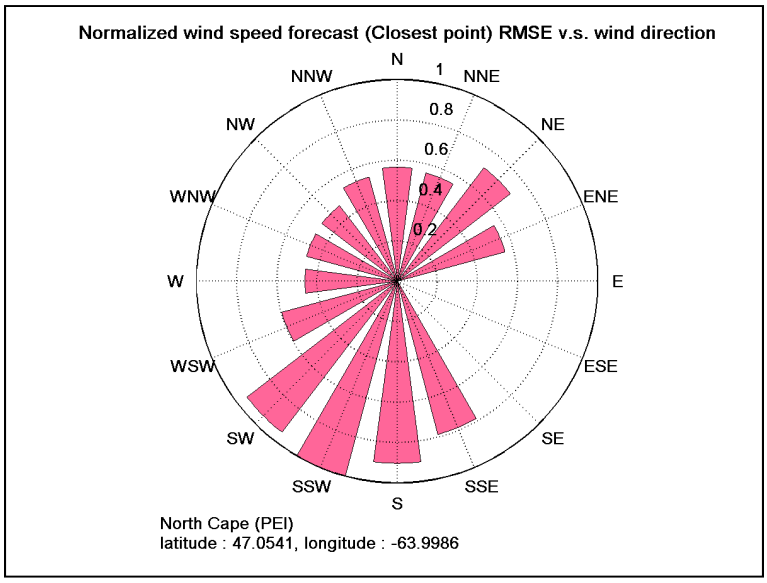

Figure 4.3 Annual wind speed forecast RMSE rose for the North Cape site (closest forecast point).

Based on this analysis and on the site inspection, it is evident that the model does not have sufficient grid spacing refinement to properly represent the meteorological phenomena on the coastal site. It is well known that the grid spacing influences the accuracy of the NWP models for complex sites, which remains a continuing concern in wind power predictions since NWP models do not solve geophysical features smaller than the grid size. Doubling the spatial and temporal resolution of the NWP models would increase the running time by a factor of at least eight, which is not computationally possible if a short term wind power forecast is needed. Also, in the present case, there is a shore line discontinuity in the surface roughness and no realistic mesh refinement could solve that condition. For these several reasons, a GMOS taking into account the site geography and the meteorological situation is developed in order to properly represent the site geography and the meteorological behaviour while being computationally inexpensive.

CHAPTER 5

GEOPHYSIC MODEL OUTPUT STATISTICS

As mentioned in the previous chapter, the preliminary analysis shows that there is a need for a Geophysic Model Output Statistics (GMOS) to reduce the topographic signature within the wind speed predictions. Therefore, many types of GMOS are developed and applied in the present section: geo-referenced weighting, linear regressions and ANN. Finally, they are compared to a reference model developed from simple mathematical interpolation methods.

5.1 Reference interpolation method

Indeed, when using NWP models in short-term numerical wind power predictions, simple mathematical methods are used to interpolate the wind speed forecast from the NWP outputs. As the closest point (nearest neighbour) interpolation, where the value of an interpolated point is the value of the closest forecast point, is the most widely used method. It is also the simplest scheme to implement. Bilinear and bicubic interpolations are also used by the wind energy industry since they can slightly improve the interpolation without being much harder to implement than the closest point method:

- Bilinear interpolation fits a linear surface through the forecast points from the NWP. This interpolation method combines the values of the four closest points, to determine the value of the interpolated forecast.

- Bicubic interpolation fits a cubic surface using the sixteen closest forecast points. Thus, keeping the first order derivatives continuous, this method produces a much smoother surface than a bilinear interpolation. On the other hand, bicubic interpolation can produce important local variations to fit the first order derivative. Therefore, precautions must be taken when using such method.

These three models are computed on a regular Cartesian grid and they are then tested for both sites. Table 5.1 - 5.2 show the improvement (see Chapter 1) on the bias, MAE and RMSE of the bilinear and the bicubic models compared to the closest point interpolation method:

Table 5.1 Improvement of different mathematical interpolation methods (bilinear and bicubic) compared to the closest point method (North Cape)

Interpolation method	**Bias (%)**	**MAE (%)**	**RMSE (%)**
Bilinear	0.25	0.12	0.07
Bicubic	0.18	0.07	0.03

Table 5.2 Improvement of different mathematical interpolation methods (bilinear and bicubic) compared to the closest point method (Bouctouche)

Interpolation method	**Bias (%)**	**MAE (%)**	**RMSE (%)**
Bilinear	-8.06	-4.00	-3.54
Bicubic	-11.28	-5.27	-5.07

When comparing the results (Table 5.1), one can conclude that, for North Cape site, the bilinear and the bicubic interpolation did not improve significantly the predictions compared to the closest point method since the measurement tower is located close to the closest forecast point (445 m). Furthermore, all the surrounding forecast points have very similar geophysical input parameters and therefore, the computed wind speeds are very similar. These two considerations cause the three interpolations schemes to give very similar results. On the other hand, at Bouctouche site, some of the surrounding forecast points used in the interpolations have very different geophysical fields which cause a significant variation in the wind speed forecast at these points. Therefore, the closest point have the topographic characteristics that correspond the most to the site characteristics and the surrounding forecast points are less representative of the site. Thus, the predictions are degraded by both

bilinear and bicubic interpolations (Table 5.2). Therefore, in the present study, the closest point scheme, which is the most widely used in the industry, is used as the reference interpolation method when comparing other statistical methods implemented in this section.

5.2 Geo-referenced weighting module

In order to reduce the topographic signature of the wind speed predictions, a geo-referenced weighting module is developed. This geo-referenced weighting module uses forecast model inputs such as topography, surface roughness, distance between grid points and measurement site as well as wind direction forecast output to weigh the closest 49 grid points in order to identify the best points that properly represent the site topography for any forecasted wind direction.. 49 grid points (17.5 x 17.5 km) are used since GEM-LAM is piloted by GEM Regional (15 km) and that the geostrophic winds are assumed to be constant within this area.

First of all, the equations computing the weighting parameters used in this interpolation module are developed. The topographic height and the surface roughness are already known since they are part of the NWP inputs. Then, the computed variables are the distance between grid points and the measurement tower as well as the direction of every grid point in relation to the tower. These parameters are computed from the Earth radius used in the NWP model, along with the latitude and the longitude of the grid and measurement points (equations 5.1 – 5.7). Figure 5.1 shows the geographical parameters to be computed:

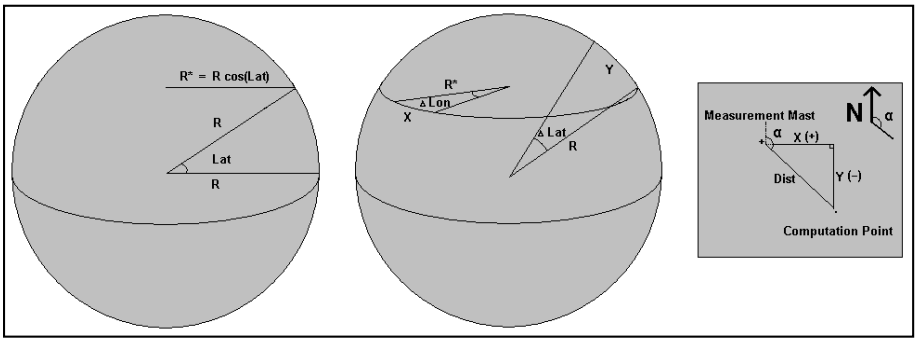

Figure 5.1 Representation of the geographical parameters.

$$R^*_{Earth} = R_{Earth}\cos(Lat^*) \tag{5.1}$$

$$X = R^*_{Earth}\,(Lon - Lon^*) \tag{5.2}$$

$$Y = R_{Earth}\,(Lat - Lat^*) \tag{5.3}$$

$$Dist = \sqrt{X^2 + Y^2} \tag{5.4}$$

$$\alpha = \cos^{-1}({}^{Y}/_{Dist}) \tag{5.5}$$

$$\alpha = \begin{cases} 360° - \alpha, & X < 0 \\ \alpha, & X \geq 0 \end{cases} \tag{5.6}$$

$$\varphi = \begin{cases} |\alpha - \beta|, & |\alpha - \beta| \leq 180 \\ 360° - |\alpha - \beta|, & |\alpha - \beta| > 180 \end{cases} \tag{5.7}$$

Where: R_{Earth} is the approximated Earth radius at the equator (0.637122 x 10^7 [m]);

- R^*_{Earth} is the axial Earth radius at the site latitude [m];
- Lat is the latitude of the grid point considered [°N];
- Lon is the longitude of the grid point considered [°E];
- Lat^* is the latitude of the WEICan measurement mast (47.054082 [°N]);
- Lon^* is the longitude of the WEICan measurement mast (296.00135 [°E]);
- X is the relative distance along the longitude axis from the measurement point [m];
- Y is the relative distance along the latitude axis from the measurement point [m];
- Dist is the total relative distance from the measurement point [m];
- α is the orientation of the grid point from the measurement point (North is at 0 °);
- β is the wind direction (β = 0 ° from North and β = 90 ° from East);
- φ is the angle between the wind direction and the grid point orientation [0 – 180 °].

Note that, as the geo-referenced weighting module is much easier to compute when using a Cartesian grid, the Earth surface curvature considered in the NWP model is neglected over the small area in this study (17.5 km x 17.5 km). Also, in this study, the NWP model horizontal grid points are not equally spaced, but as mentioned earlier, for simplicity purposes, it is considered to be equally spaced by the average grid spacing distance (2.5018 km). To verify that this consideration is not biased, the STD of the grid spacing to the average has been computed for that area. A STD of $2\text{x}10^{-3}$ km compared to an average value of 2.5018 km shows that this approximation is not causing any harm to the methodology, nor to the results.

Before implementing a geo-referenced interpolation module with all the parameters, it is necessary to validate that every proposed parameters are essential to the method. Simple interpolation modules are first implemented using one parameter at a time and are compared to the closest point interpolation method. The base weighting factors (W) are computed (equation 5.8) at each computation grid point and for each interpolation parameter: angle between the wind direction and the grid point orientation, distance between measurement and forecast points, surface roughness and topography. For all the parameters, the weighting factors are defined as inversely proportional to the parameter (equations 5.9 - 5.12). As an example, the closest points (small distance) have higher weights than farther computation grid points. In each case, the base weighting factor is normalized using the summation of each computation point parameter as defined previously.

$$W_i = \frac{Parameter_i}{\sum_i (Parameter_i)} \tag{5.8}$$

$$W_{Dist\,i} = \frac{{}^{1}/_{Dist_i}}{\sum_i \left({}^{1}/_{Dist_i}\right)} \Rightarrow Dist_i \geq 1\% \times Resolution_{GEM-LAM} \tag{5.9}$$

$$W_{\varphi_i} = \frac{{}^{1}/_{\varphi_i}}{\sum_i \left({}^{1}/_{\varphi_i}\right)} \Rightarrow \varphi_i \geq 1\% \times 360° \tag{5.10}$$

$$W_{z_{0_i}} = \frac{1/|z_{0_i} - z_{0_{Site}}|}{\sum_i \left(1/|z_{0_i} - z_{0_{Site}}|\right)} \Rightarrow \left|z_{0_i} - z_{0_{Site}}\right| \geq 1\% \times z_{0_{Site}} \quad (5.11)$$

$$W_{H_{Topo_i}} = \frac{1/\left|H_{Topo_i} - H_{Topo_{Site}}\right|}{\sum_i \left(1/\left|H_{Topo_i} - H_{Topo_{Site}}\right|\right)} \Rightarrow \left|H_{H_{Topo_i}} - H_{Topo_{Site}}\right| \geq 1\% \times H_{Topo_{Site}} \quad (5.12)$$

Note that for each parameter, a lower limit (1 % of the environment characteristics) is applied to the value in order to avoid any division by 0: if the value is lower than the limit, it is forced to the limit value, thus considering every point. Then, the wind speed forecast (U) is interpolated by multiplying each grid point value by its respective base weighting parameter (equations 5.13 - 5.16).

$$U_{Dist} = \sum_i \left(W_{Dist_i} \times U_i\right) \quad (5.13)$$

$$U_{\varphi} = \sum_i \left(W_{\varphi_i} \times U_i\right) \quad (5.14)$$

$$U_{z_0} = \sum_i \left(W_{z_{0_i}} \times U_i\right) \quad (5.15)$$

$$U_{H_{Topo}} = \sum_i \left(W_{H_{Topo_i}} \times U_i\right) \quad (5.16)$$

Where: Dist is the total relative distance from the measurement point [m];

- φ is the absolute angle between the wind direction and the grid point orientation [°];
- z_0 is the surface roughness in the model [m];
- $z_{0_{Site}}$ is the surface roughness of the North Cape site (0.25 [m]);
- H_{Topo} is the topographic height of each grid point [m];
- $H_{Topo_{Site}}$ is topographic height at the North Cape site (10.3 [m]);

- W_i is the base weighting factor for every grid point [-];
- U_i is the vertically interpolated wind speed for every grid point [m/s].

Table 5.3 presents the improvement done by interpolating the wind speed predictions using the simple geo-referenced weighting modules compared to the closest point method. Each value presents the improvement of a weighting method compared to the closest point.

Table 5.3 Improvement of different simple geo-referenced weighting schemes compared to the closest forecast point

Interpolation method	**Bias (%)**	**MAE (%)**	**RMSE (%)**
U_{Dist}	4.60	1.60	1.43
U_{φ}	11.93	4.43	4.37
U_{z_0}	18.97	5.77	5.36
$U_{H_{Topo}}$	15.64	5.28	4.94

Analysing Table 5.3, one can see that each and every base weighting parameter improves the wind predictions compared to the reference interpolation model (closest point). Certainly, in this case, the model based on distance slightly improves the forecast since the closest grid point has an important weight compared to other points. However it is expected that this parameter improves the interpolation when coupled with other parameters. Thus, it is important to assure that the interpolation module considers the closest points. Table 5.3 also shows that weighting models based on the wind direction, the surface roughness and the topographic height significantly improve the forecast. Note that a weighting models based on the topographic mask (ground cover ratio) is also tested and compared to the weighting models based on the topographic height. As they give similar results, the model based on the topographic height is kept since it is more convenient: it can be applied to non-coastal sites. Similar results are observed for the Bouctouche site (see Annex V: Table A.V.1).

Overall, all these individual weighting parameters are successfully implemented and they are compared to the closest point interpolation model. In each and every case, the basic geo-referenced weighting significantly improves the forecast compared to the reference method by reducing considerably the MAE and the RMSE. This shows that all these variables are indeed necessary and they are all implemented into a complete geo-referenced interpolation module. Different algorithms can be developed using diverse combining rules such as the weighted product rule or the weighted sum rule (Kittler et al., 1998). These two methods can be applied to merge the different and independent base weighting parameters without any training data set (fixed combining rules). In the present situation, as the base weighting parameters can have high variations in their outcomes, it is suggested to employ the product rule (Duin, 2002). Furthermore, the surface roughness and the topographic height could be correlated. Then it is again recommended to use the product rule for possibly correlated parameters (Bilmes and Kirchhoff, 2000 and Tax et al., 2000). Equation 5.17 details the computation of the product rule to implement the final geo-referenced weighting module:

$$U_{Geo} = \frac{\sum_i \left(W_{Dist_i} \times W_{\varphi_i} \times W_{z_{0_i}} \times W_{H_{Topo_i}} \times U_i \right)}{\sum_i \left(W_{Dist_i} \times W_{\varphi_i} \times W_{z_{0_i}} \times W_{H_{Topo_i}} \right)} \tag{5.17}$$

Where: U_{Geo} is the interpolated wind speed and U_i is the forecasted wind speed [m/s]. Once the interpolation module is implemented, it can be compared to the reference interpolation models, which is the closest point (see section 5.6).

5.3 Linear regressions

Linear regressions using observed data are applied to model the relationship between the NWP and the wind speed measurements by fitting a linear equation. The minimization of the least mean squared (LMS) error method is the most common approach for fitting these regression lines since it is conceptually simple and computationally straightforward, while performing better than the double bias correction (Liu, 2009). It computes the best fitting line for the observed data by minimizing the sum of the squares of the deviations between

each data point and the regression line. Equation 5.18 details the computation of a simple linear regression rule and the minimization of the least square error. It is shown in the matrix representation of equations 5.19 - 5.22:

$$U_{Measure} = A \times U_{Forecast} + B \tag{5.18}$$

$$Matrix = [A\ B]^T \tag{5.19}$$

$$U_{Matrix} = [U_{Forecast}\ 1] \tag{5.20}$$

$$U_{Measure} = U_{Matrix} \times Matrix \tag{5.21}$$

$$Matrix = ({U_{Matrix}}^T \times U_{Matrix})^{-1} \times ({U_{Matrix}}^T \times U_{Measure}) \tag{5.22}$$

Where: $U_{Forecast}$ is the forecast wind speed from the NWP [m/s];

- $U_{Measure}$ is the measured wind speed [m/s];
- Matrix is the matrix containing the statistical parameters to optimize [-];
- U_{Matrix} is the matrix containing the forecast wind speed [m/s].

As mentioned earlier, the GMOS developed and applied to the NWP shall reduce the directional and topographic signature of the wind speed prediction error. Therefore, linear regressions can be applied to weight the different forecast points within the studied area. As the geo-referenced weighting module uses geographic parameters to weigh the different grid points, a linear regression can be used to weigh the surrounding 49 forecasts points (Multi-Point (MP) linear regression), since each one have different geographic characteristics. This GMOS is developed following equation 5.23. Thereafter, as the wind direction seems to be also an important characteristic (see Table 5.3), a linear regression using the same ensemble of 49 predictors can be applied for the different wind directions (Directional Multi-Point (D-MP) linear regression). This method is detailed through equation 5.24:

$$U_{MP\ linear} = \sum_i (A_i \times U_{Forecast_i}) + B \quad (5.23)$$

$$U_{D-MP\ linear_\varphi} = \sum_i (A_{\varphi_i} \times U_{Forecast_{\varphi_i}}) + B_\varphi \quad (5.24)$$

Where: $U_{Forecast_i}$ is the NWP forecasted wind speed from each of the forecast points [m/s];

- A and B are the statistical parameters to optimize [-];
- $U_{MP\ linear}$ is the interpolated wind speed using the MP linear regression method [m/s];
- $U_{D-MP\ linear_\varphi}$ is the interpolated wind speed for each sector of the direction rose (φ) using the D-MP linear regression method [m/s].

Then, the MP linear model equation (5.23) can be solved using the methodology described in the previous sub-section (equations 5.18 - 5.22). However, the D-MP linear model equation (5.24) cannot be solved using the regular least mean square regression (derivative method) because data are too few in some wind directions to fit the regression line, thus, generating large uncertainties. The training dataset being too small to be representative of the general situation, it does not fit properly all the statistical parameters of the model: the model "memorizes" the learning dataset, but generalizes poorly for the new data included in the test database. This situation is called over-learning. Therefore, to train the D-MP linear regression model, it is necessary to use back-propagation training (batch training) algorithm using a gradient descent technique (Hinton, 1989):

1. Initialize the statistical weights (A_{φ_i} and B_φ) to random values.

2. Process all the training data to compute the gradient ($\frac{\partial E}{\partial A_{\varphi_i}}$) of the average error function.

$$E = \frac{1}{2}\left(U_{Measure_\varphi} - U_{D-MP\ Linear_\varphi}\right)^2 \quad (5.25)$$

$$\frac{\partial E}{\partial A_{\varphi_i}} = \left(U_{Measure_{\varphi}} - U_{D-MP\ linear_{\varphi}}\right) \times \frac{\partial\left(\sum(A_{\varphi_i} \times U_{Forecast_{\varphi_i}}) + B_{\varphi}\right)}{\partial A_{\varphi_i}} \qquad (5.26)$$

3. Update the weights (A_{φ_i} and B_{φ}) by subtracting the gradient times a learning rate (lr) and by subtracting the previous adjustment times a momentum constant (mc). Note that the momentum is used to avoid falling in local minima and it speeds up the convergence rate (considering the former update "$\Delta A_{\varphi_i}(t-1)$") since it acts like a damper, which avoids oscillations during the training.

$$\Delta A_{\varphi_i}(t) = -lr \times \frac{\partial E(t)}{\partial A_{\varphi_i}(t)} - mc \times \Delta A_{\varphi_i}(t-1) \qquad (5.27)$$

4. Repeat steps 2 & 3 until the gradient of the average error function for the training set becomes small enough (10^{-10}) or if the average error function for the cross-validation set is not decreased for the last five consecutive iterations. There is no restriction in terms of number of iterations and training time to avoid limiting the performance of the model.

This learning method is also implemented in the MP linear regression module in order to make sure that this methodology does not produce large uncertainties. Applied to the MP linear regression, the batch learning (gradient descent) and the derivative approach gave the exact same results. Therefore, the batch learning methodology permits to the D-MP linear module to find statistical parameters minimizing the quadratic error, since the cross-validation prevents over-learning process due to the lack of data.

5.4 Artificial Neural Networks

As the linear regression are developed to model the relationship between the NWP and the wind speed measurements using different architectures, similar models are developed using Artificial Neural Networks (ANN) to verify if non-linear regressions can perform better than

linear ones for the surface wind prediction problematic. Multilayer Feed Forward ANN, also called Multilayer Perceptron (MLP), are complex non-linear systems inspired by the functioning of the biological nervous system that are constituted of many neurons highly interconnected by synapses.

In the ANN technique, the weighted sum of the inputs (altered by weights) is fed to the neurons of the first layer which process the input signal using an activation function: $f\left(\sum W_{ij} \times z_i\right)$. Then the output of each neuron (z_j) are fed as new inputs to other neurons, constituting the next layer of the network, and so on. The output layer of a multilayer feed forward ANN contains as much neurons as expected model outputs. In the current project, the desired output is the regressed wind speed forecast, so there shall be only one output neuron. In addition, it is possible to use different types of activation functions depending on the nature of the problem to solve: linear, unipolar or bipolar binary function, unipolar (log-sigmoid) or bipolar (tan-sigmoid) continuous function, etc. In the current work, a unipolar continuous function (log-sigmoid) is used since wind speed always has positive values. Figure 5.2 shows the architecture of the current MLP:

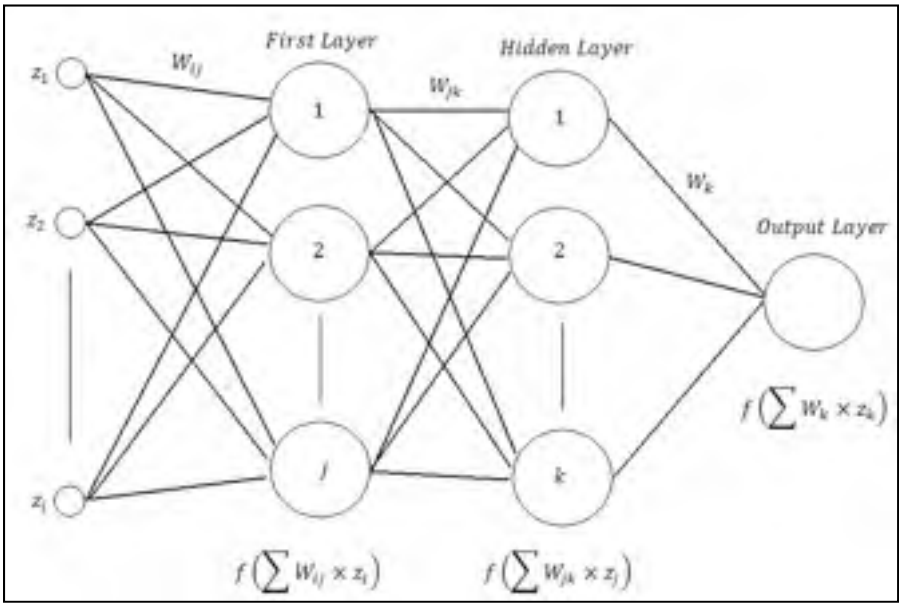

Figure 5.2 Representation of the multilayer ANN architecture.

Subsequently, the network has to be trained using the batch training method as explained earlier: during the training phase, the connection weights are continuously modified. Only when the training process is done, it is possible to test the network by processing the test data. In order to compare non-linear ANN to linear regression for the wind forecast problematic, the same architectures are implemented and tested: an ANN processing the closest forecast point (simple ANN); an ANN processing an ensemble of the 49 closest predictions points (MP ANN) and finally, a group of ANN processing an ensemble of the 49 predictions for each direction of the wind (D-MP ANN). Also, as a proof of concept, a linear regression has been modeled using a single layer containing only one neuron with a linear activation function. When evaluating the simple ANN, the results are the exact same as the simple linear regression outputs. Consequently, ANN have the capability to replicate the linear regression done by simple LMS linear regressions. Now, multilayer non-linear ANN can be implemented to test how they can solve the wind forecast for the atmospheric boundary layer.

Before evaluating such Multilayer Feed Forward ANN, it is important to set the training parameters (momentum constant, learning rate and cross-validation ratio) and to fix the architecture of the Network (number of nods on the first and on the hidden layers). To do so, many different models are trained and validated for different parameter values. For each and every parameter set, 30 replications are made in order to have statistically valid results and the median value is kept. Note that the average value is not used since it is much more influenced by outlying data than the median. As the results of a network are not linearly correlated to its parameters, it is necessary to perform many iterations changing one parameter at a time to approach the optimal value for each parameter. Figure 5.3 shows the results for the different parameters value of the last iteration done.

Looking at this figure, one can see that, as the number of nods on a layer increases, the results are first improved, but by a certain limit, the error starts to increase. This is due to the fact that a network having a large number of nods is able to describe a much more complex phenomenon (higher order of non linearity). But then, as the number of neurons increases,

the number of statistical parameters to set also increases and the network needs more data to be trained to avoid over-learning, thus explaining the "V" shape of the error at the convergence points (two neurons on the first layer and three nods on the hidden layer). On the other hand, the error seems to increase along with the value of the learning rate, showing that a low learning rate (0.01) allows the network to explore, step by step, a large area within the possible solutions. Conversely, the momentum rate converged to a relatively high value (90 %), acting like a strong damper to avoid oscillations during the training and to avoid falling in local minima. Finally, the cross validation rate converged to a value of 75 %, showing that 75 % of the data shall be used to train the network and 25 % for the cross-validation. This is also Matlab's default value (60 % training, 20 % cross-validation and 20 % test), since a totally separate test data series is used.

5.5 Model verification

As previously seen, during model training, the cross-validation helps to avoid over-learning. This technique is especially crucial for the models that have small training database, such as the D-MP linear and D-MP ANN models. These models are using data for the specific wind direction range included in a rose sector. Therefore, they have only part of the total database to be trained (~ 1/16). Subsequently, even if cross-validation is used, these models could still be poorly trained due to the lack of data and may suffer from over-learning. Consequently, the convergence of the error for both the training and validation data shall be verified, in order to assure that they learned properly. Figure 5.4 shows the evolution of the model error on the training and validation database. The graphs contained in Figure 5.4 are plotted using the wind speed database for the northern direction sector since the database related to this sector has fewer data than the other directions (see Figure 5.5 for the frequency distribution of the wind direction).

Verifying the convergence of the models error in Figure 5.4, one can observe that the training and the validation errors converge very closely. This shows that both models (D-MP linear and D-MP ANN) seem not to be affected by any over-learning situation.

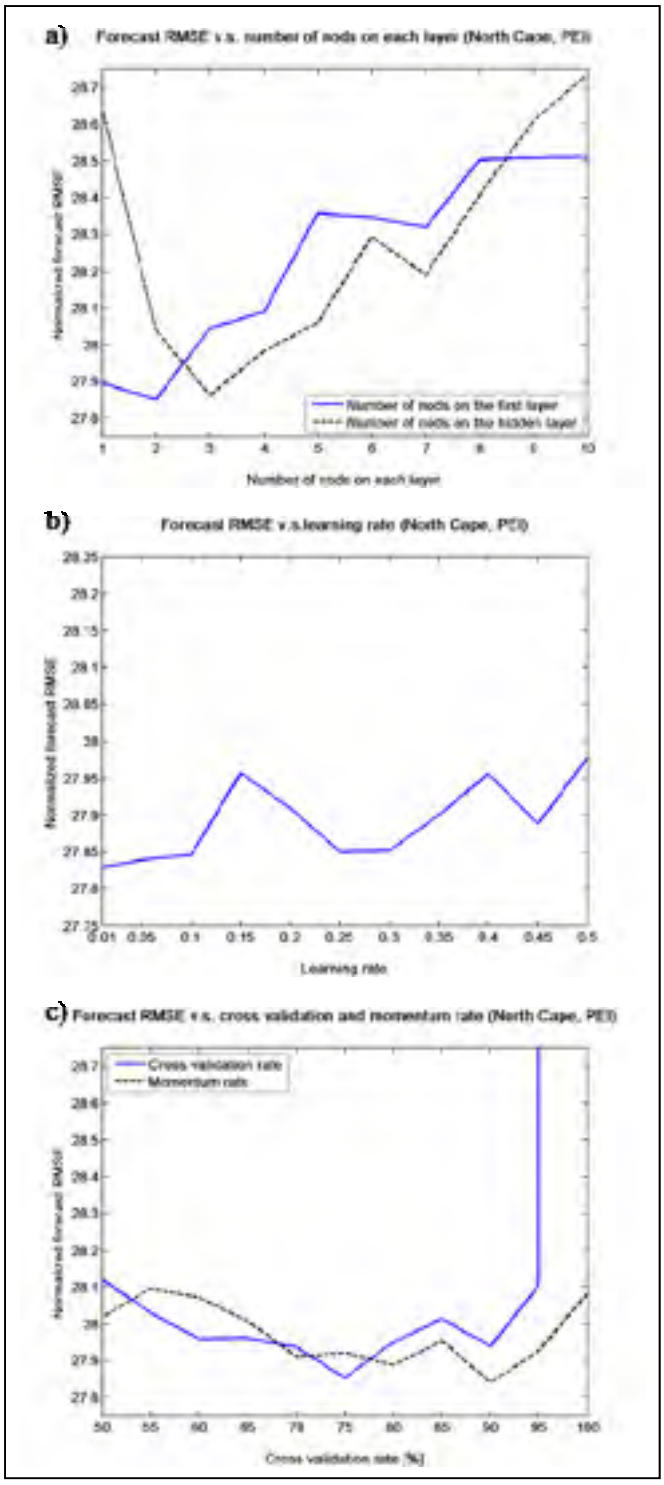

Figure 5.3 ANN forecast RMS error for different parameters: a) number of nods, b) learning rate and c) cross validation and momentum rate.

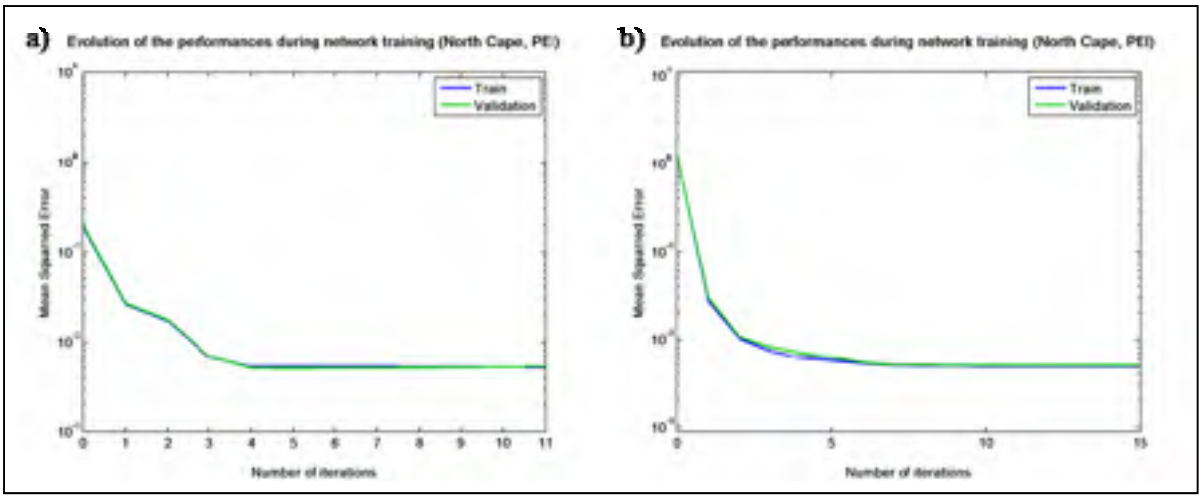

Figure 5.4 Evolution of the performance of the a) D-MP linear and b) D-MP ANN.

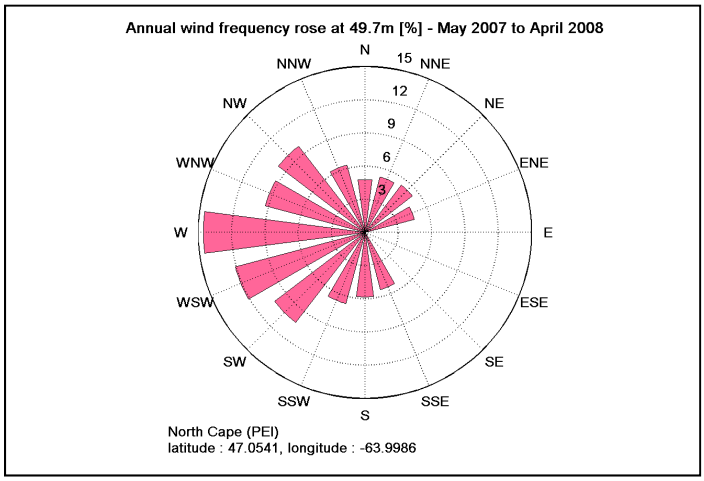

Figure 5.5 Measured annual wind frequency rose.

Now, as each and every model has sufficient data to be trained, the models are tested to verify that they do not induce outlying data. For this purpose, two simple verifications are performed. The first test case verifies that there is no coding error that could influence the quality of the results. The different GMOS are trained and applied to a homogeneous solution (zero forecasted and measured wind speeds) and each GMOS gives zero wind speed outputs, as expected. Then, the second test case applies the different GMOS to a virtual site

having the same geographical location and characteristics as the closest forecast point in order to verify the theoretical performance limit and therefore, the reliability of these models. The outputs of the GMOS are compared to the closest forecast point data and the error is computed for each module. Overall, the mean annual RMSE introduced by the GMOS are very close to zero: the highest RMSE introduced (0.55 %) is attributed to the D-MP ANN. This showed that every module has a theoretical performance limit that is much higher than the NWP performance (36.77 %). Hence, they are all well adapted for GMOS applications.

Finally, the verification of the proposed modules done in this section shows that each GMOS has sufficient data to be trained without being affected by any over-learning situation, that there is no coding error and that the theoretical performance limit of the proposed modules are sufficiently high to be used along with the NWP at Environment Canada. These different GMOS are then validated and compared using the test data in the next section.

5.6 Comparison of the different GMOS

As all parameters are set for every method, each interpolated NWP can now be compared. The improvement of the different regression methods is detailed for the North Cape site (PEI) and the forecast error is analysed for different time series and different meteorological variables. As the same conclusions are found for Bouctouche site, the results are presented in Annex V (see Table A.V.2). Table 5.4 shows the detailed performance improvement of the different regression methods compared to the closest point for the North Cape site:

Looking at Table 5.4, one can easily conclude that all implemented GMOS improve significantly the NWP. As the geo-referenced method is well suited for application where no historical atmospheric records are available, there is a significant improvement to use such past recorded data to train the GMOS (linear regressions or ANN). In addition, both linear and non-linear (ANN) methodologies gain to use the surrounding forecast points (MP architecture). This is due to the fact that these forecast points have different geographical characteristics that are taken into account indirectly when weighting each of them. This

improvement is comparable to the improvement done when integrating the geographical characteristics into the geo-referenced approach (with no historical atmospheric records). In every case, except for the D-MP architecture, the ANN has an advantage on the linear scheme. However, the integration of the wind direction (D-MP architecture) in the GMOS improved once more the wind predictions, especially for the linear scheme (D-MP linear). For this architecture (D-MP), there isn't much difference between the results of the linear and the ANN approaches. Moreover, the improvements results of the MP ANN and the D-MP ANN are almost the same. Therefore, it is possible to conclude that, for this particular correlation problem, the non-linearity in the relation between the NWP and the wind speed measurements have almost completely been taken into account by the geographical parameters and especially the wind direction. Subsequently, there seems to be no need of ANN methods (non-linear) to resolve this correlation problem, since it is shown that the non-linearity can be detailed by physical parameters which are known a priori. Figure 5.6 presents the scatter plot of the measured wind speed vs the forecasted wind speed for a selected wind direction sector (North). This graph shows that the correlation between the forecasted and measured wind speed is almost linear for low wind speed in a given wind direction. Therefore, as the cut-out speed of a wind turbine is generally set to 15 m/s, even if the ANN slightly outperforms the linear model for the D-MP architecture, the difference may not be perceived in terms of wind power generated.

Table 5.4 Improvement of the different regression methods

Interpolation method	**Bias (%)**	**MAE (%)**	**RMSE (%)**
Geo-referenced	21.16	7.76	7.75
Simple linear regression	96.61	16.11	17.68
MP linear regression	97.37	19.87	17.24
D-MP linear regression	98.70	27.67	27.07
Simple ANN	98.28	17.87	19.33
MP ANN	96.56	25.68	25.93
D-MP ANN	95.99	28.36	27.70

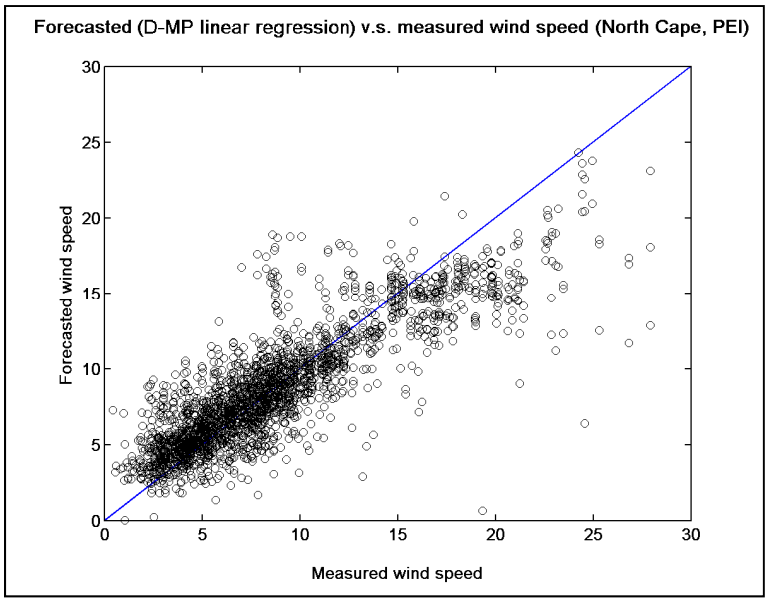

Figure 5.6 Scatter plot of the measured and the forecasted wind speed (northern direction sector).

Afterwards, the results for some of the main interpolation modules are incorporated on common graphs for comparison purposes for the North Cape site (see Figures 5.7 - 5.10). Note that in every figure presented, the wind speed forecast error is normalized with the annual mean wind speed. Each graph shows the performance of the closest point interpolation, the geo-referenced weighting module, the linear regressions modules (simple, MP and D-MP architecture), the MP ANN and the D-MP ANN models. For readability purposes, the two other modules are not plotted in order to not overload the graphs. Consequently, Figure 5.7 presents the forecasted error for different time series (diurnal cycle and 24h forecast time horizon). In the forecast horizon comparison, the interpolation modules are also compared with the new reference model (see Chapter 2) developed by Nielsen et al. (1998). Figure 5.8 presents the forecasted error for different meteorological conditions and Figure 5.9 shows the wind speed forecast error rose of each interpolation method. Similarly, Figure 5.10 shows the improvement of each interpolation method compared to the closest point method for each wind direction sector. Note that the values in each graph are normalized with the highest value in the respective graph. Again, because of

the similarity of the results, the results for the Bouctouche site are presented in the annexes (see Annex V: Figures A.V.1 – A.V.4). The only difference that can be seen between the two sites is that, as expected, the forecast error (when compared to the new reference model) is greater for the Bouctouche site since the NWP model does not take into account the displacement of the surface height due to the density of the forest canopy (see section 2.2).

Analysing Figure 5.7, one can easily conclude that all regression modules implemented improve the closest point NWP output. However, the D-MP linear regression and D-MP ANN still perform better than all other methods for all time horizons and for the complete diurnal cycle. Moreover, Figure 5.7 shows that the modules using this architecture perform better than the new reference model from a 2 h horizon instead of 4 h if no GMOS is applied. This is a significant improvement since the persistence offers exceptional forecast capabilities for short-term forecasts up to 3 - 6 h (Landberg and Watson, 1994; Liu, 2009).

Furthermore, the D-MP GMOS improves the wind speed forecast for most of the meteorological conditions in Figure 5.8. On the other hand, there are few meteorological events where regression modules do not improve significantly the NWP: for highly unstable convective atmospheric boundary layer (only for the North Cape site) and for high wind speeds (higher than 12 m/s).

Analysing Figure 5.9 - 5.10, one can see that the general performance of the geo-referenced weighting module slightly reduces the topographic signature of the forecast error that is observed mainly for southern winds. But, when looking further, it is evident that the linear regressions and the ANN modules are superior to the closest point method and the geo-referenced weighting module for each wind direction. Using those methods, the topographic signature within the error rose is significantly decreased. Also, it is interesting to note that the general error and its geographic signature are almost totally eliminated when using the D-MP modules.

Finally, the D-MP linear method always performs better than all other schemes implemented and tested, except for the D-MP ANN which had similar results. This finding is valid for all time series and almost all atmospheric conditions, including critical meteorological conditions such as low pressure systems. Although the GMOS has been validated using a second complex site, there might be some limitations on the improvement that can be achieved on surface wind forecast (compared to micro-scale models based on computational fluid dynamics (CFD)) for highly mountainous sites or for very simple sites (flat terrain or off-shore). Conversely, as such statistical module integrates geophysical parameters as well as the forecasted wind direction, one can consider that it will still outperform regular MOS that does not assimilate such physical characteristics. Also, GMOS using historical data as training dataset can easily integrate effects (e.g. wind turbine wake effect) that are not simple to integrate into CFD codes, which present another advantage using statistical methods such as GMOS. Since the main goal of this regression module is to reduce the topographic signature of the forecast error and to improve the NWP without being computationally expensive, the D-MP linear approach is used as the GMOS to process the NWP outputs for wind power forecast.

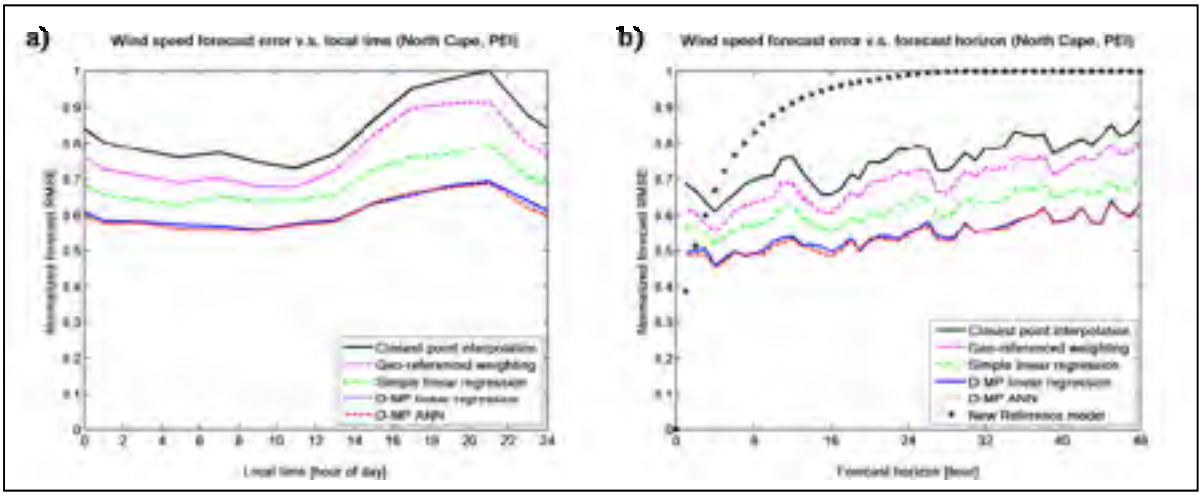

Figure 5.7 Wind speed forecast RMS error for different time series at the North Cape site: a) local time and b) forecast horizon (up to 48 h).

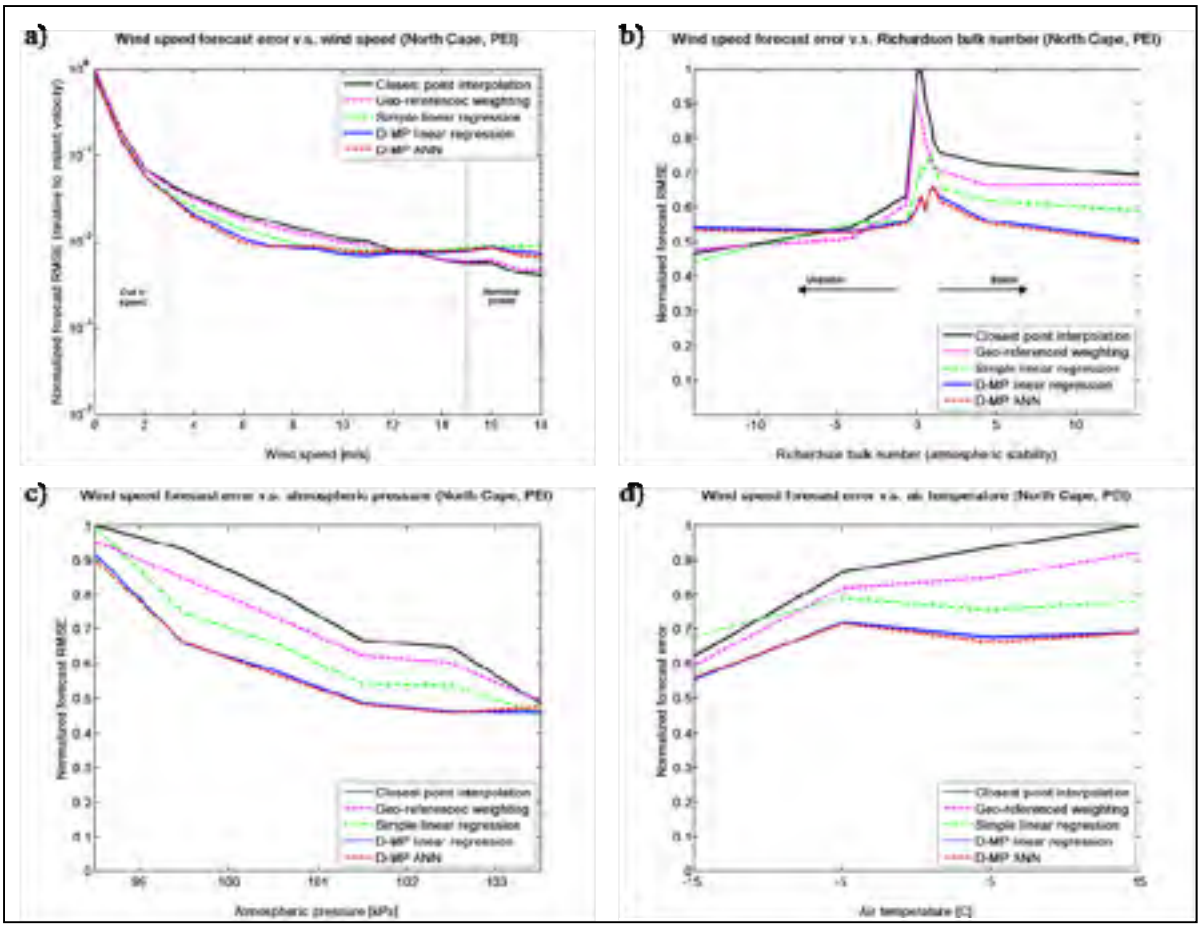

Figure 5.8 Wind speed forecast RMS error for different meteorological parameters at the North Cape site: a) wind speed, b) atmospheric stability (bulk Richardson number), c) atmospheric pressure and d) air temperature.

Figure 5.9 Wind speed forecast RMS error rose of each regression method at the North Cape site: a) closest point, b) geo-referenced weighting, c) simple linear regression, d) D-MP linear regression and e) D-MP ANN.

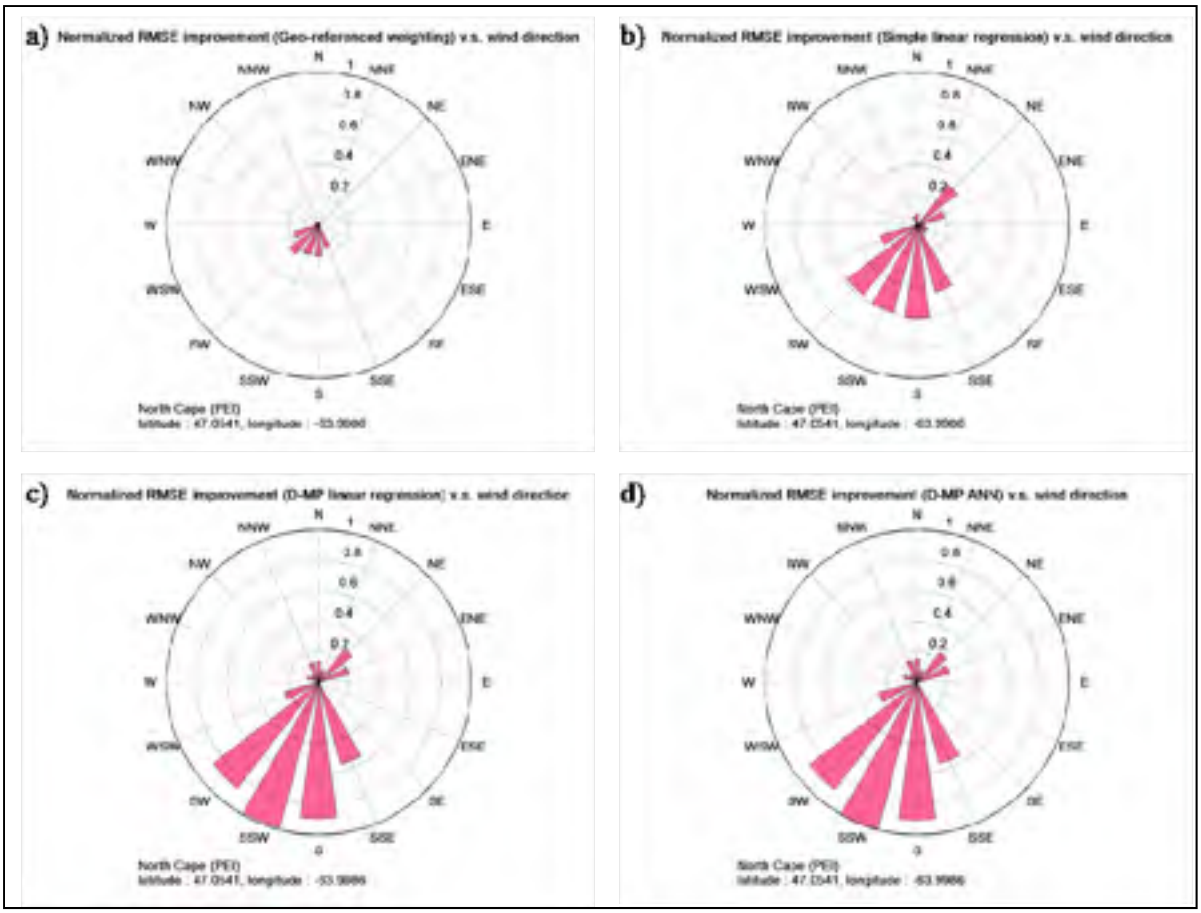

Figure 5.10 Improvement rose of each regression module compared to the closest point at the North Cape site: a) geo-referenced weighting, b) simple linear regression, c) D-MP linear regression and d) D-MP ANN.

CHAPTER 6

STATISTICAL ANALYSIS AND NWP MODEL VALIDATION

As the forecast error due to the lack of horizontal resolution in the NWP model has been significantly reduced using a GMOS, it is now possible to assess and understand the NWP errors on their amplitude and phase for different meteorological situations. Therefore, a methodology is presented in the first section of this chapter (section 6.1) to decompose the forecast error into phase and amplitude parts. This methodology is then validated in section 6.2 and finally, section 6.3 presents the results of this error assessment on the NWP for complex sites.

6.1 Assessment of the phase and amplitude error contributions

In his PhD thesis, Lange (2003) described simple algebraic expressions to decompose the RMSE into bias and STD from the basic definitions of the error ($\in$):

$$\in = U_{Forecast} - U_{Measure} \tag{6.1}$$

$$RMSE = \sqrt{\overline{\in^2}} \tag{6.2}$$

$$RMSE^2 = \overline{\in^2} \tag{6.3}$$

$$bias = \overline{\in} \tag{6.4}$$

$$bias^2 = \overline{\in}^2 \tag{6.5}$$

$$STD^2 = \overline{(\in - \overline{\in})^2} \tag{6.6}$$

$$STD^2 = \overline{(\in^2 + \overline{\in}^2 - 2\ \in\overline{\in})} \tag{6.7}$$

$$STD^2 = \overline{\in^2} + \overline{\overline{\in}^2} - \overline{2\ \in\overline{\in}} \tag{6.8}$$

$$STD^2 = \overline{\in^2} + \overline{\in}^2 - 2\ \overline{\in}^2 \tag{6.9}$$

$$STD^2 = \overline{\epsilon^2} - \bar{\epsilon}^2 \tag{6.10}$$

$$RMSE^2 = bias^2 + STD^2 \tag{6.11}$$

Then, following the notation from Hou et al. (2001), the STD is decomposed in two parts related to phase and amplitude of the error. The idea here is to isolate the systematic error (bias) and the amplitude component of the error to find the mathematical expression describing the dispersion (DISP) between the forecasted and the measured wind speed (i.e. phase error). The amplitude error is defined as the difference between the STD (SDBias) of the forecasted and measured wind speed:

$$SDBias = \sigma(U_{Forecast}) - \sigma(U_{Measure}) \tag{6.12}$$

Therefore, the STD can be decomposed as:

$$STD^2 = \overline{(U_{Forecast} - \overline{U_{Forecast}} - (U_{Measure} - \overline{U_{Measure}}))^2} \tag{6.13}$$

$$STD^2 = \overline{(U_{Forecast} - \overline{U_{Forecast}})^2} + \overline{(U_{Measure} - \overline{U_{Measure}})^2} - \overline{2(U_{Forecast} - \overline{U_{Forecast}})(U_{Measure} - \overline{U_{Measure}})} \tag{6.14}$$

Using the cross-correlation (r), the linear dependence of two variables is described as:

$$r(U_{Forecast}, U_{Measure}) = \frac{\overline{(U_{Forecast} - \overline{U_{Forecast}})(U_{Measure} - \overline{U_{Measure}})}}{\sigma(U_{Forecast})\sigma(U_{Measure})} \tag{6.15}$$

$$STD^2 = \sigma^2(U_{Forecast}) + \sigma^2(U_{Measure}) - 2\sigma(U_{Forecast})\sigma(U_{Measure})r(U_{Forecast}, U_{Measure}) \tag{6.16}$$

$$STD^2 = \sigma^2(U_{Forecast}) + \sigma^2(U_{Measure})$$
$$-2\sigma(U_{Forecast})\sigma(U_{Measure}) + 2\sigma(U_{Forecast})\sigma(U_{Measure})$$
$$-2\sigma(U_{Forecast})\sigma(U_{Measure})r(U_{Forecast}, U_{Measure}) \quad (6.17)$$

$$STD^2 = \left(\sigma(U_{Forecast}) - \sigma(U_{Measure})\right)^2$$
$$+2\sigma(U_{Forecast})\sigma(U_{Measure})\left(1 - r(U_{Forecast}, U_{Measure})\right) \quad (6.18)$$

$$STD^2 = SDBias^2 + 2\sigma(U_{Forecast})\sigma(U_{Measure})\left(1 - r(U_{Forecast}, U_{Measure})\right) \quad (6.19)$$

Then, the DISP can be express as the following mathematical expression (equation 6.20). Thus, it gives a relation between the RMSE, the systematic error (bias), the amplitude error (SDBias) and the phase error (DISP):

$$DISP^2 = 2\sigma(U_{Forecast})\sigma(U_{Measure})\left(1 - r(U_{Forecast}, U_{Measure})\right) \quad (6.20)$$

$$RMSE^2 = bias^2 + SDBias^2 + DISP^2 \quad (6.21)$$

6.2 Validation of the error assessment methodology

Following the definition of the amplitude error (SDBias), the mathematical expressions derived in section 6.1 permits to express the RMSE as a function of the systematic error (bias), the amplitude error (SDBias) and the phase error (DISP). Therefore, before applying such mathematical decomposition to assess the NWP uncertainty, it is important to validate that the definition of the amplitude error is adequate, as the mathematical decomposition relies on that hypothesis. To do so, this methodology is applied to three simple test cases using synthetic wind measurements over 24 h where the type of error is known a priory (see Figure 6.1):

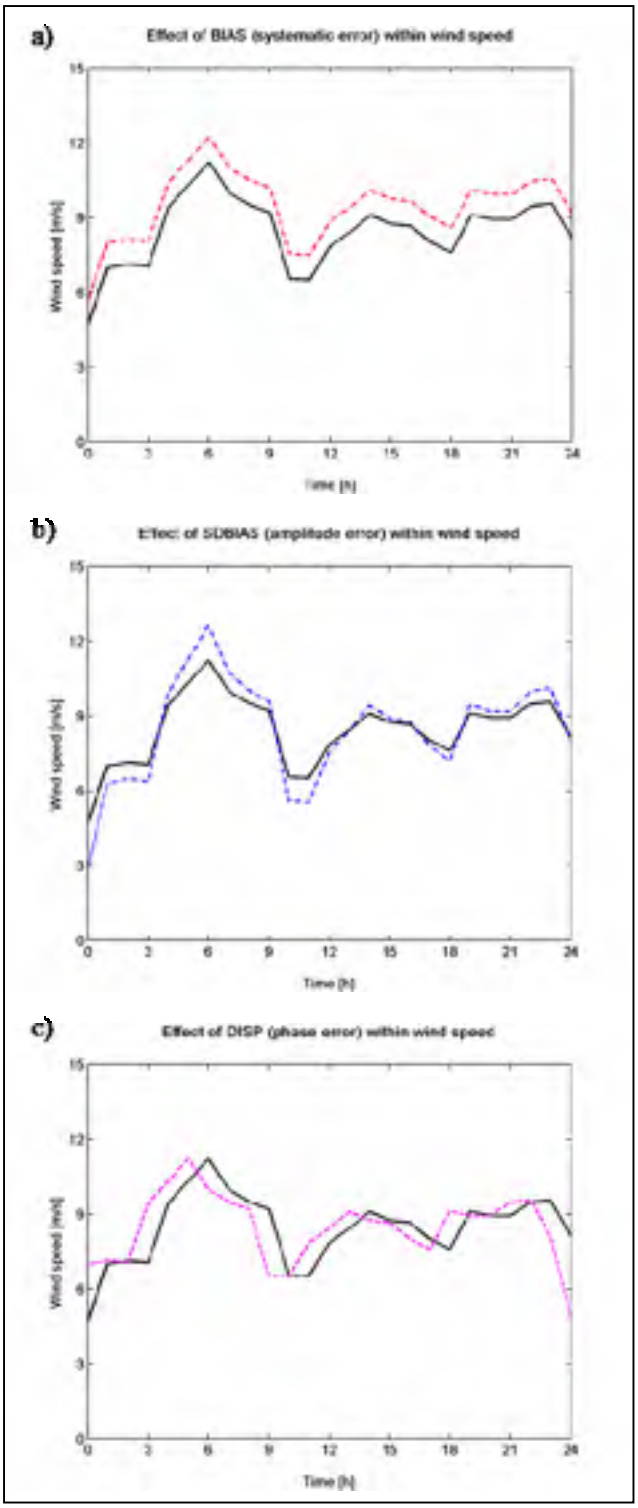

Figure 6.1 Simple test cases on a) systematic, b) amplitude and c) phase errors.

- Systematic error (bias): To express the bias, the wind speed is systematically increased of 1 m/s (no phase or amplitude error).

- Amplitude error (SDBias): To simulate an amplitude error, the wind speed is modified using a linear function, thus keeping the same 24 h average value (bias=0).

- Phase error (DISP): To reproduce a phase error, a 1 h time lag has been introduced in the wind speed time series. Therefore, there shall be no systematic nor amplitude errors.

Then, the mathematical expressions derived in section 6.1 are applied to these three test cases in order to verify the validity of the methodology. The results of this experiment are shown in Table 6.1. Looking at Table 6.1, one can see that this methodology is able to describe properly each type of error: when a time lag is introduced, it only perceives a phase error (DISP); for a systematic increase of the wind speed, the mathematical decomposition indicates a bias; finally, for a linear scaling error keeping the same average wind speed, the method point out an amplitude error, which is correct. Moreover, note that, in every case, the quadratic sum of the bias, the SDBias and the DISP always equals the RMSE, which respects equation 6.9.

A second validation has been conduced to verify that the DISP parameter could effectively describe the phase error in a wind forecast application. In that experiment, for each measured data within a one year database, the best wind speed forecast has been selected in a time window of fixed duration. Therefore, one can expect that as the time window duration increases, the phase error is reduced accordingly. Note that, in order to keep the graphs as clear as possible, the legend appearing in Figure 6.2 is used to describe the curves appearing in every figures of the present chapter. Subsequently, Figure 6.3.a shows the variation of the wind speed forecast error as a function of the time window duration. The time windows shown range from zero to twice the autocorrelation time scale (before and after the forecast time stamp) which is computed (Chapter 2, equation 2.15) using the autocorrelation function

of the wind speed shown in Figure 6.3.b. The computed autocorrelation time scale is approximately 3 h.

Table 6.1 Results of the test cases on systematic, amplitude and phase errors

Test Case	**Criteria**	**Error (%)**
Systematic error	$RMSE^2$	1.4
	$Bias^2$	1.4
	$SDBias^2$	0.0
	$DISP^2$	0.0
Amplitude error	$RMSE^2$	0.7
	$Bias^2$	0.0
	$SDBias^2$	0.7
	$DISP^2$	0.0
Phase error	$RMSE^2$	2.3
	$Bias^2$	0.0
	$SDBias^2$	0.0
	$DISP^2$	2.3

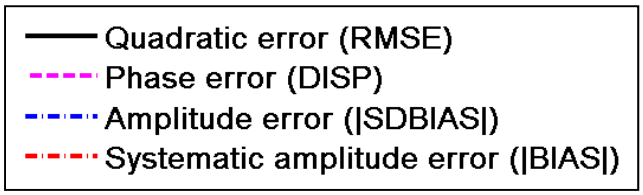

Figure 6.2 Legend for the NWP uncertainty assessment on amplitude and phase errors.

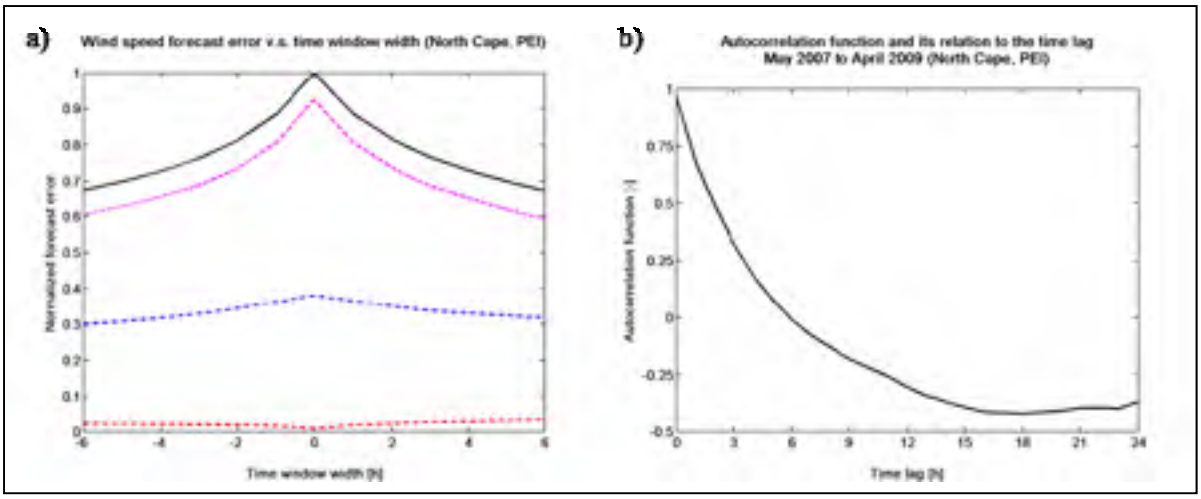

Figure 6.3 a) Variation of the wind speed forecast error as a function of the time window duration and b) autocorrelation function of the forecasted wind speed.

Looking at Figure 6.3, one can see that, as expected, the phase error decreases as the time window duration increases and conversely, the amplitude and the systematic errors tend to stay more or less constant. Thus, these two validations showed that this mathematical decomposition can be applied to assess the phase and amplitude errors of the NWP.

6.3 Assessment of the forecast errors for complex sites (NWP with GMOS)

As the methodology detailed in section 6.1 shows the capacity to identify phase and amplitude errors within the wind predictions, it is applied to the NWP outputs to detail the forecast errors for the North Cape and the Bouctouche sites. The RMSE characteristics (phase, amplitude and systematic errors) are computed for different time series and different meteorological conditions in all wind directions (including dynamical events). The results for the North Cape site are shown in Figures 6.4 - 6.7, while those for the Bouctouche site can be found in the annexes since the results are very similar for both sites (see Annex VI: Figures A.VI.1 – A.VI.5).

Looking at Figures 6.4 - 6.6, one can see that for most meteorological conditions, for all wind directions and all time series, the phase error is dominant compared to the bias and the amplitude errors. This is partially due to the fact that the GMOS is applying a linear regression which mainly reduces the systematic errors related to the geophysical fields such as topography, land use, etc. Moreover, the use of 49 GEM-LAM grid points, covering an area of 17.5 x 17.5 km, reduces the phase errors, but also reduces the forecast sharpness which degrades the amplitudes errors (Liu, 2009). Nonetheless, as the RMSE improvement done by applying the GMOS (~ 27 %) are mainly observed in terms of bias and phase errors, the phase errors remain dominant on the amplitude errors with or without using GMOS.

Moreover, in almost all cases (Figures 6.4 - 6.6), the bias is negligible compared to both phase and amplitude errors. Indeed, this fact can be observed for all time series (diurnal cycle and 0 to 48 h forecast horizon in Figure 6.4), for all wind directions (Figure 6.6) and for most meteorological conditions (Figure 6.5): low and high pressure systems; stable, neutral and unstable flow; cold or warm weather. However, when looking at the graph presenting the forecast error in relation with the wind speed (Figure 6.5.a), one can see that the bias is only negligible for wind speeds close to 8 m/s. This is mainly due to the fact that the GMOS has been trained with data having an annual mean value close to 8 m/s and, following the Weibull distributions (see Chapter 2: Figure 2.12), data having a wind speed close to that value present a high frequency of occurrence. Consequently, when getting away from the median value (generally close to the mean), the frequency of occurrence decreases. Therefore, as the statistical module is trained by minimizing the forecast error (mainly bias and amplitude error) for one year of data, the bias tends to be lower for data having a higher probability of occurrence (i.e. close to the mean).

On the same graph (Figure 6.5.a), it is also possible to observe that the normalized errors (RMSE, bias, SDBias and DISP) are quite higher for low wind speeds, which is normal since these values are normalized using the instantaneous wind speed. Therefore, the relative contribution of a 1 m/s error is five times higher for a nominal wind speed of 2 m/s than for 10 m/s. Moreover, the high forecast error for very low wind speed can be partially explained

by the fact that a minimum floor number of 2 m/s is set for wind speed when computing the surface fluxes in GEM-LAM (momentum, latent and sensible heat fluxes). This operation is mostly done to avoid decoupling of the surface and of the atmosphere in low wind and stable conditions, but also to mediate the impact of unrealistic surface roughness in the regional model which is too high. Therefore, by setting a minimum wind speed on the ground when computing the surface fluxes, the vertical exchanges in the atmospheric boundary layer are increased, which also influence the resulting wind speed forecast by slightly increasing its value. This issue has been pointed out by Environment Canada team and they are currently working to correct that problem in the NWP model. Nonetheless, the forecast error for the database used in the current study presents that imperfection and it partially explains the high forecast error for low wind speed. Nevertheless, this imperfection does not affect much the wind power forecast since the cut in speed of the turbines is generally higher than 2 m/s and, therefore, the power production is null for these low wind speeds.

Moreover, when looking at the forecast error in relation with the atmospheric stability (Figure 6.5.b), it is possible to point out that the model does not perform as well for the neutral case as it does for unstable and stable cases. Indeed, this intermediate situation, which generally occurs in the day-night transition, is quite hard to predict as the atmosphere slowly becomes stable: the thin stable layer is developed from above the ground and increases in height as the ground temperature cools down. As a matter of fact, as the two first computation levels are approximately located at 45 and 135 m AGL, the vertical resolution in the NWP model cannot describe properly the development of this thin stable layer ranging from zero to a few hundred meters during the day-night transition (neutral atmospheric conditions). The difficulty to model the development of the stable boundary layer also explains the increase in the forecast error at the sunset, which can be observed in Figure 6.4.a. This is consistent with the conclusions of Lange (2003) and Liu (2009).

Subsequently, looking at Figure 6.5.c, one can conclude that the barometric pressure influences the forecast precision since low pressure systems, which tend to produce dynamical events, are associated with larger forecast errors than high pressure ones. Indeed,

when looking at Figure 6.7, it is possible to confirm that these dynamical events (rapid changes of the wind speed, the pressure or the temperature), generally associated with low pressure systems, produce a large forecast errors. When verifying the error details, one can see that, during these events, the systematic and the amplitude errors increase as the phase error remains constantly high. Therefore, as noted by Liu (2009), it is possible to conclude that the NWP model generally produces high phase errors for most time series, wind directions and meteorological conditions; high systematic and high amplitude errors are mainly observed during ramping events, which are quite hard to predict due to their dynamical behaviour.

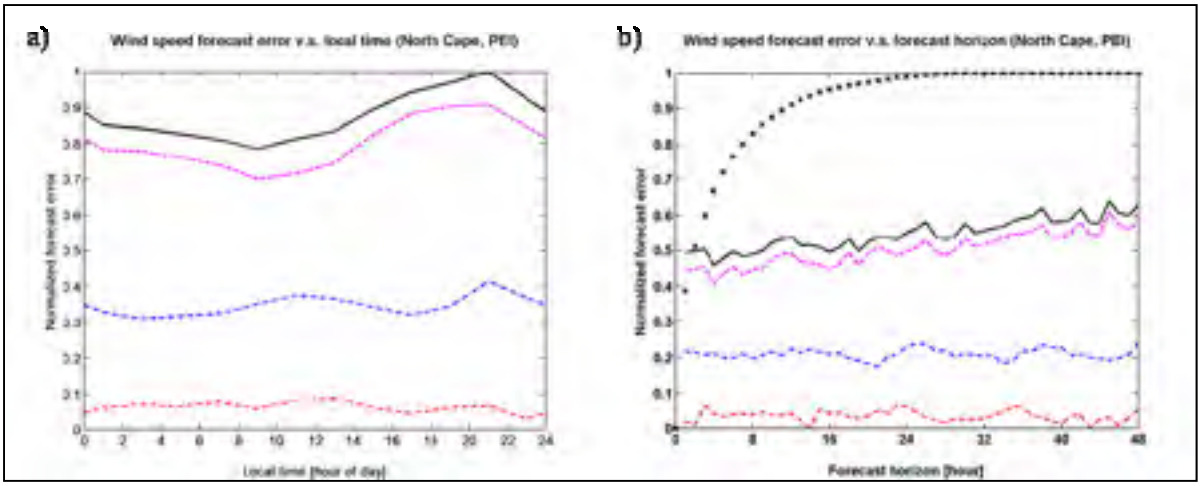

Figure 6.4 Wind speed forecast errors for different time series at the North Cape site: a) local time and b) forecast horizon (up to 48 h).

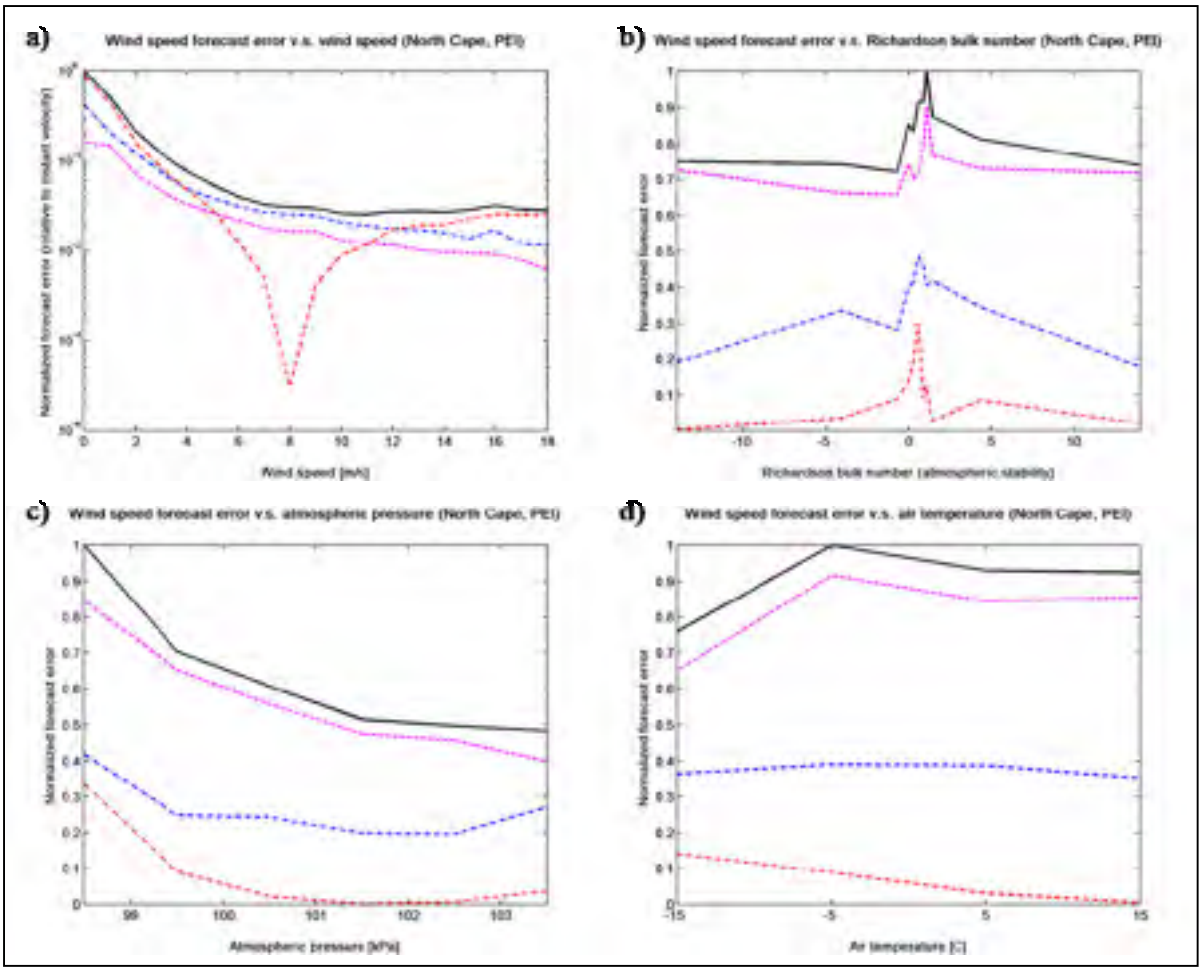

Figure 6.5 Wind speed forecast errors for different meteorological conditions at the North Cape site: a) wind speed, b) atmospheric stability (bulk Richardson number), c) atmospheric pressure and d) air temperature.

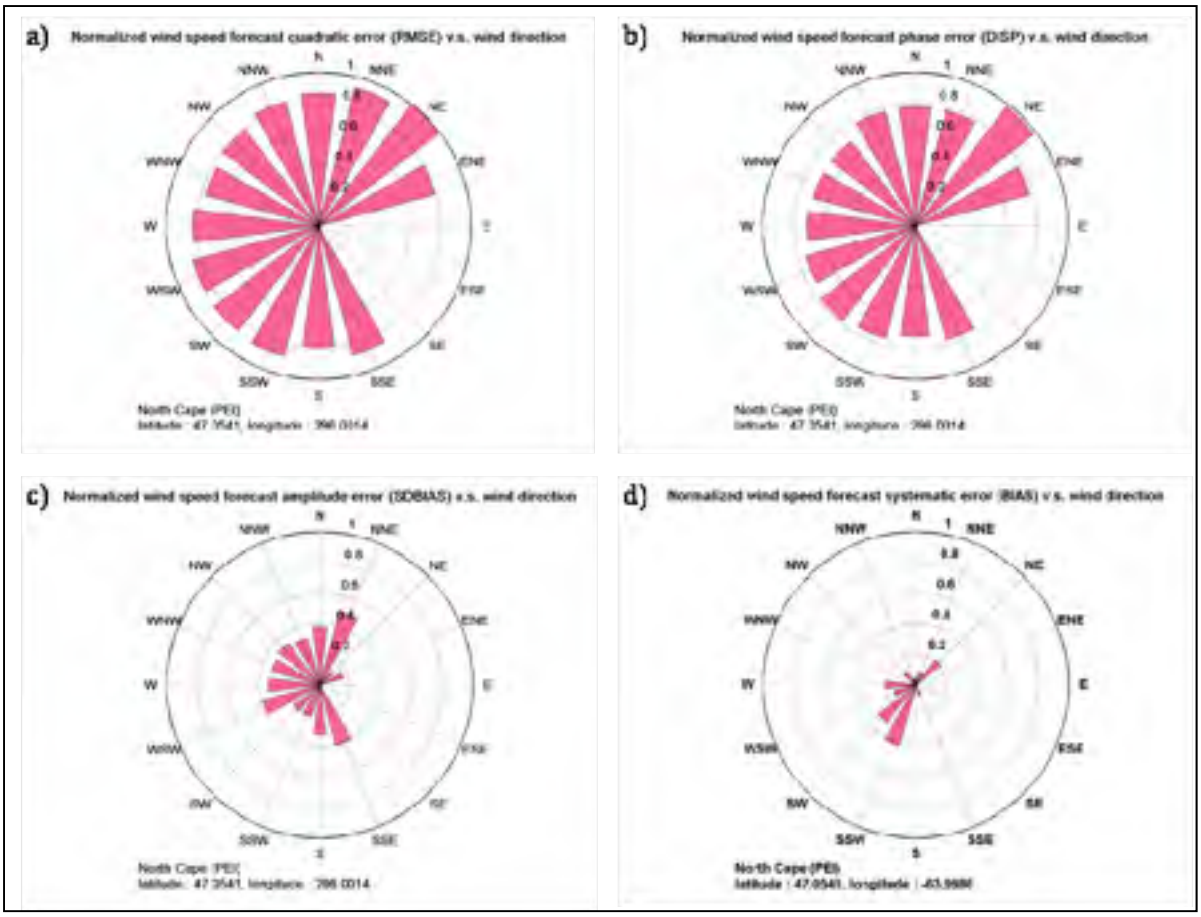

Figure 6.6 Wind speed forecast error roses at the North Cape site: a) RMSE, b) phase error, c) amplitude error and d) systematic errors.

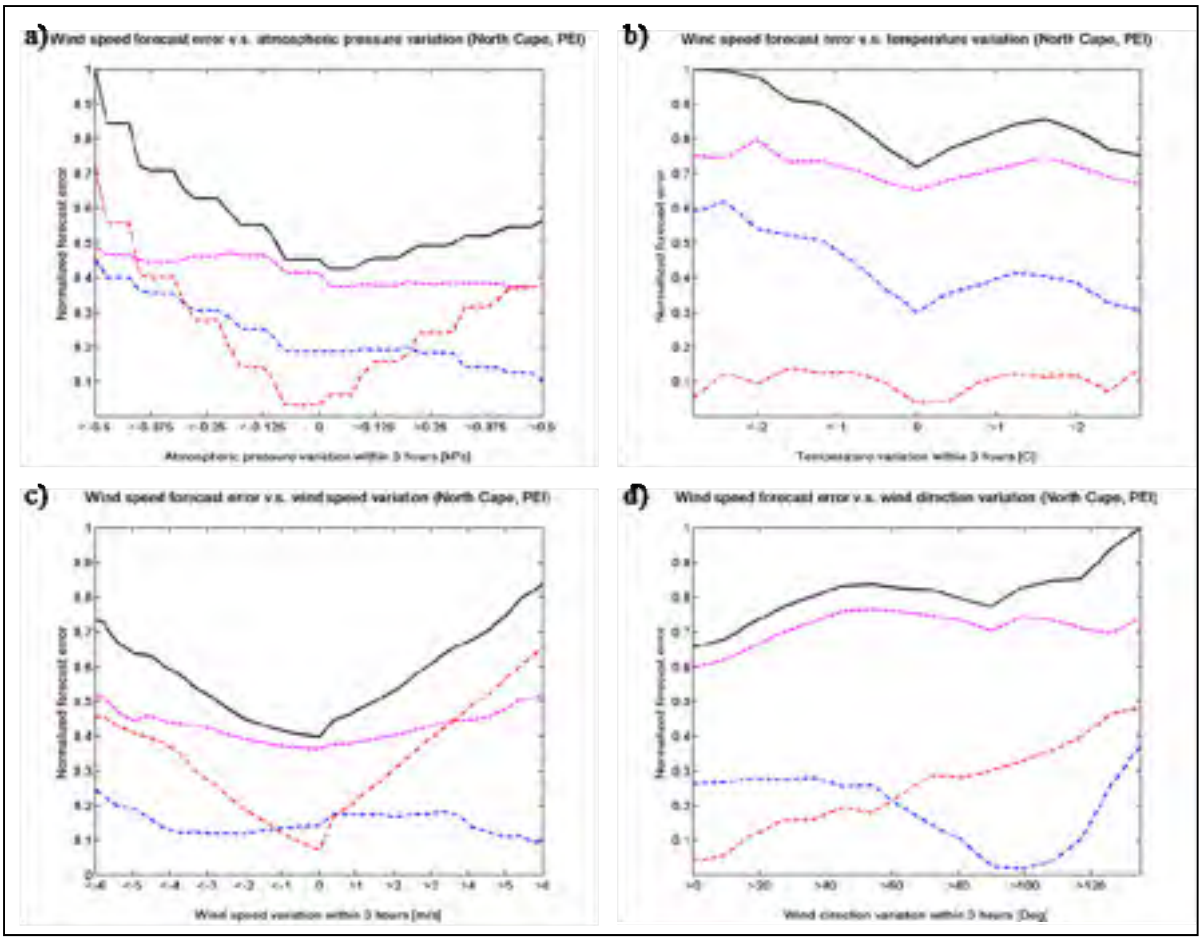

Figure 6.7 Wind speed forecast errors for dynamic meteorological events at the North Cape site: a) pressure variations, b) temperature variations, c) wind speed variations and d) wind direction variations.

CONCLUSION

In preparation for this work, a detailed literature review allowed to understand the wind forecast problem for complex sites. As there is a need for more accurate wind power forecast to properly integrate the wind energy in the electrical utility, the objective of this research work is to present a number of variables that influence the forecast errors and that can be implemented in a statistical module to improve the wind forecasts. Therefore, after performing the data quality analysis and after assessing the errors of the atmospheric measurements, the wind characteristics are established for both analyzed sites (North Cape, PEI and Bouctouche, NB).

Subsequently, the forecasted wind speeds are interpolated vertically. To do so, several vertical interpolation methods are implemented and tested in order to determine which one is the most suitable for wind energy assessments. It appears that simplified non-neutral logarithmic profile, considering the atmospheric stability to be constant with height, do properly represents stable, neutral and unstable air flows in the surface layer. The selection of a proper vertical profile is essential since the behaviour of the atmospheric boundary layer over complex sites is greatly influenced by the atmospheric stability. This assessment also allows to point out that, for dense forest canopies such as seen at the Bouctouche site, the surface roughness is greater than what is expected due to a virtual vertical displacement of the ground surface. Since the NWP model does not consider such vertical displacement to correct the surface roughness, the vertical profile of the wind speed computed does not properly represent the behaviour of the flow for forested sites. It is therefore recommended to consider introducing a vertical displacement in the NWP model for wind profile calculation in densely forested sites. Such misrepresentation of surface properties leads to a systematic underestimation of the wind speed which can be easily corrected by using a MOS.

This led to the conduct of a preliminarily statistical analysis of the GEM-LAM model using one year of meteorological data at North Cape (PEI). This analysis shows that the wind forecast errors are strongly related to the wind direction and the geographical characteristics

of the sites. For this reason, the NWP are downscaled to the test sites using different configuration of GMOS, such as: geo-referenced weighting module, linear LMS regressions and ANN. In subsequent statistical analyses, the different statistical modules are analyzed and compared. The GMOS using the surrounding forecast points as well as the wind direction (D-MP architecture) appears to be superior to all other tested modules. However, the statistical analysis shows that the non-linearity in the correlation between the forecasted and measured wind speed could be resolved using physical parameters (site characteristics and wind direction). Therefore, there appears to be no need to use sophisticated non-linear statistical tools such as ANN since they perform as well as the linear ones when using the D-MP architecture for this particular problem. It is important to note that the batch learning and cross validation methodologies are also helpful to train such model to prevent over-learning situations due to the lack of data. GMOS differs from other MOS that are widely used by meteorological centers and the strengths of this innovative approach are based on the following aspects:

- GMOS dynamically selects a different linear model depending on the forecasted wind direction.

- It optimally exploits the physical simulations done by the NWP model for the surrounding forecasting points which have different geographic characteristics (surface roughness, terrain height, etc.).

- It can be applied to any forecast model providing wind speed and direction.

- It can be used without any historical data although a training phase using one year of data is recommended for further improvements. This characteristic is well suited for new sites where no data are available.

Globally, the D-MP linear model shows significant improvement over all other methods: this GMOS improves the GEM-LAM 2.5 km forecasts RMSE at the North Cape site by 25-30%.

These improvements can be appreciated among all time series and almost all meteorological conditions. Moreover, the present model combined with the GMOS outperformed the new reference model (persistence + climatology) from a 2 h horizon instead of 4 h without using the GMOS, which is a significant progress according to the literature. Also, the D-MP linear GMOS reduces considerably the topographic signature of the forecast errors, which is the main objective of the present study. This is due to the fact that this model exploits the physical simulations of the NWP model by using an ensemble of the surrounding forecasting points, having different geographic characteristics. Therefore this statistical model is able to integrate the fine scale local effects in the wind predictions which were not taken into account by the closest forecast point due to the relatively coarse spatial resolution of the NWP model. Finally, the GMOS developed for the North Cape site was applied and validated at another site located in Bouctouche (New Brunswick). Similar improvements on the GEM-LAM 2.5km forecasts were observed, thus showing the general applicability of the GMOS.

After applying the "optimal" GMOS, a dynamic approach is used to analyze and characterize the uncertainty of the short-term wind forecasts on the amplitude and phase error for different meteorological events. It appears that the phase errors are dominant over the bias and amplitude errors for all time series, for all wind directions and for most meteorological conditions. However, the amplitude errors and the bias become significant during less predictable dynamic events such as low pressure systems, wind ramps, rapid changes in the temperature or in the barometric pressure. These statistical analyses also show a higher forecast uncertainty for low wind speeds due to an incorrect forcing in the NWP model for wind speeds lower than 2 m/s. Also, the vertical resolution of the NWP model appears to be insufficiently fine in the surface layer to represent the formation of the thin stable atmospheric boundary layer, thus generating high forecast uncertainty at sunset (neutral atmospheric stability), when the atmosphere slowly turns stable from the convective unstable condition. Environment Canada team is now working to correct the surface fluxes forcing at low wind speed and it is intended to refine the vertical resolution of the GEM-LAM. These modifications should improve the NWP ability to forecast the wind speed for complex sites.

In future work, it would be interesting to provide probabilistic forecasts. This could be achieved by using the ensemble of surrounding forecast points to examine what are the different scenarios possible or by running an ensemble of ANN using different replications of the D-MP architecture as detailed in the literature review. This methodology could be useful to reduce the forecast uncertainty, but mostly to give the confidence interval of the forecast, which is more than valuable in energy trades. As cited in the previous paragraph, the NWP would greatly benefit from phase error reduction. Following that conclusion, it would be interesting to perform high resolution data assimilation for the GEM-LAM or to implement a Kalman filter. Similarly, a phase correction tool could also be developed using the MP methodology: indeed, the surrounding forecast points could provide useful information with regard to the phase of the dynamical events occurring. Also, to describe the geophysical parameters, it could be relevant to investigate the use of: the topographic slope instead of the topographic height and the surface roughness inverse logarithm instead of the roughness length itself. GMOS could also be coupled to micro-scale models for further improvements.

As concluding remarks, according to the needs of the wind energy industry, a GMOS has been developed and applied to improve the wind forecast from a NWP model, particularly in complex terrain. The methodology used to assess and understand the forecast uncertainty and error tendencies will also greatly improve wind power forecasts as it helped identifying meteorological events with high forecast uncertainties. Also, model errors being decomposed into phase, amplitude and systematic errors, the phase errors are found to be dominant compared with the two other types of errors. This finding will help to define the research priority in improving wind energy forecasting. A better knowledge of prediction uncertainties and a better wind forecast will increase the economic value of wind energy in the market by increasing wind energy confidence for energy trades and by simplifying the issues of energy transmission, electricity grid balancing and power generation dispatch.

ANNEX I

DATA RECOVERY RATE AT THE BOUCTOUCHE SITE

Table A.I.1 Data recovery rates for every month
of the sample year (Bouctouche)

Month	**Records Available Ratio (%)**	**Valid Records Ratio (%)**	**Upwind Records Ratio (%)**	**Available Forecast Ratio (%)**	**Data Recovery Rate (%)**
January	83.33	93.06	93.41	100.0	72.44
February	83.48	90.64	94.20	100.0	71.28
March	86.02	88.83	92.44	100.0	70.63
April	95.56	92.59	86.50	100.0	76.53
May	97.45	92.14	85.33	100.0	76.62
June	93.89	94.67	80.16	100.0	71.25
July	93.88	93.20	88.40	100.0	77.35
August	94.42	94.45	89.75	100.0	80.04
September	97.71	92.89	94.26	100.0	85.55
October	96.44	90.94	88.97	100.0	78.03
November	52.08	93.07	92.26	100.0	44.72
December	90.86	92.68	89.70	100.0	75.54
Annual	**88.13**	**92.34**	**90.24**	**100.0**	**73.44**

ANNEX II

ANEMOMETER RELIABILITY AT THE BOUCTOUCHE SITE

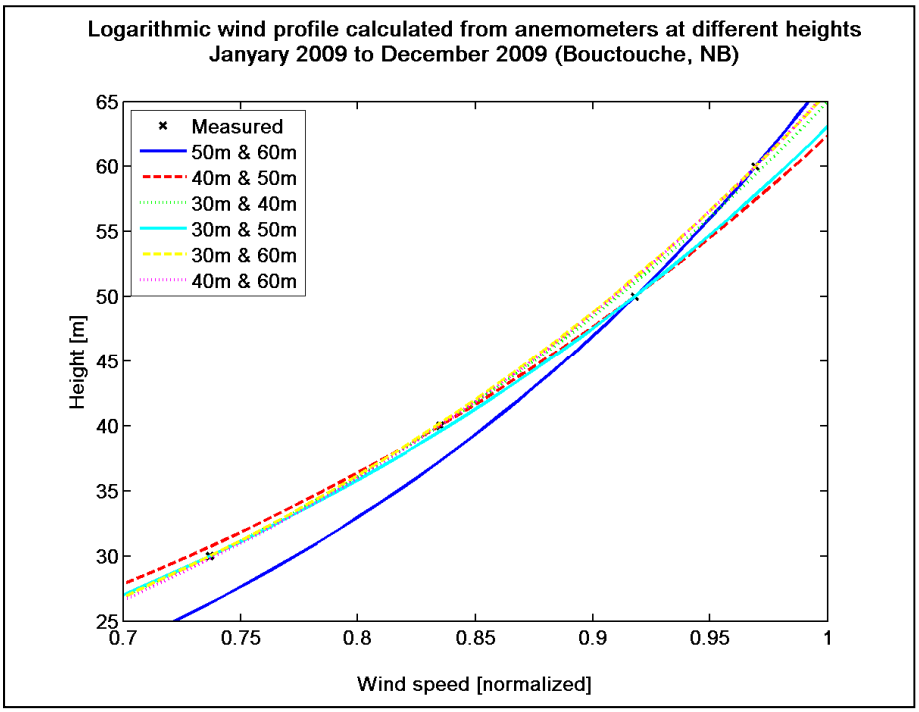

Figure A.II.1 Logarithmic vertical wind speed profiles plotted from the mean wind speed at two different heights.

ANNEX III

CHARACTERISTICS OF THE WIND AT THE BOUCTOUCHE SITE

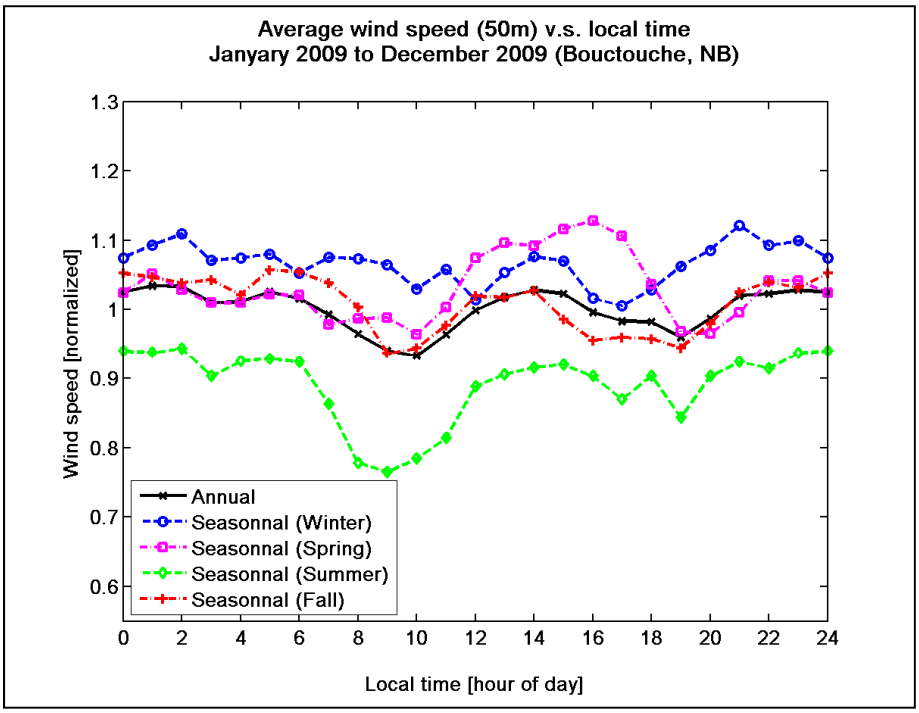

Figure A.III.1 Annual and seasonal average wind speed diurnal cycles at the Bouctouche site.

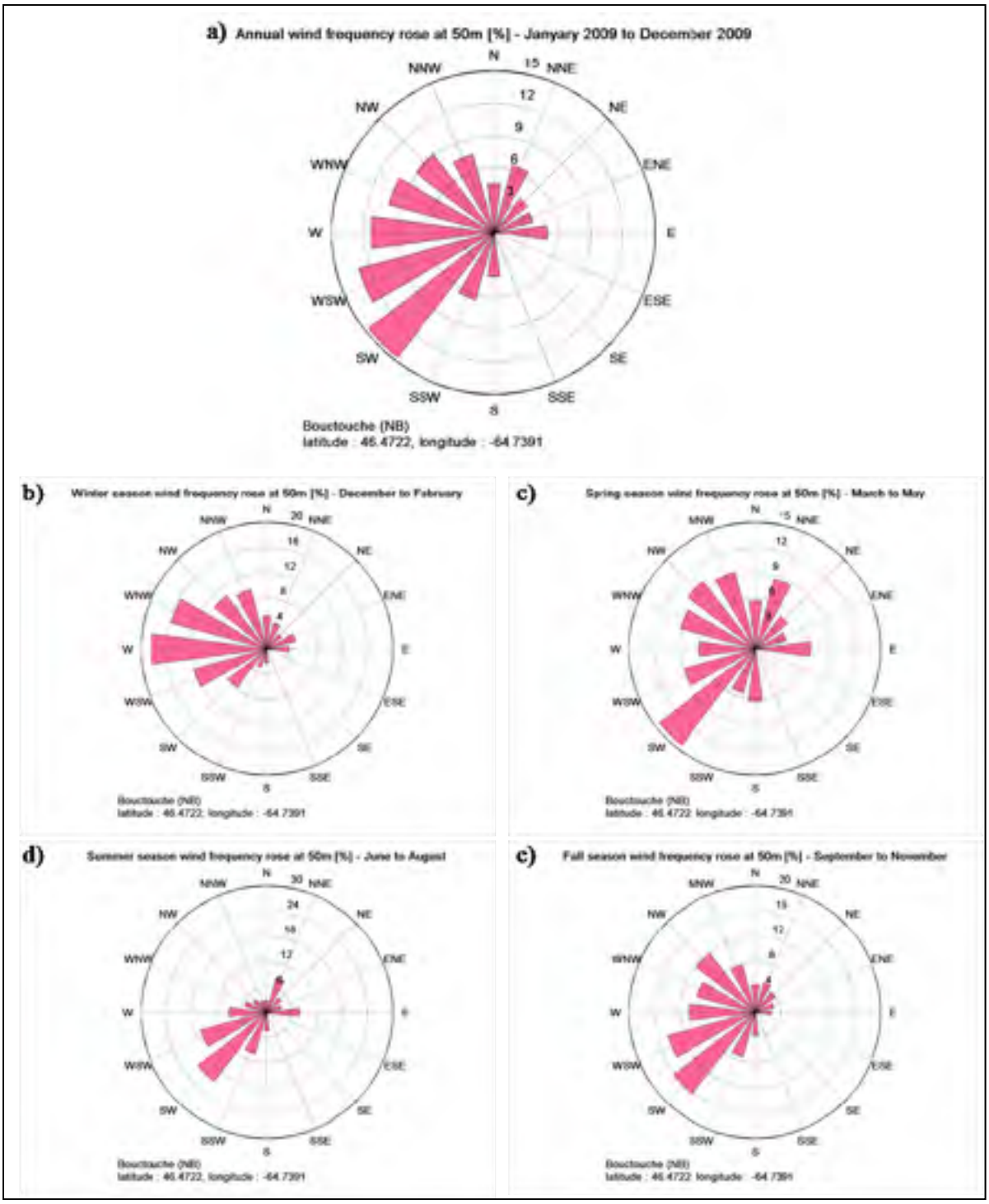

Figure A.III.2 Annual and seasonal wind frequency roses at the Bouctouche site: a) annual, b) winter, c) spring, d) summer and e) fall.

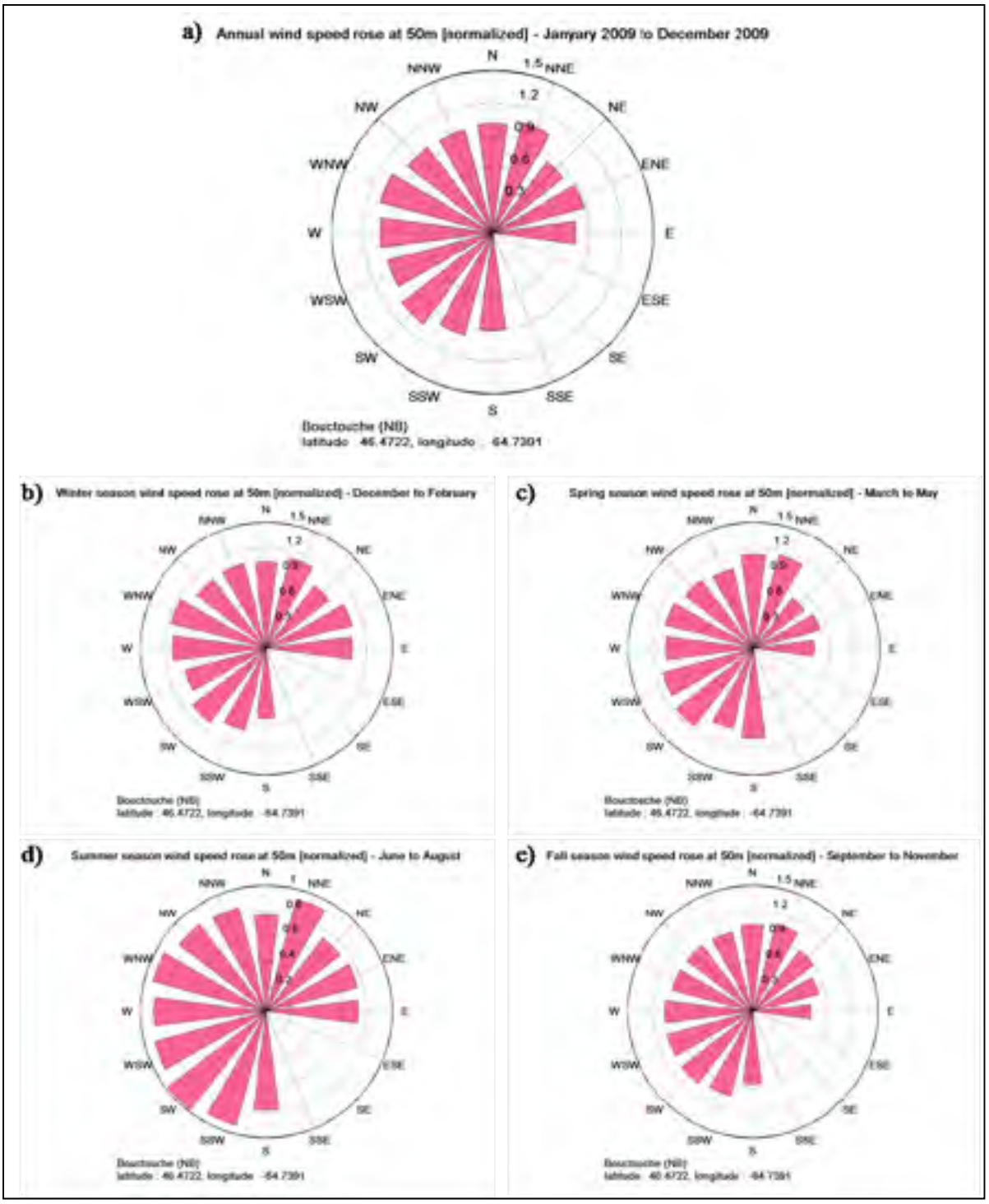

Figure A.III.3 Annual and seasonal average wind speed roses at the Bouctouche site: a) annual, b) winter, c) spring, d) summer and e) fall.

Figure A.III.4 Annual and seasonal wind energy roses at the Bouctouche site: a) annual, b) winter, c) spring, d) summer and e) fall.

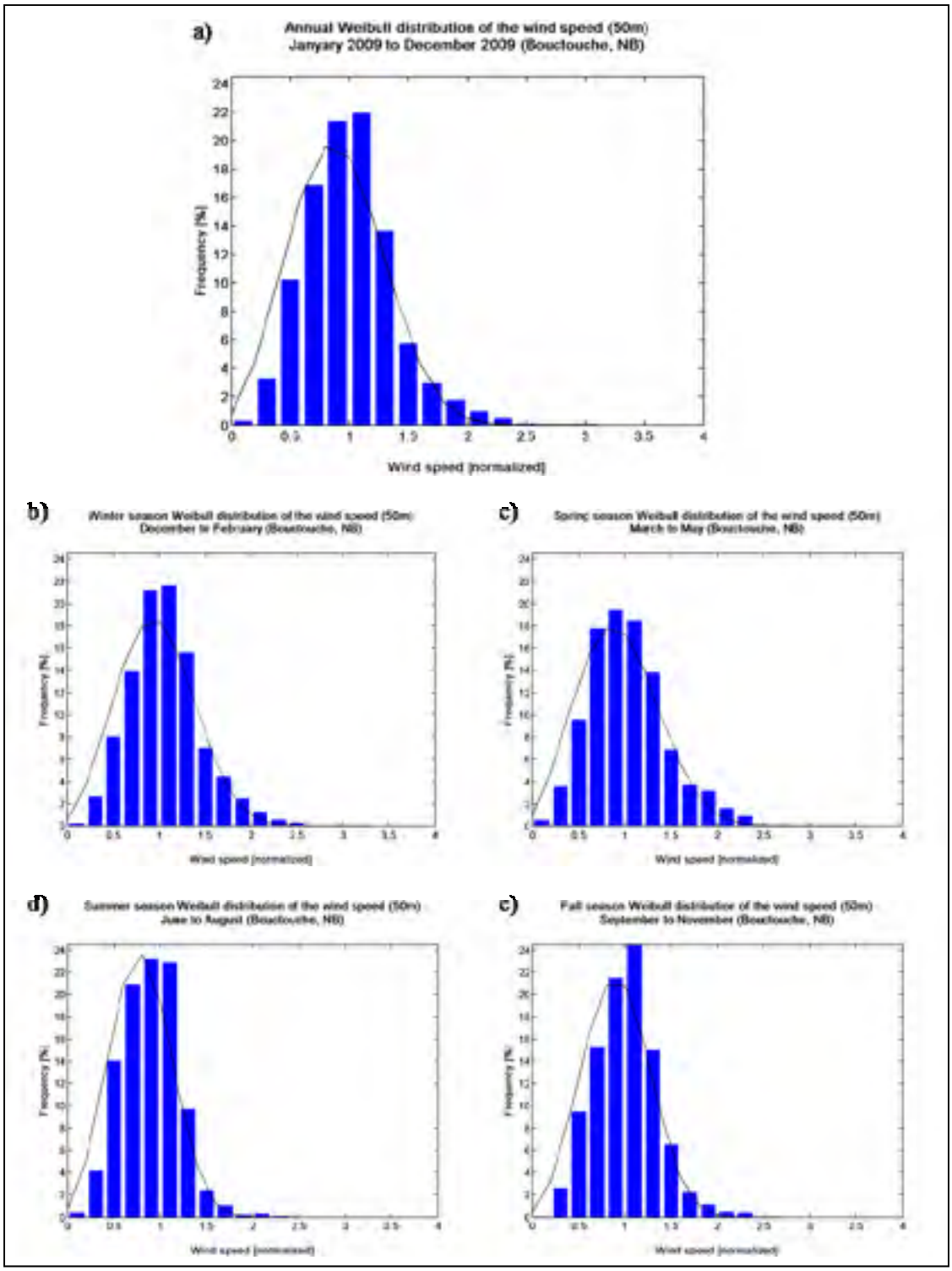

Figure A.III.5 Annual and seasonal Weibull distributions of the wind speed at the Bouctouche site: a) annual, b) winter, c) spring, d) summer and e) fall.

ANNEX IV

VERTICAL INTERPOLATION AT THE BOUCTOUCHE SITE

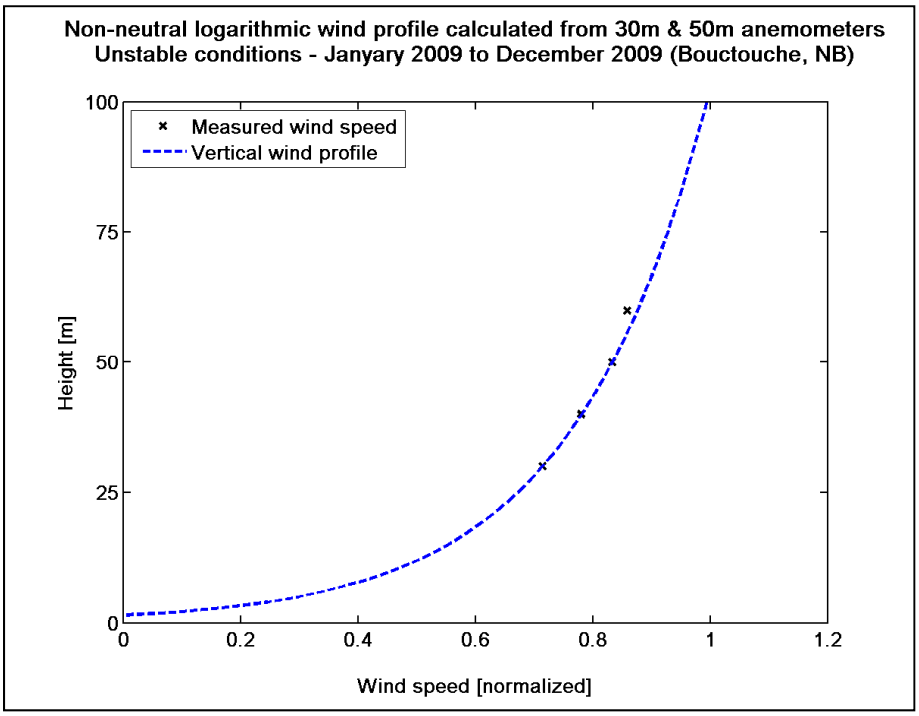

Figure A.IV.1 Non-neutral logarithmic wind profile under unstable/neutral atmospheric conditions at the closest NWP point to the measurement mast (Bouctouche).

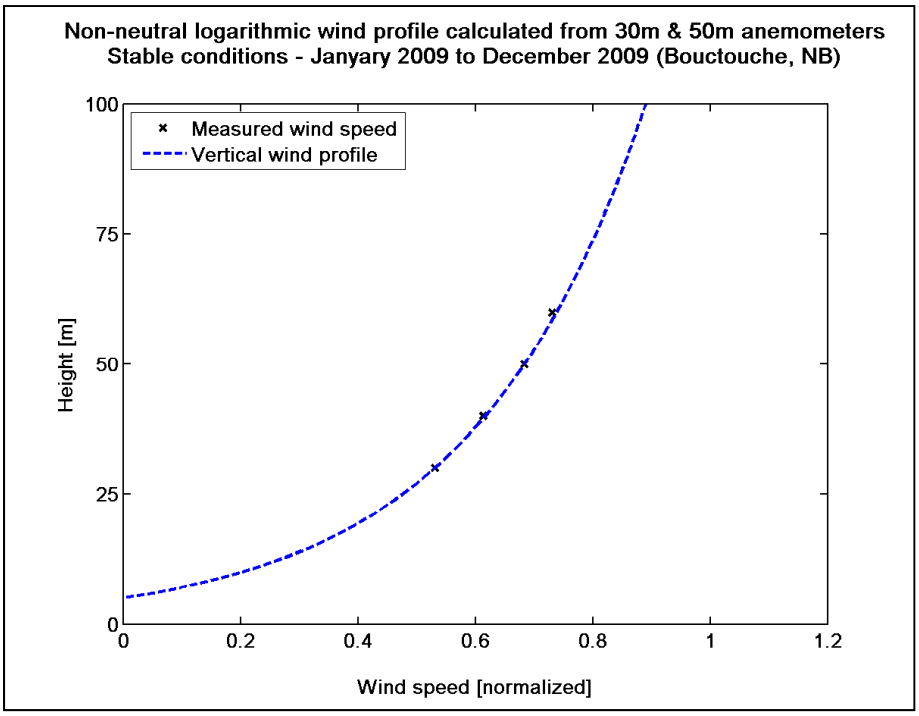

Figure A.IV.2 Non-neutral logarithmic wind profile under stable atmospheric conditions at the closest NWP point to the measurement mast (Bouctouche).

ANNEX V

COMPARISON OF THE GMOS AT THE BOUCTOUCHE SITE

Latitude of the Bouctouche measurement mast: 46.472217 °N.

Longitude of the Bouctouche measurement mast: 295.2609 °E.

Surface roughness of the Bouctouche site: 3.5 m.

Topographic height of the Bouctouche site: 30 m.

Table A.V.1 Improvement of different simple geo-referenced weighting schemes compared to the closest forecast point

Interpolation method	**Bias (%)**	**MAE (%)**	**RMSE (%)**
U_{Dist}	15.90	8.64	8.28
U_{φ}	24.40	6.03	1.73
U_{z_0}	29.52	14.52	13.98
$U_{H_{Topo}}$	51.43	21.84	20.59

Table A.V.2 Improvement of the different regression methods

Interpolation method	**Bias (%)**	**MAE (%)**	**RMSE (%)**
Geo-referenced	44.47	17.45	15.43
Simple linear regression	89.93	31.24	31.15
MP linear regression	90.93	33.77	33.86
D-MP linear regression	90.00	35.38	34.56
Simple ANN	89.70	31.50	31.81
MP ANN	91.75	34.48	34.91
D-MP ANN	92.03	36.23	35.63

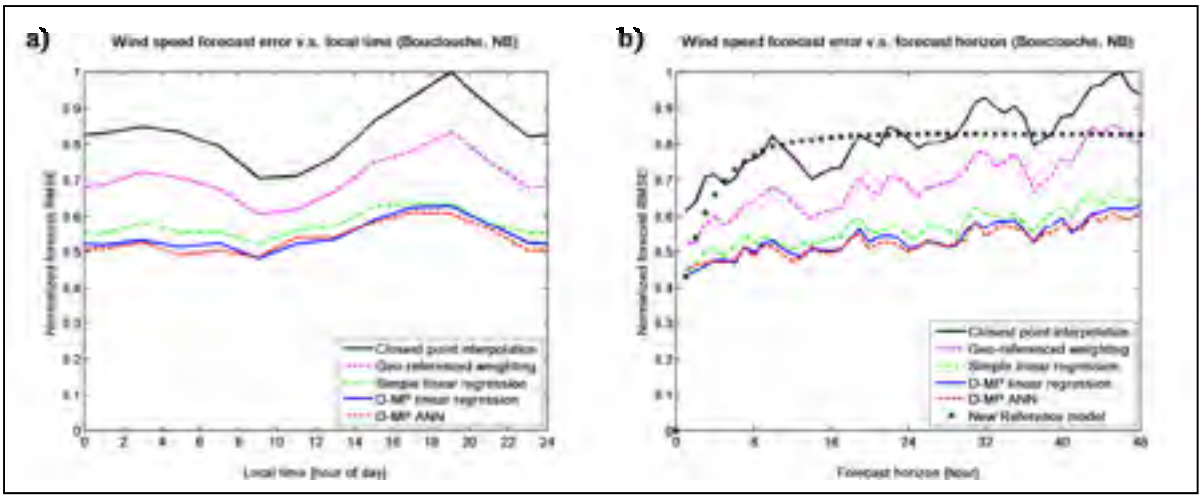

Figure A.V.1 Wind speed forecast RMS error for different time series: a) local time and b) forecast horizon (up to 48 h).

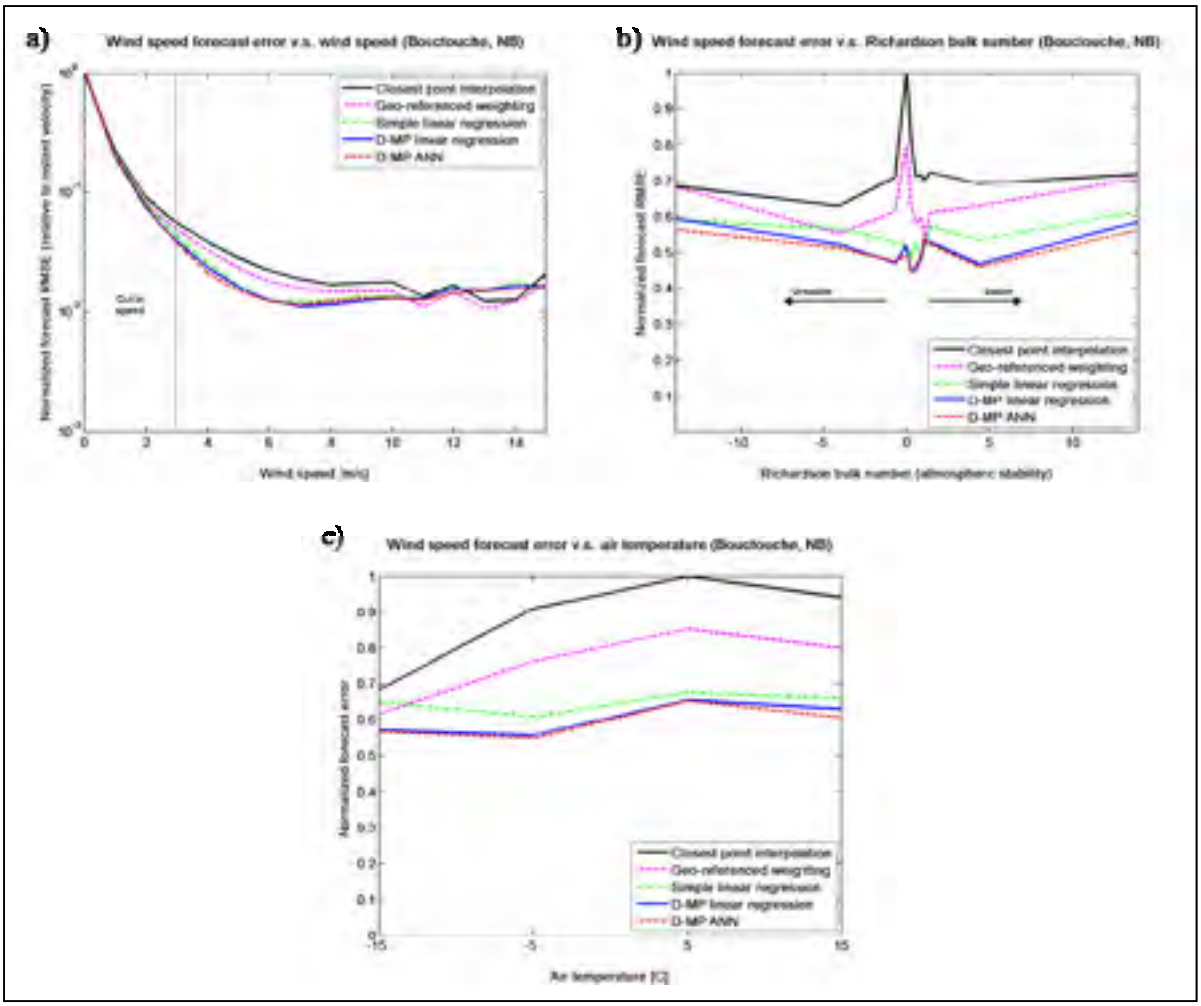

Figure A.V.2 Wind speed forecast RMS error for different meteorological parameters: a) wind speed, b) atmospheric stability (bulk Richardson number) and c) air temperature.

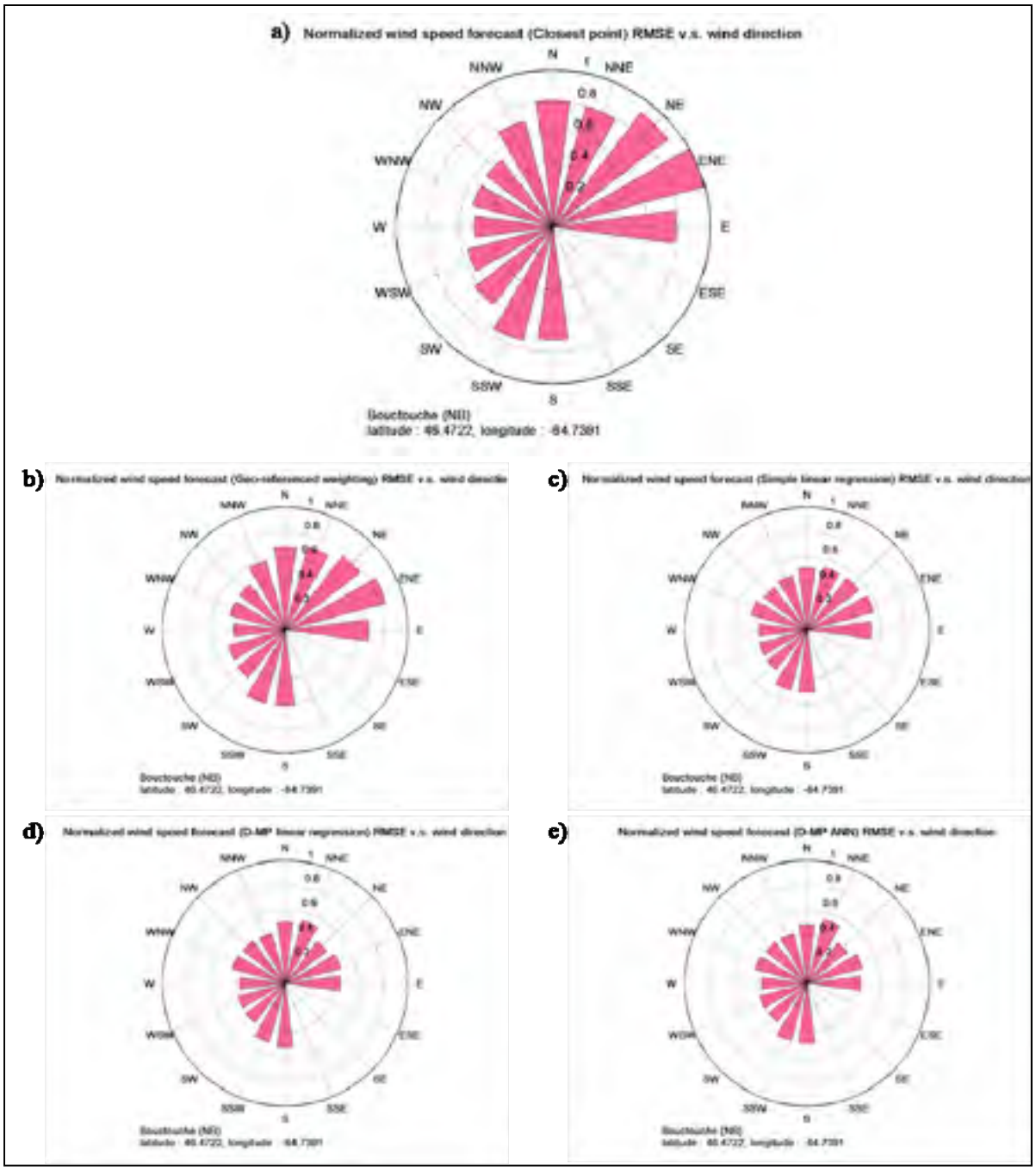

Figure A.V.3 Wind speed forecast RMS error rose of each regression method: a) closest point, b) geo-referenced weighting, c) simple linear regression, d) D-MP linear regression and e) D-MP ANN.

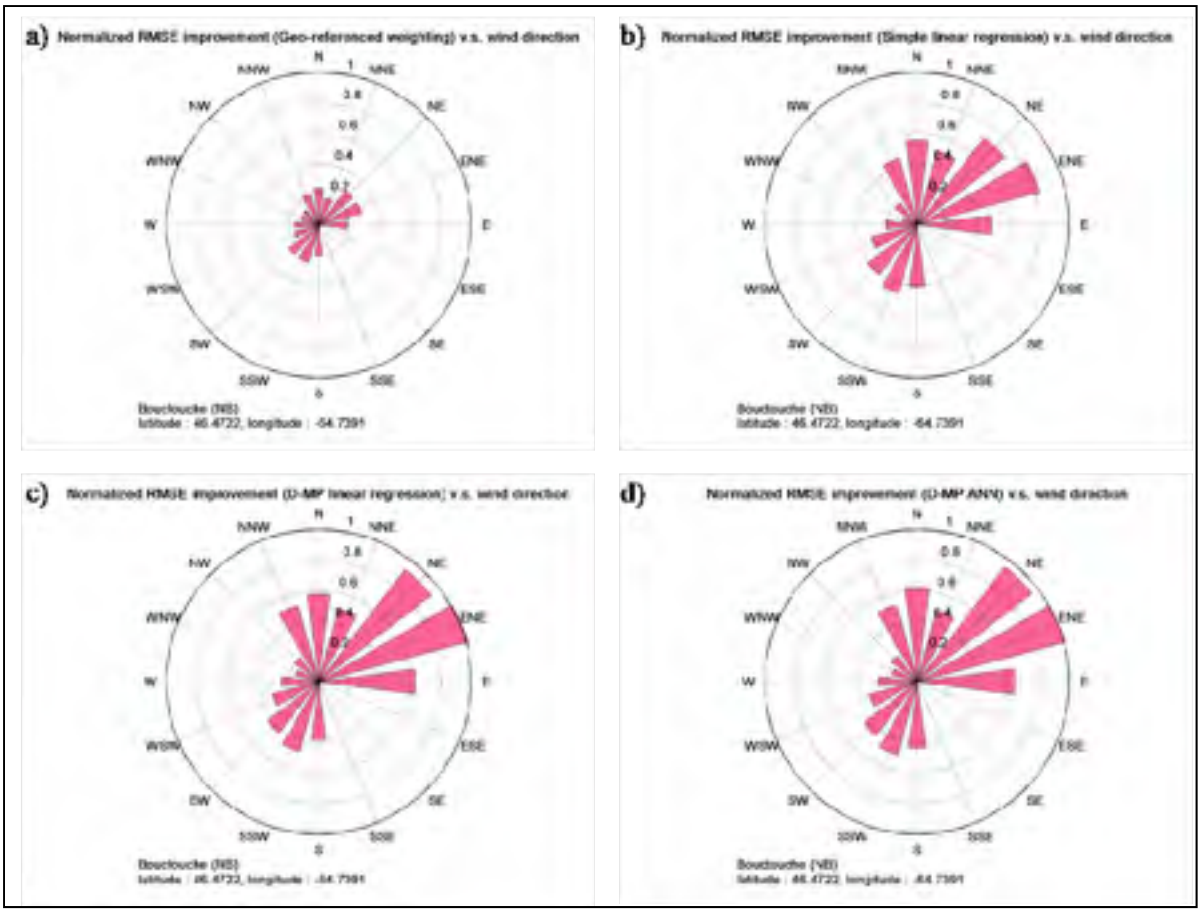

Figure A.V.4 Improvement rose of each regression module compared to the closest point: a) geo-referenced weighting, b) simple linear regression, c) D-MP linear regression and d) D-MP ANN.

ANNEX VI

NWP MODEL VALIDATION AT THE BOUCTOUCHE SITE

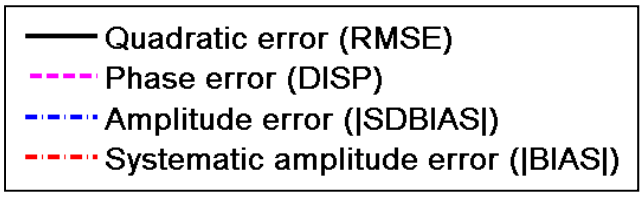

Figure A.VI.1 Legend for the NWP uncertainty assessment on amplitude and phase error.

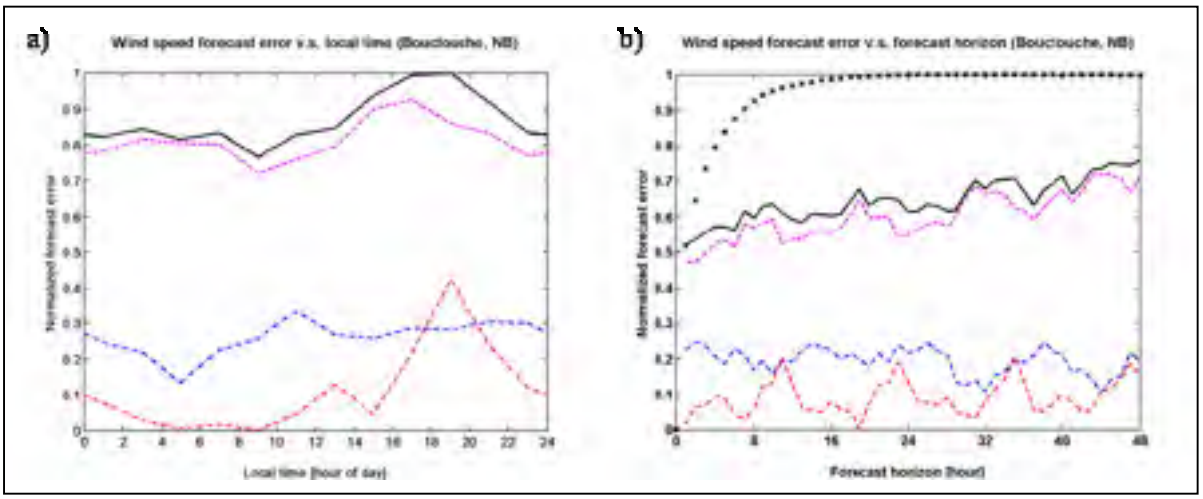

Figure A.VI.2 Wind speed forecast errors for different time series at the Bouctouche site: a) local time and b) forecast horizon (up to 48 h).

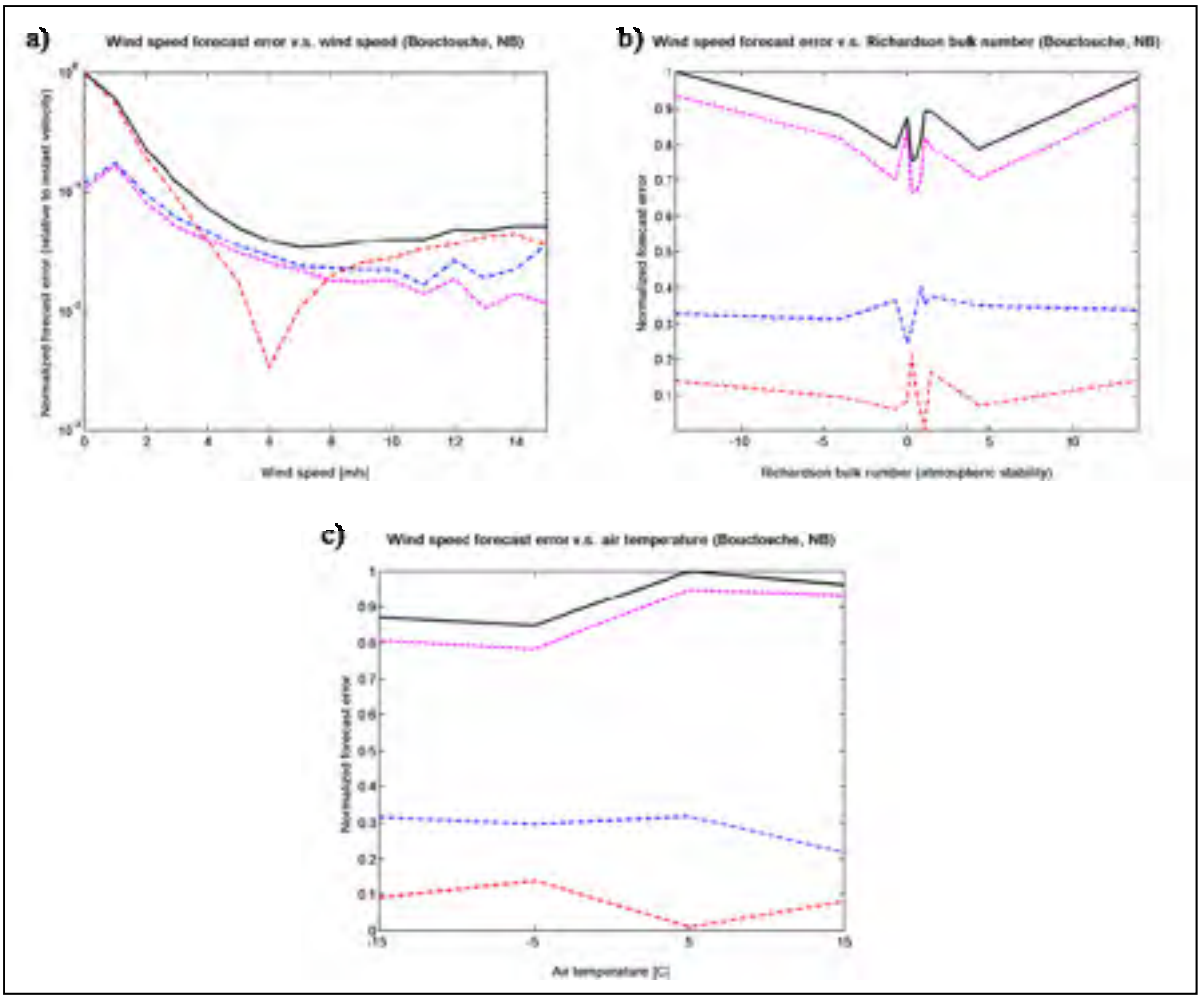

Figure A.VI.3 Wind speed forecast errors for different meteorological conditions at the Bouctouche site: a) wind speed, b) atmospheric stability (bulk Richardson number) and c) air temperature.

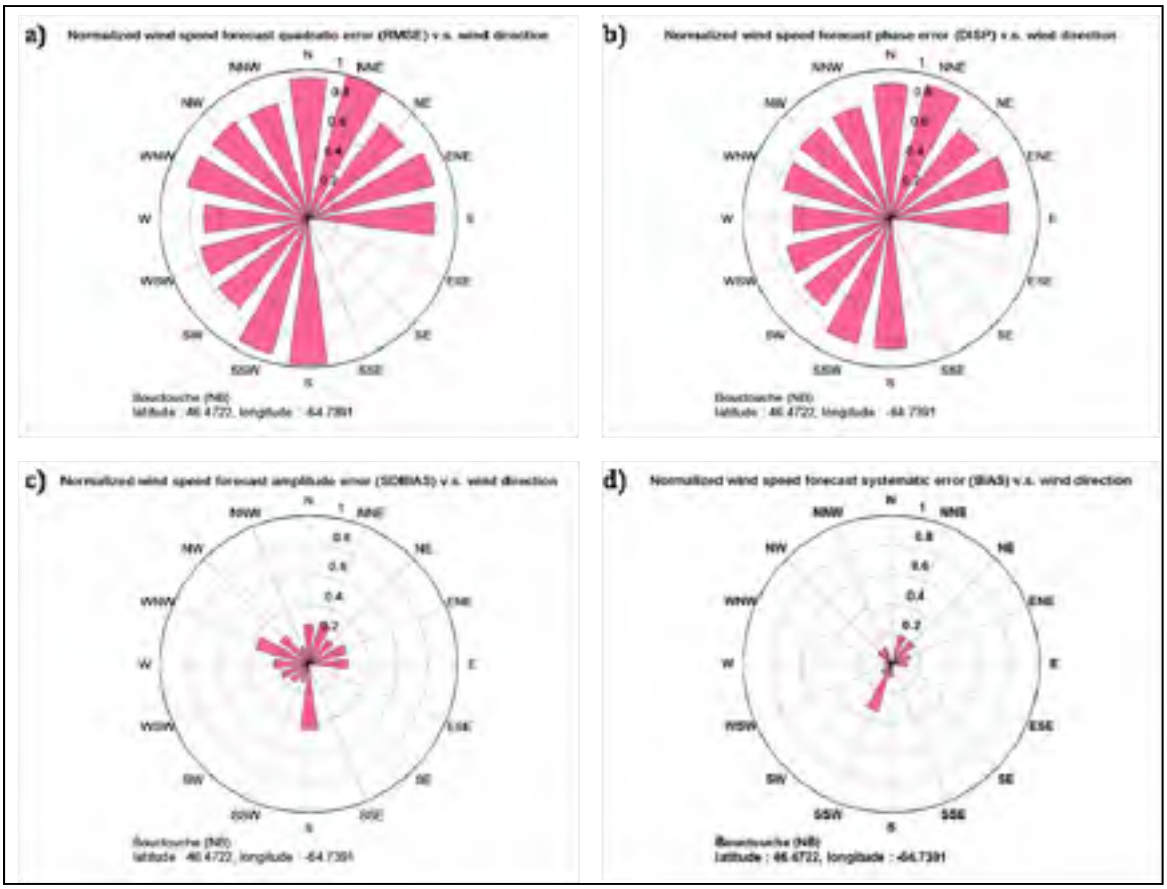

Figure A.VI.4 Wind speed forecast error roses at the Bouctouche site: a) RMSE, b) phase error, c) amplitude error and d) systematic errors.

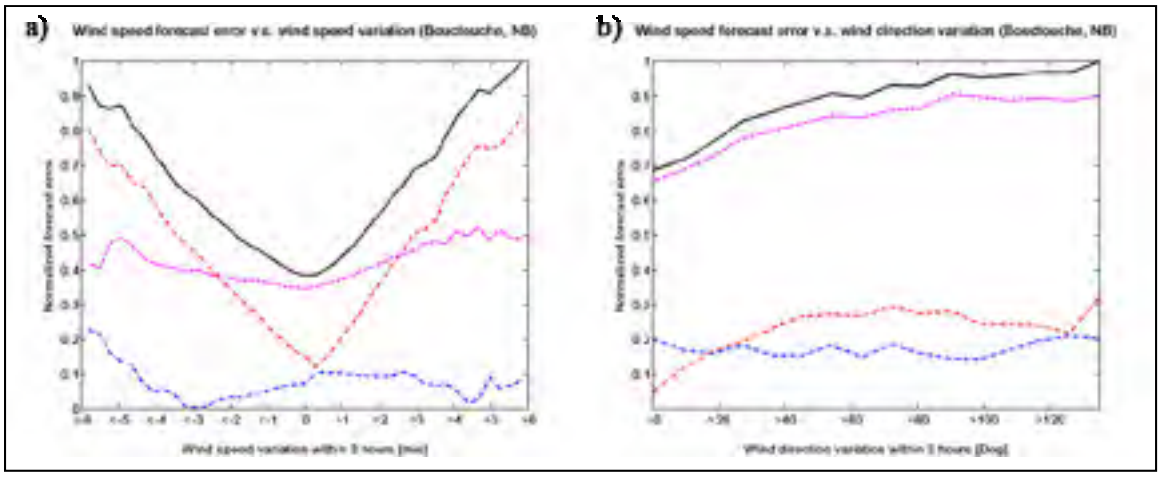

Figure A.VI.5 Wind speed forecast errors for dynamic meteorological events at the Bouctouche site: a) wind speed variations and b) wind direction variations.

REFERENCES

AWS Scientific Inc., 1997. "Wind Resource Assessment Handbook: Fundamentals for Conducting a Successful Monitoring Program". National Renewable Energy Laboratory, TAT-5-15283-01. Golden (Colorado), 79p.

Bilmes J. and Kirchhoff K., 2000. "Directed Graphical Models of Classifier Combination: Application to Phone Recognition". In: International Conference on Acoustics, Speech, and Signal Processing, Beijing (China), October 2000.

Businger J.A., Wyngaard J.C., Izumi Y. and Bradley E.F., 1971. "Flux-Profile Relationships in the Atmospheric Surface Layer". Atmospheric Science, Vol. 28, pp. 181-189.

Côté J., Gravel S., Méthot A., Patoine A., Roch M. and Staniforth A., 1998. "The Operational CMC/MRB Global Environmental Multiscale (GEM) Model: Part I - Design Considerations and Formulation". Monthly Weather Review, Vol. 126, (June), pp. 1373-1395.

Counihan J., 1975. "Adiabatic Atmospheric Boundary Layers: A Review and Analysis of Data Collected from the Period 1880- 1972". Atmospheric Environment, Vol. 9, pp. 871-905.

Cutler N., Kay M., Jacka K. and Nielsen T.S., 2007. "Detecting, Categorizing and Forecasting Large Ramps in Wind Farm Power Output Using Meteorological Observations and WPPT". Wind Energy, Vol. 10, pp. 453-470.

Delage Y. and Girard C., 1992. "Stability Functions Correct at the Free Convection Limit and Consistent for Both the Surface and Ekman Layers". Boundary-Layer Meteorology, Vol. 58, pp. 19-31.

Delage Y., 1988 "The Position of the Lowest Level in the Boundary Layer of Atmospheric Circulation Models". Atmosphere-Ocean, Vol. 26, pp. 329-340.

Delage Y., 1997. "Parameterising Sub-Grid Scale Vertical Transport in Atmospheric Models Under Statically Stable Conditions". Boundary-Layer Meteorology, Vol. 82, pp. 23-48.

Duin R.P.W., 2002. "The Combining Classifier: to Train or Not to Train?". In: 16th International Conference on Pattern Recognition, Québec, August 11-15 2002, Vol. 2, pp. 765-770.

Gasset N., Poitras G.J., Gagnon Y. and Brothers C., 2005. "Study of Atmospheric Boundary Layer Flows Over a Coastal Cliff". Wind Engineering, Vol. 29, No. 1, pp. 3-24.

Giebel G., Kariniotakis G. and Brownsword R., 2003. “The State-Of-The-Art in Short-Term Forecasting of Wind Power. A Literature Overview”, Deliverable report for the Anemos project. 36 p.

Global Wind Energy Council, 2008. “Global Wind Energy Outlook 2008”. Online, 60 p. <http://www.gwec.net/fileadmin/images/Logos/Corporate/GWEO_A4_2008_lowres.pdf >. Consulted on Dec. 12th 2008.

Hinton G.E., 1989. “Connectionist Learning Procedures”. Artificial Intelligence, Vol. 40, (September), pp. 185-234.

Hou D., Kalnay E. and Droegemeier K.K., 2001. “Objective Verification of the SAMEX ’98 Ensemble Forecast”, Monthly Weather Review, Vol. 129, pp. 73-91.

Hunter R.S., Pedersen B.M., Pedersen T.F., Klug H., Van Der Bord N., Kelley N., Dahlberg J.Å., 1999. “Recommended Practices From Wind Turbines Testing - 11. Wind Speed Measurements and Use of Cup Anemometry”. Report from IEA Wind Agreement Executive Committee. 50 p.

IEC. 2004. “WIND TURBINES - Part 121: Power Performance Measurements of Electricity Producing Wind Turbines”. IEC 61400-121. International Electrotechnical Commission, 2004, 85 p.

Justus, C.G., 1978. “Winds and Wind System Performance”. Franklin Institute Press, Philadelphia (PA). 120 p.

Kaimal J.C. and Finnigan J.J., 1994. “Atmospheric Boundary Layer Flows - Their Structure and Measurement”. Oxford University Press, New-York. 289 p.

Kariniotakis G., Martì I., Casas D., Pinson P., Nielsen T.S., Madsen H., Giebel G., Usaola J., Sanchez I., Palomares A.M., Brownsword R., Tambke J., Focken U., Lange M., Louka P., Kallos G., Lac C., Sideratos G. and Descombes G., 2004. “What Performance Can Be Expected by Short-Term Wind Power Prediction Models Depending on Site Characteristics?”. In: European Wind Energy Conference, London (UK), 2004.

Kittler J., Hatef M., Duin R.P.W., and Matas J., 1998. “On Combining Classifiers”. IEEE Transactions On Pattern Analysis And Machine Intelligence, Vol. 20, No. 3, (March), pp. 226-239.

Landberg L., 1998. “A Mathematical Look at a Physical Power Prediction Model”, Wind Energy, Vol. 1, pp. 23-28.

Landberg L. and Watson S.J., 1994. “Short-Term Predictions of Local Wind Conditions”. Boundary-Layer Meteorology, Vol. 70, pp. 171-195.

Landberg L., Giebel G., Nielsen H.A., Nielsen T.S. and Madsen H., 2003. "Short-Term Prediction - An Overview", Wind Energy, Vol. 6, pp. 273-280.

Lange M., 2003. "Analysis of the Uncertainty of Wind Power Predictions", PhD Thesis, Carl von Ossietzky Universität, Oldenburg, Germany, 127 p.

Lange M. and Heinemann D., 2003. "Relating the Uncertainty of Short-Term Wind Speed Predictions to Meteorological Situations with Methods from Synoptic Climatology". In: European Wind Energy Conference, Madrid, 2003.

Lange M., Focken U., Meyer R., Denhardt M., Ernst B. and Berster F., 2006. "Optimal Combination of Different Numerical Weather Models for Improved Wind Power Predictions". In: International Workshop on Large-Scale Integration of Wind Power and Transmission Networks for Offshore Wind Farms, Delft, 2006.

Liu H., 2009. "Wind Speed Forecasting for Wind Energy Application", PhD Thesis, York University, Toronto, Canada, 240 p.

Lumley J.L. and Panofsky H.A., 1964. "The Structure of Atmospheric Turbulence". Wiley Interscience Publishers, New York. 239 P.

Madsen H., Kariniotakis G., Nielsen H.A., Nielsen T.S. and Pinson P., 2004. "A Protocol For Standardizing The Performances Evaluation of Short-Term Wind Power Prediction Models". Deliverable report for the Anemos project. 16 p.

Mailhot J., Bélair S., Benoit R., Bilodeau B., Delage Y., Filion L., Garant L., Girard C. and Tremblay A., 1998. "Scientific Description of RPN Physics Library - Version 3.6". Report from Recherche en Prévision Numérique group, Environment Canada Atmospheric Environment Service. 188 p.

Mailhot J., 1992. "Numerical Simulation of Air Mass Transformation Over the Gulf of Mexico". Journal of Applied Meteorology, Vol. 31, pp. 946-963.

Manwell J.F., McGowan J.G. and Rogers A.L., 2002. "Wind Energy Explained - Theory, Design and Application". John Wiley & Sons Ltd, England. 590 P.

Nielsen H.A., Pinson P., Christiansen L.E., Nielsen T.S., Madsen H., Badger J., Giebel G. and Ravn H.F., 2007a. "Improvement and Automation of Tools for Short-Term Wind Power Forecasting". In: European Wind Energy Conference, Milan (Italy), 2007.

Nielsen H.A., Nielsen T.S., Madsen H., Badger J., Giebel G., Landberg L., Sattler K. and Feddersen H., 2004. "Comparison of Ensemble Forecasts with the Measurements from the Meteorological Mast at Risø National Laboratory". Project report for the Anemos project. 45 p.

Nielsen H.A., Nielsen T.S., Madsen H., San Isidro Pindado M.J. and Martì I., 2007b. "Optimal Combination of Wind Power Forecasts", Wind Energy, Vol. 10, pp. 471-482.

Nielsen T.S., Joensen A., Madsen H., Landberg L. and Giebel G., 1998. "A New Reference Model for Wind Power Forecasting". Wind Energy, Vol. 1, pp. 29-34.

Panofsky H.A. and Dutton J.A., 1983. "Atmospheric Turbulence - Models and Methods for Engineering Applications". John Wiley & Sons Ltd, England. 397 p.

Stull R.B., 1988. "An Introduction to Boundary Layer Meteorology". Kluwer Academic Publishers, Netherlands. 666 p.

Tax D.M.J., Van Breukelen M., Duin R.P.W. and Kittler J., 2000. "Combining Multiple Classifiers by Averaging or by Multiplying?". Pattern Recognition, Vol. 33, pp. 1475 - 1485.

Tennekes H. and Lumley J.L., 1972. "A first Course in Turbulence". The Massachusetts Institute of Technology Press, Cambridge, Massachusetts. 300 p.

Van Der Hoven I., 1957. "Power Spectrum of Horizontal Wind Speed in the Frequency Range from 0.0007 to 900 Cycles per Hour". Journal of Meteorology, Vol. 14, pp. 160-164.